Universitat Autònoma de Barcelona

Tesi doctoral

Excited state intramolecular proton transfer reactions coupled with non adiabatic processes: electronic structure and quantum dynamical approaches

Juan Manuel Ortiz Sánchez

Directors: Miquel Moreno Ferrer i Ricard Gelabert Peiri

Programa de doctorat: Química Teòrica i Computacional

Departament de Química, Facultat de Ciències

Universitat Autònoma de Barcelona

2009

Paper IV

J. M. Ortiz-Sánchez, R. Gelabert, M. Moreno and J. M. Lluch. A comparative study on the photochemistry of two bipyridyl derivatives: [2,2'-pipyridyl]-3,3'-diamine and [2,2'-bipyridyl]-3,3'-diol. *ChemPhysChem* 8(8): 1199 – 1206, 2007.

ARTICLES

DOI: 10.1002/cphc.200600771

A Comparative Study on the Photochemistry of Two Bipyridyl Derivatives: [2,2′-Bipyridyl]-3,3′-diamine and [2,2′-Bipyridyl]-3,3′-diol

Juan Manuel Ortiz-Sánchez, Ricard Gelabert, Miquel Moreno,* and José M. Lluch[a]

The two isoelectronic bipyridyl derivatives, [2,2′-bipyridyl]-3,3′-diamine and [2,2′-bipyridyl]-3,3′-diol, are experimentally known to undergo very different excited-state double-proton-transfer processes, which result in fluorescence quantum yields that differ by four orders of magnitude. Herein, density functional theory (DFT), time-dependent DFT (TDDFT), and complete active space self-consistent field (CASSCF) calculations are used to study the double-proton-transfer processes in the ground and first singlet $\pi\rightarrow\pi^*$ excited state. The quantum-chemistry calculations indicate 1) the existence of only one energy minimum in the ground electronic state corresponding to reactants (thus avoiding the possibility of a fast fluorescent relaxation process from the photoproducts region), 2) an endoergic process of the complete double proton transfer, and 3) the presence of a conical intersection in the excited intermediate region of [2,2′-bipyridyl]-3,3′-diamine. These facts explain the very low fluorescence quantum yield in [2,2′-bipyridyl]-3,3′-diamine compared to [2,2′-bipyridyl]-3,3′-diol.

1. Introduction

Photoinduced intramolecular proton transfer is a ubiquitous process in chemistry and biology.[1–4] Excited-state intramolecular proton-transfer (ESIPT) processes are usually ultrafast ($\tau < 10^{-12}$ s) and reversible. These properties lead to a huge number of applications in the technological world based on ESIPT, such as rewritable molecular memories, photostabilizers, and UV-filter materials.[5–7]

Even if there is a large diversity of molecules known to experience ESIPT, it is well-accepted that ESIPT processes are usually initiated by a HOMO(π)→LUMO(π^*) electronic excitation (HOMO: highest occupied molecular orbital; LUMO: lowest unoccupied molecular orbital) that reverses the acid–base characteristics of the H-donor and H-acceptor fragments of the molecule. In other words, the potential energy surfaces of the ground (S_0) and first singlet excited (S_1) electronic states are very different, so that the more stable tautomer in S_0 becomes less stable (or even unstable) in S_1.

The use of modern experimental techniques such as time-resolved laser spectroscopy or coherent transient data has provided a wealth of knowledge about these ultrafast processes. However, the vast majority of studies have dealt with single ESIPT processes. Excited-state intramolecular double proton transfer (ESIDPT) is far less well-known. In ESIDPT, the reaction is expected to be more complicated, since two possible limiting mechanisms can be envisaged. In the first limiting mechanism, the two protons transfer in a single step (concerted mechanism), whereas in the second, one proton transfer precedes the other so that the mechanism involves a zwitterionic intermediate (stepwise mechanism).

A few years ago, some of us reported a theoretical study on the ESIDPT in [2,2′-bipyridyl]-3,3′-diol [hereafter referred to as $BP(OH)_2$].[8] This molecule had been carefully studied by Glasbeek and co-workers,[9–13] who carried out a series of time-resolved experiments in the sub-picosecond time range. From these studies it was concluded that the ESIDPT in $BP(OH)_2$ was a branched mechanism and consisted of: 1) a concerted reaction channel, where both protons exchange sites simultaneously and 2) a stepwise channel, where one proton transfers first and the other proton transfers upon completion of the first step. The two processes involve three different chemical species (Scheme 1) named by Glasbeek and co-workers as dienol (DE), monoketo (MK), and diketo (DK) after the reactant, intermediate, and product tautomers, respectively. The same nomenclature was used in our previous theoretical work on $BP(OH)_2$,[8] and it is also used herein. The characteristic times of both concerted and stepwise channels were very different: the concerted path was completed in about 100 fs, and the same timescale was reported for the first step of the stepwise mechanism, whereas the second step needed a much longer time (10 ps). Electronic-structure calculations based on density functional theory (DFT) and time-dependent DFT (TDDFT) methodology showed that the stepwise mechanism was ener-

[a] J. M. Ortiz-Sánchez, Dr. R. Gelabert, Dr. M. Moreno, Prof. J. M. Lluch
Departament de Química
Universitat Autònoma de Barcelona
08193 Bellaterra, Barcelona (Spain)
Fax: (+34) 93-581-2920
E-mail: mmf@qf.uab.es

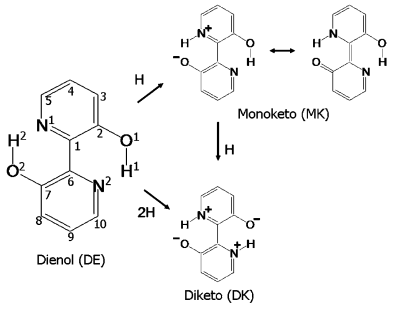

Scheme 1. Concerted and stepwise mechanism for double proton transfer in [2,2′-bipyridyl]-3,3′-diol, including atom numbering. The charges shown are formal charges in the context of a Lewis structure and do not necessarily correspond to the actual charge distribution.

getically favored over a concerted process.[8] However, quantum dynamical simulations performed on a representation of the S_1 potential-energy surface showed branching of the wavepacket between the two routes, thus confirming the experimental findings. Also, the reasons behind the longer timescale of the second step in the stepwise mechanism were identified as intramolecular vibrational energy redistribution (IVR).[8]

Recently, the group of Glasbeek reported on a very similar system, [2,2′-bipyridyl]-3,3′-diamine [henceforth $BP(NH_2)_2$] in which the two hydroxyl groups are replaced by amine groups (Scheme 2).[14] A femtosecond fluorescence upconversion study

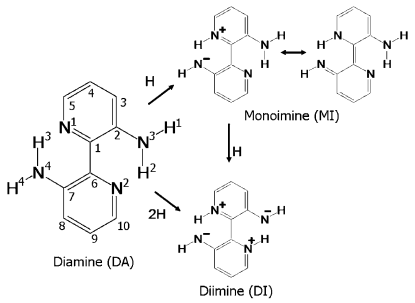

Scheme 2. Concerted and stepwise mechanism for double proton transfer in [2,2′-bipyridyl]-3,3′-diamine, including atom numbering. The charges shown are formal charges in the context of a Lewis structure and do not necessarily correspond to the actual charge distribution.

of $BP(NH_2)_2$ revealed two fluorescent bands, band I (425 nm) and band II (585 nm) with a rise time faster than 100 fs, and both bands presenting a 250 fs emission decay. The quantum yield (QY) for both emission bands was estimated to be as low as 10^{-5}, irrespective of the solvents used. This finding is in sharp contrast with the fluorescence spectrum of $BP(OH)_2$ in cyclohexane (QY = 0.32).[14] These results have been interpreted in terms of a branched mechanism leading to the ESDIPT product. On the one hand, there is a concerted double proton transfer within about 100 fs, followed by a twisting of the product that takes place in around 250 fs. On the other hand, there is a slower process involving simultaneous twisting and double proton transfer with an overall reaction time of approximately 250 fs. In the case of $BP(NH_2)_2$, there is no evidence of an intermediate single-proton-transfer state being involved in the process. Scheme 2 depicts the hypothetical concerted and stepwise mechanisms for $BP(NH_2)_2$. The chemical species involved have been named employing a similar terminology to that used for $BP(OH)_2$: diamine (DA), monoimine (MI), and diimine (DI) for the reactant, intermediate, and product tautomers, respectively.

Despite the molecular structural similarities between $BP(OH)_2$ and $BP(NH_2)_2$, the notable differences experimentally detected for the respective ESIDPT process and the very dissimilar quantum yields are striking, so we have carefully analyzed the ESIDPT process in $BP(NH_2)_2$ from a theoretical point of view. As some of the theoretical techniques and analysis to be performed here for $BP(NH_2)_2$ are different from those used in our previous study of $BP(OH)_2$,[8] we will also carry out some comparative calculations on the $BP(OH)_2$ system.

2. Results and Discussion

2.1. Comparison of the Potential Energy Profiles of Double Proton Transfer

The topology of the proton-transfer process in both the S_0 and the S_1 state has been obtained and compared for $BP(NH_2)_2$ and $BP(OH)_2$. The stationary points in the S_0 state have been localized by full minimization and characterized at the DFT level of calculation, while only the zeroth-order stationary points in the S_1 state have been directly located at the TDDFT level. At present, to characterize stationary points in the TDDFT scheme, numerical second derivatives should be computed (due to the unavailability of analytic second derivatives), which is a fairly expensive calculation. Instead of using this method, relaxed potential-energy profiles for both concerted and stepwise proton transfer in $BP(NH_2)_2$ and $BP(OH)_2$ were computed, using as a reaction coordinate the distance between the hydrogen and the acceptor atoms and encompassing the full range from the minimum of the reactants to that of the products.

2.1.1. $BP(NH_2)_2$

Exploration of the electronic ground state at the DFT level led to the localization of a sole stationary point corresponding to the diamine (DA) energy minimum. This structure is characterized by a small out-of-plane torsion of the pyridyl rings (C2–C1–C6–N2 = 11.4°, see Scheme 2 for atom numbering) and pyramidalization of the NH_2 groups (H1–N3–C2–H2 = 145.9°). The calculated value of the vertical excitation energy for the $S_0 \rightarrow S_1$ transition is 3.17 eV ($\lambda = 391$ nm), which is in reasonable agreement with the experimental value (ca. 370 nm).[14] All attempts to locate energy minima corresponding to the inter-

mediate of the stepwise mechanism and the product of the double transfer, the monoimine (MI) and diimine (DI) tautomers, respectively, reverted to the DA minimum.

Our first approach to the topology of the S_1 state led to the direct optimization of the DA and DI tautomers. The DA structure presents (as observed in the S_0 state) a small out-of-plane torsion angle of the pyridyl rings (C2–C1–C6–N2 = 12.2°), while the DI structure (6.60 kcal mol^{-1} above DA) is planar.

Optimization of the proton-transfer intermediate was not straightforward. All attempts to obtain an energy minimum in the MI region by free optimization in S_1 led to a twisted conformation of the two pyridyl rings (C2–C1–C6–N2 ≈ 90°), with a relative energy 50 kcal mol^{-1} below the energy minimum of the reactants: a highly unphysical situation, where the energy of this conformation almost matches the electronic ground-state energy. Visual inspection of the molecular orbitals involved in the excitation that leads to S_1 for such a twisted structure (Figure 1) reveals a clear intramolecular charge-transfer state, described by a single-electron excitation from the HOMO (π) located on the (donor) pyridyl ring to the LUMO (π) located on the other (acceptor) ring. It has been stated in several theoretical reports[15,16] that TDDFT overstabilizes charge-transfer states. To our knowledge, few semiquantitative procedures have been proposed to correct this shortcoming of TDDFT,[17–20] but optimization turns out to be cumbersome, and the correct TDDFT description of such a state is still an unsolved problem.

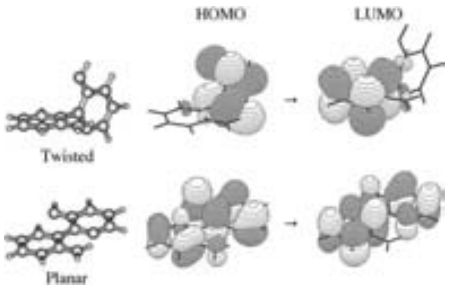

Figure 1. Probability isodensity surfaces corresponding to the molecular orbitals involved in the $S_0 \rightarrow S_1$ excitation for the twisted (ca. 90° torsion in the pyridyl rings; top) and planar (bottom) conformations of the monoimine (MI) tautomer of [2,2′-bipyridyl]-3,3′-diamine.

We have observed, however, that forcing absolute planarity (i.e. C_S symmetry) in the geometry optimizations causes the molecular orbitals involved in the description of the charge-transfer state to become delocalized over the two pyridyl rings (see comparison of molecular orbitals in Figure 1). The relative energy of the DA tautomer with respect to DI does not vary substantially when planarity is imposed, thus not appreciably modifying the endoergic nature of the double-proton-transfer process (6.60 kcal mol^{-1} in non-planar conformation instead of 6.40 kcal mol^{-1} in planar conformation). Besides, the MI structure was reoptimized at the CIS level. The result was a structure with a small out-of-plane torsion angle (C2–C1–C6–N2 = 20.5°), thus suggesting that the approximation of forcing planarity in the intermediate of the double proton transfer is acceptable.

Moreover, ESIDPT in $BP(NH_2)_2$ has been described as an ultrafast process, and considering that the reactants are almost planar, it is a reasonable approximation to consider that protons will transfer before the two pyridyl rings can undergo a twist with respect to the central C–C bond. In order to maintain homogeneity in our results, the stationary points in the S_0 and S_1 states were recalculated within C_S symmetry. In the discussion below, we restrict ourselves to the C_S (planar) symmetry group. Thus, the stationary points located are not true stationary points. However, the planar approximation allows us to estimate the energy of the hypothetical zwitterionic intermediate, MI.

Within the planar restriction, the DA tautomer in S_0 shows few differences in its relative energy and Franck–Condon excitation (3.22 eV, λ = 385 nm), and neither the MI nor the DI tautomer exists as an energy minimum. In contrast, the S_1-state topology exploration shows three different C_S "minima", corresponding to the DA, MI, and DI structures. The most stable structure is the MI tautomer, which lies only 0.95 kcal mol^{-1} below the DA minimum, whereas, as noted above, the DI tautomer lies 6.40 kcal mol^{-1} above the DA tautomer. Thus, forcing planarity does not change the endoergodicity of the double proton transfer in S_1, whereas the single proton transfer is slightly exoergic.

To complete this electronic-structure study, relaxed potential-energy profiles have been computed for both concerted and stepwise proton-transfer mechanisms in order to estimate the locations of the energy maxima for the different mechanisms. These maxima can be considered a good estimation of the transition states of the processes in S_1. Different reaction coordinates have been considered for each mechanism, as depicted in Figure 2. For the first proton-transfer process, the N4–H3 distance has been gradually modified from a DA-like conformation to a MI-like conformation. For each point of the profile, the optimal energy has been computed by allowing the structure to relax, and the energy has been represented as a function of the difference between the N4–H3 and N1–H3 distances. Analogously, for the second proton-transfer process, the N3–H2 distance has been lengthened from a MI-like conformation to a DI-like conformation. The energy of each point in the profile has been represented in terms of the difference between the N3–H2 and N2–H2 distances. For the concerted mechanism, both N4–H3 and N3–H2 distances have been modified synchronously, so that their value is the same at every point. The energy of the profile has been represented in terms of the difference between the N4–H3 and N1–H3 distances (which is equivalent to the difference between the N3–H2 and N2–H2 distances).

As seen in Figure 2, the energy barriers along the relaxed potential-energy surface for the DA→MI and MI→DI processes lie 2.96 kcal mol^{-1} and 7.97 kcal mol^{-1}, respectively, above the DA minimum. In contrast, the direct transformation DA→DI lies 11.60 kcal mol^{-1} above the DA minimum. It is likely that the

CHEMPHYSCHEM M. Moreno et al.

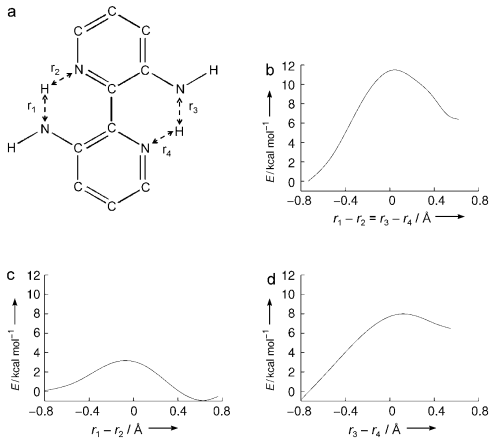

Figure 2. Relaxed potential-energy profiles in S_1 for proton transfer in [2,2′-bipyridyl]-3,3′-diamine. a) Reaction coordinates used for each profile. b) Profile for the concerted mechanism. c) Profile for the first proton transfer in the stepwise mechanism. d) Profile for the second proton transfer in the stepwise mechanism. All profiles have been referred to the diamine (DA) minimum.

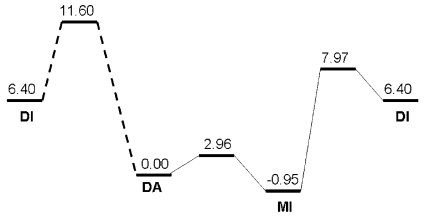

Figure 3. Relative energies [kcal mol^{-1}] of the planar structures in S_1 relevant to double proton transfer in [2,2′-bipyridyl]-3,3′-diamine, referred to the diamine (DA) minimum. Dashed lines depict the concerted transformation diamine→diimine (DA→DI). The monoimine (MI) tautomer only exists as an energy minimum when C_S symmetry is imposed.

DA→DI process goes through a second-order transition state (according to the Murrell–Laidler theorem) and is thus not in the topological reaction path.

We summarize in Figure 3 the general landscape for the proton-transfer process in the $BP(NH_2)_2$ molecule in the S_1 state. It can be seen that the most stable structure is the MI tautomer, which lies only 0.95 kcal mol^{-1} below the DA minimum, but we must note that we can only locate the MI tautomer as an energy minimum using TDDFT when planar symmetry is imposed.

2.1.2. $BP(OH)_2$

As mentioned in the Introduction, some of us previously reported a theoretical study on the ESIDPT in $BP(OH)_2$,[8] and hence the exploration of the topology in S_0 and S_1 has already been reported (see Figure 2 in ref. [8]). However, only unoptimized S_1-state energies were obtained by vertical excitation energy calculations. The TURBOMOLE package allows us to revisit and update these results with TDDFT minimizations in S_1. Results on S_0 (presented in ref. [8]) are briefly overviewed.

In contrast with the $BP(NH_2)_2$ results, three energy minima exist for $BP(OH)_2$ in S_0. The most stable structure is the dienol (DE) tautomer (Figure 4). The monoketo tautomer (MK), that is,

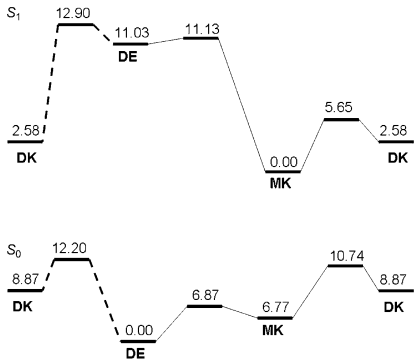

Figure 4. Relative energies [kcal mol^{-1}] of the structures in S_0 (bottom) and S_1 (top) relevant to the double proton transfer in [2,2′-bipyridyl]-3,3′-diol, referred to the monoketo (MK) minimum. Dashed lines depict the concerted transformation dienol→diketo (DE→DK). The monoketo (MK) tautomer only exists as an energy minimum in S_1 when C_S symmetry is imposed.

the intermediate in the stepwise mechanism, lies 6.77 kcal mol^{-1} above the DE structure, and the diketo (DK) tautomer (final product of the double proton transfer), lies 8.87 kcal mol^{-1} above the DE tautomer. All three optimized structures present a coplanar conformation of the two aromatic rings. The higher-order stationary points correspond to the transition-state structures for the transformations DE→MK (6.87 kcal mol^{-1}) and MK→DK (10.74 kcal mol^{-1}) and to a second-order saddle point, where a tentative transition state for the concerted mechanism should be, with an energy of 12.20 kcal mol^{-1} with respect to the DE structure. The double-proton-transfer reaction happens to be an endoergic process in S_0.

The update of our previously published results in S_1[8] with TDDFT optimizations leads to a situation very similar to that for $BP(NH_2)_2$ described in the previous section. While energy minima were directly obtained for the DE and DK tautomers (already in planar conformations), the free TDDFT optimization of the MK tautomer suffered from the same problems encountered while optimizing the MI tautomer in $BP(NH_2)_2$. For this reason, the MK tautomer has been optimized with imposed C_S symmetry.

As can be seen in the upper half of Figure 4, the TDDFT optimizations on the S_1 state unveil an exoergic profile for the double proton transfer, with important decreases in the energy barriers as compared to S_0. The MK tautomer appears to be the most stable structure, 11.03 kcal mol^{-1} below the DE mini-

mum and 2.58 kcal mol^{-1} below the DK minimum. As in BP(NH$_2$)$_2$, the energy maxima in S_1 have been located through relaxed potential-energy profiles (Figure 5). For the first and

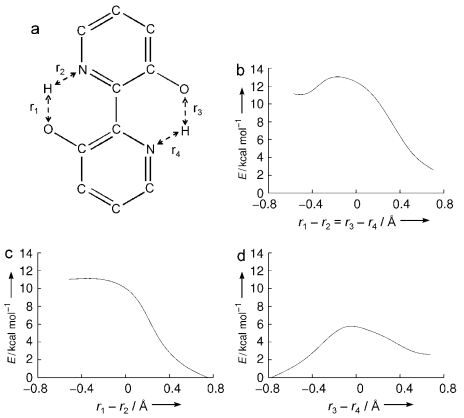

Figure 5. Relaxed potential-energy profiles in S_1 for proton transfer in [2,2′-bipyridyl]-3,3′-diol. a) Reaction coordinates used for each profile. b) Profile for the concerted mechanism. c) Profile for the first proton transfer in the stepwise mechanism. d) Profile for the second proton transfer in the stepwise mechanism. All profiles have been referred to the monoketo (MK) minimum.

second proton-transfer processes, the O2–H2 and O1–H1 distances, respectively, have been considered (see Scheme 1 for atom numbering). For the concerted mechanism, both distances have been modified synchronously so that their values were the same at every point. In all three cases, the energy has been represented in terms of the difference between the hydrogen atom–donor atom and the hydrogen atom–acceptor atom distances. The estimated transition-state structures for the DE→MK and MK→DK processes have energies of 11.13 kcal mol^{-1} and 5.65 kcal mol^{-1} respectively, relative to the MK minimum. The maximum found in the direct transformation DE→DK (12.90 kcal mol^{-1} with respect to the MK minimum) was demonstrated to be a maximum with respect to the motion of any proton in the previous exploration of S_1,[8] which supports the idea that topologically, the process is best described as stepwise in S_1, exactly as in BP(NH$_2$)$_2$.

It is remarkable that the TDDFT fully optimized results within planarity on BP(OH)$_2$ in S_1 differ only slightly from our previous results.[8] The values of the energy barriers and the relative stability of the stationary points (except for the MK tautomer) are quite similar. Taking into account these small changes in the S_1 state, the quantum dynamical simulations for the double-proton-transfer process carried out in the previous study are now validated.

To conclude this electronic-structure study, we emphasize that the results obtained for BP(OH)$_2$ and BP(NH$_2$)$_2$ reveal several notable differences. The energy profile of the double proton transfer in S_1 for BP(OH)$_2$ is clearly exoergic, with low energy barriers for both concerted and stepwise mechanisms. These results suggest, as demonstrated by experimental[11] and theoretical studies,[8] that the overall process in BP(OH)$_2$ can occur through both mechanisms, while from a purely topological point of view, the process would be described solely as stepwise.

In contrast, the ESIDPT energy profile for BP(NH$_2$)$_2$ presents an endoergic profile with higher energy barriers, which represent a great obstacle for the proton-transfer process. However, Glasbeek and co-workers have reported that a very small portion of photoexcited DA molecules evolve to products with QY = 10^{-5}.[14] According to our theoretical results, the Franck–Condon excitation energy from the DA S_0 minimum to the S_1 state leads the system only 0.22 kcal mol^{-1} below the barrier for the transfer of the first proton. This indicates that upon photoexcitation, the DA molecules can easily reach the intermediate region but not the final product region.

2.2. Nonradiative Processes in BP(NH$_2$)$_2$ and BP(OH)$_2$

As stated in the Introduction, the differences detected experimentally for the ESIDPT process in BP(OH)$_2$ and BP(NH$_2$)$_2$ are notable. Special attention should be placed on the comparison of the residual lifetimes of the tautomeric product state, which is very short in the case of BP(NH$_2$)$_2$ (ca. 1–10 ps).[14] According to Glasbeek and co-workers, this short lifetime is indicative of efficient nonradiative deactivation paths of the fluorescence state. On the basis of these results, the existence of a conical intersection between the S_1 and S_0 potential-energy surfaces has been proposed for a twisted conformation of the BP(NH$_2$)$_2$ tautomeric product.[14] Such deactivation processes have been proposed for twisted conformations of similar compounds, such as [2,2′-bipyridyl]-3-ol[21] and derivatives of biphenyl-type systems.[22]

To further explore the existence of a conical intersection, the possibility that such an approach between the S_0 and S_1 states could be located either in the reactant, intermediate, or product region should be taken into account. Considering that the TDDFT level fails to describe the charge-transfer state corresponding to the twisted conformation of the MI tautomer, we have employed the CASSCF level to explore the region where the conical intersection is expected.

As a first qualitative insight as to where the conical intersection might lie, energy profiles around the twisting C2-C1-C6-N2 dihedral angle have been obtained through CASSCF (10,10) state-average single-point calculations of the DA, MI, and DI tautomers, taking a range from 0° to 180°. All the other coordinates have been kept fixed. It is inferred from our results that the S_0 and S_1 states corresponding to the DA tautomer do not approach each other, as they are separated by an energy gap of 100 kcal mol^{-1}. At high values of the torsion coordinate (>140°), the energy rapidly increases owing to steric effects between the two amino groups. In comparison, S_0 and S_1 in the DI tautomer are closer, but the smallest energy gap between these states never drops below 40 kcal mol^{-1} (again disregarding the region over 140°). Even when considering that these CASSCF qualitative profiles have not been obtained through full optimizations, 40 kcal mol^{-1} is too large an energy

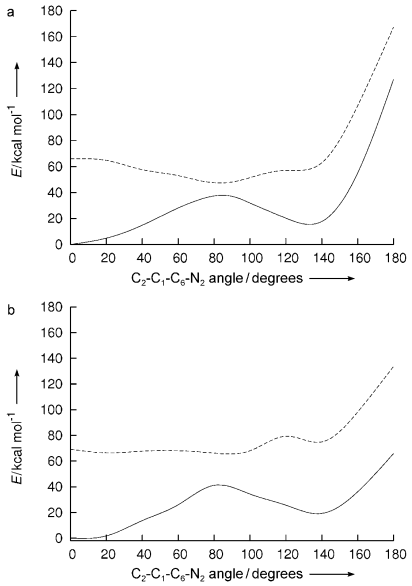

Figure 6. Ground state (——) and first singlet excited state (- - - -) CASSCF (10,10) energy profiles along the C2-C1-C6-N2 torsion angle for the intermediate tautomers of a) [2,2′-bipyridyl]-3,3′-diamine and b) [2,2′-bipyridyl]-3,3′-diol. See Schemes 1 and 2 for atom numbering.

gap between two electronic states to suggest the possibility of a conical intersection. However, the energy profile corresponding to the MI tautomer (Figure 6a) depicts a continuous approach between the two electronic states from 0° to reach a minimal difference of less than 10 kcal mol^{-1} at approximately 85°. This narrow energy gap between the electronic states is small enough, even at this qualitative level, to seriously consider the existence of a conical intersection between S_0 and S_1 in the region corresponding to a twisted conformation of the MI tautomer.

The question remains as to whether anything similar occurs in $BP(OH)_2$. Our prior study on $BP(OH)_2$[8] was focused on the dynamics of the double proton transfer and not on the possibility of the existence of a conical intersection. Because of this fact, the theoretical model of the molecule was restricted to planarity. No available experimental study suggested the possibility or relevance of a nonradiative relaxation pathway. However, in recent years the existence of conical intersections for biphenyl-type systems at twisted conformations has been proposed.[22] In order to check the possibility of the existence of a conical intersection in $BP(OH)_2$, the same procedure described above was used. Our results show that the S_0 and S_1 states corresponding to the DE tautomer do not approach each other and show a separation of approximately 110 kcal mol^{-1}. The S_0 and S_1 states in the DK tautomer are closer, but the minimal energy gap is still 60 kcal mol^{-1}. The energy profile corresponding to the MK tautomer (Figure 6b) is similar to the MI tautomer. However, the energy of the S_1 state does not approach that of the S_0 state. Rather, the energy of the S_0 state increases to reach a maximum near 85°, where the difference between the two electronic states is approximately 20 kcal mol^{-1}. At this qualitative level, it is reasonable to reject the existence of a conical intersection in the region of the DE and DK tautomers because of the wide energy gap between S_0 and S_1 (>60 kcal mol^{-1}). In contrast, the energy gap found in the MK tautomer, which is 10 kcal mol^{-1} larger than that found in the MI tautomer, casts some doubts about the existence of a conical intersection in this case. A more accurate electronic study will be necessary to get a better description of the S_0 and S_1 states at the twisted conformation of the MK tautomer.

There is no definite answer as to where exactly these conical intersections lie and to what role they play in the global photochemical process. More accurate electronic calculations at the CASSCF level and a dynamical treatment of these nonadiabatic processes will be necessary to understand the actual photochemistry of $BP(NH_2)_2$ and $BP(OH)_2$. Work devoted to this aim is currently in progress in our laboratory.

3. Conclusions

In this section we discuss our model for the photochemistry of $BP(NH_2)_2$ and $BP(OH)_2$ (Figure 7) as inferred from our prior results for the ground and first singlet excited electronic states. A plausible explanation of the experimental results observed by Glasbeek and co-workers,[14] placing a special stress on the very low quantum yield in $BP(NH_2)_2$, will be also presented. We highlight that dynamical effects can be [and, in fact, for $BP(OH)_2$ have been shown to be] critical to explain the complete photophysics of the system. Herein, we are making an "educated guess" on the photochemistry solely on the basis of the topological data. This is by no means complete. For instance, without the dynamics, the concerted reaction channel in $BP(OH)_2$ could not be understood.

After vertical excitation of the neutral form DA (point *a* in Figure 7a) following the Franck–Condon principle, the excited DA lies less than 1 kcal mol^{-1} below the energy barrier corresponding to the first proton-transfer process. Thus, it is highly likely that the first proton transfer, perhaps assisted by proton tunneling, will occur in competition with vibrational relaxation to the excited DA minimum in S_1. Once the excited MI region has been accessed, the step leading to the DI product is endoergic (3.66 kcal mol^{-1} above the Franck–Condon excitation) and has a high energy barrier (5.23 kcal mol^{-1} above the Franck–Condon excitation). Hence, it is predicted that only a very small fraction of molecules will make their way to the excited DI region. At any rate, whatever small fraction of systems does make its way to the DI region, it will do so in a much longer time than 100 fs. There are several reasons for this conclusion: first, the concerted reaction pathway presents a prohibitively large energy barrier; second, even though the stepwise mechanism is energetically more favorable, in the second step (MI→DI) competition with IVR would occur. It has been shown previously that IVR can greatly delay these transfers.[8] Besides, the absence of a minimum in the DI region of S_0

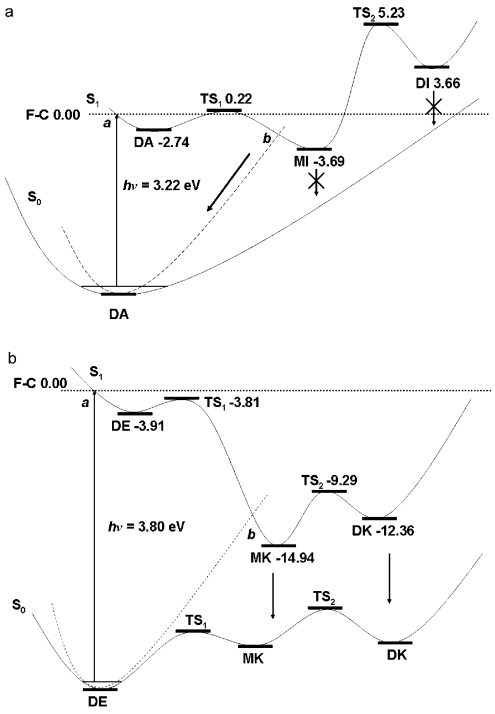

Figure 7. Model for the photochemistry of a) [2,2′-bipyridyl]-3,3′-diamine and b) [2,2′-bipyridyl]-3,3′-diol, both in C_s symmetry, as inferred from our quantum chemical calculations. All relative energies (in kcal mol^{-1}) in S_1 are referred to the Frank–Condon excitation energy of the reactant tautomer in S_0. Marked point *a* represents the energy arrival of the Franck–Condon excitation, and point *b* represents the tentative location of the possible conical intersection between S_1 and S_0.

would make radiative relaxation by fluorescent decay of the excited DI a very unlikely process.

Our quantum chemical calculations suggest that the electronically excited MI, after vibrational relaxation, can undergo a twisting of the two pyridyl rings. When this coordinate nearly reaches perpendicularity, a conical intersection between S_1 and S_0 occurs (point *b* in Figure 7a). The MI molecules can then decay nonradiatively to S_0 along a path which mainly includes two coordinates: 1) the twisting back of the two pyridyl rings to planarity, and 2) the back-proton-transfer coordinate. This path leads from the excited MI minimum in S_1 to the DA minimum in S_0. Hence, the fast decay of the emission bands I and II in $BP(NH_2)_2$ should correspond to a species structurally analogous to the MI tautomer, and not to the DI tautomer, as suggested by Glasbeek and co-workers.[14]

In the discussion below, we try to justify the experimentally measured decay times for bands I and II. When the excited DA systems are created after photonic excitation, they evolve very rapidly through the stepwise reaction channel (first step) to the excited MI because of the minuscule energy barrier that separates DA and MI. In these conditions, this process can occur within a few tens of femtoseconds.[8] Once in the MI region, the system can evolve further by undergoing a twist of the two rings and transfer to S_0 through the conical intersection. This process could be responsible of the measured decay time of approximately 250 fs in band II. These systems can relax by fluorescence to S_0 only very slowly, given the lack of a minimum for MI in S_0. Globally, this would be in agreement with the very low QY of band II.[14]

What can be said for band I? The systems arriving at MI from DA in S_1 come with excess energy, and some of them will not relax to the bottom of the MI minimum (and cross to S_0 through the conical intersection). Rather, being prevented from reaching the final product DI owing to their lack of energy, they will bounce back, reverting to the DA region, where they can start the whole process again. Given that the usual fluorescence from S_1 to S_0 has a rate constant in the order of 10^9 s^{-1},[23] one concludes that excited DA depopulates mainly through the conical intersection in the MI region, a much faster process than DA (S_1)→DA (S_0) fluorescence. This situation would also explain the decay time for band I.

According to our previous (and now updated) quantum chemical calculations on $BP(OH)_2$, the photochemistry of $BP(OH)_2$ is somewhat different than that just presented for $BP(NH_2)_2$ because of the exoergic nature of the double proton transfer in S_1 and the existence of an energy minimum for the MK and DK tautomers in S_0.

After vertical excitation of the neutral form DE (3.80 eV, $\lambda =$ 326 nm), the excited DE lies 14.94 kcal mol^{-1} and 12.36 kcal mol^{-1} above the excited MK and DK minima, respectively (Figure 7b). As we showed in our previous theoretical report,[8] it is highly likely that a part of the excited DE will evolve directly to the excited DK region through a concerted double-proton-transfer mechanism that occurs simultaneously with a stepwise mechanism. Once in the excited DK region, in contrast to the $BP(NH_2)_2$ system, the presence of a minimum in the DK region of S_0 makes radiative relaxation by fluorescent decay of the excited DK a quite feasible process. Another fraction of the initially excited DE will make its way to the DK region through a stepwise mechanism. In that trip, it passes the MK region, where a conical intersection could be present. Additionally, fluorescence from the MK intermediate is not so difficult in this case (there is a corresponding MK minimum in S_0), so that relaxation through a conical intersection, if present, will compete with this additional relaxation process and with the second proton transfer that is now also feasible.

Computational Methods

Electronic density functional based methods have been used to explore the topology of the ground (S_0) and first $\pi\pi^*$ singlet excited (S_1) electronic states. Density functional theory (DFT) and time-dependent DFT (TDDFT)[24] optimizations have been performed for the S_0 and S_1 states, respectively. TDDFT has been succesfully used to study other ESIPT systems.[8,25–27] The three-parameter hybrid functional of Becke with the correlation functional of Lee, Yang

and Parr (B3LYP)[28,29] has been chosen. The TURBOMOLE program (Version 5.4),[30,31] which implements analytical gradients at the TDDFT level, has been used to perform the TDDFT calculations.

Multireference complete active space self-consistent field method (CASSCF)[32] calculations have been carried out with the MOLCAS program (Version 6.4).[33] The electronic energy of S_0 and S_1 states has been obtained using a state average with equal weights for both states with an active space of ten electrons and ten molecular orbitals, which includes the five highest occupied and the five lowest unoccupied molecular orbitals. This active space is probably not large enough to correctly describe the whole potential energy surface (i.e. the DA, MI, and DI regions), so that it has just been used to analyze the presence of conical intersections between the S_0 and S_1 states. A larger active space would be necessary to compare the different regions of the potential-energy surface.

In all cases, to obtain a good description of the proton- and charge-transfer processes on excited states, the 6-31G(d,p)[34,35] basis has been used for the hydrogen and carbon atoms, while additional diffuse functions [6-31G+(d,p) basis][34,35] have been added to the oxygen and nitrogen atoms.

Acknowledgements

The authors are grateful for financial support from the "Ministerio de Educación y Ciencia" and the "Fondo Europeo de Desarrollo Regional" through project CTQ2005-07115/BQU, and from the "Generalitat de Catalunya" (2005SGR00400). Use of computational facilities at the "Centre de Supercomputació de Catalunya" is also acknowledged.

Keywords: density functional calculations · excited states · femtochemistry · proton transfer · reaction mechanisms

[1] H. Bouas-Laurent, H. Durr, *Pure Appl. Chem.* **2001**, *73*, 639–665.
[2] P. F. Barbara, L. E. Brus, P. M. Rentzepis, *J. Am. Chem. Soc.* **1980**, *102*, 5631–5635.
[3] P. T. Chou, Y. C. Chen, W. S. Yu, Y. H. Chou, C. Y. Wei, Y. M. Cheng, *J. Phys. Chem. A* **2001**, *105*, 1731–1740.
[4] E. T. J. Nibbering, T. Elsaesser, *Chem. Rev.* **2004**, *104*, 1887–1914.
[5] D. A. Parthenopoulos, D. McMorrow, M. Kasha, *J. Phys. Chem.* **1991**, *95*, 2668–2674.
[6] S. Moller, K. B. Andersen, J. Spanget-Larsen, J. Waluk, *Chem. Phys. Lett.* **1998**, *291*, 51–56.
[7] R. C. Haddon, F. H. Stillinger in *Molecular Electronic Devices*, Marcel Dekker, New York, **1987**.
[8] R. Gelabert, M. Moreno, J. M. Lluch, *ChemPhysChem* **2004**, *5*, 1372–1378.
[9] H. Zhang, P. Van der Meulen, M. Glasbeek, *Chem. Phys. Lett.* **1996**, *253*, 97–102.
[10] D. Marks, H. Zhang, M. Glasbeek, P. Borowicz, A. Grabowska, *Chem. Phys. Lett.* **1997**, *275*, 370–376.
[11] P. Toele, H. Zhang, M. Glasbeek, *J. Phys. Chem. A* **2002**, *106*, 3651–3658.
[12] D. Marks, P. Prosposito, H. Zhang, M. Glasbeek, *Chem. Phys. Lett.* **1998**, *289*, 535–540.
[13] P. Prosposito, D. Marks, H. Zhang, M. Glasbeek, *J. Phys. Chem. A* **1998**, *102*, 8894–8902.
[14] P. Toele, M. Glasbeek, *Chem. Phys. Lett.* **2005**, *407*, 487–492.
[15] L. Serrano-Andrés, M. Merchán, *J. Mol. Struct. THEOCHEM*, **2005**, *729*, 99–108.
[16] R. Gelabert, M. Moreno, J. M. Lluch, *J. Phys. Chem. A* **2006**, *110*, 1145–1151.
[17] A. Dreuw, G. R. Fleming, M. Head-Gordon, *J. Phys. Chem. B* **2003**, *107*, 6500–6503.
[18] Y. Tawada, T. Tsuneda, S. Yanagisawa, T. Yanai, K. Hirao, *J. Chem. Phys.* **2004**, *120*, 8425–8433.
[19] M. Chiba, T. Tsuneda, K. Hirao, *J. Chem. Phys.* **2006**, *124*, 144106.
[20] J. Neugebauer, O. Gritsenko, E. J. Baerends, *J. Chem. Phys.* **2006**, *124*, 214102.
[21] K. Tokumura, O. Oyama, H. Mukaihata, M. Itoh, *J. Phys. Chem. A* **1997**, *101*, 1419–1421.
[22] W. Rettig, V. Kharlanov, M. Maus, *Chem. Phys. Lett.* **2000**, *318*, 173–180.
[23] J. Michl, V. Bonacić-Koutecký, *Electronic Aspects of Organic Photochemistry*, Wiley, New York, **1990**.
[24] R. Bauernschmitt, R. Ahlrichs, *Chem. Phys. Lett.* **1996**, *256*, 454–464.
[25] A. L. Sobolewski, W. Domcke, *Phys. Chem. Chem. Phys.* **1999**, *1*, 3065–3072.
[26] A. J. A. Aquino, H. Lischka, C. Hattig, *J. Phys. Chem. A* **2005**, *109*, 3201–3208.
[27] J. M. Ortiz-Sánchez, R. Gelabert, M. Moreno, J. M. Lluch, *J. Phys. Chem. A* **2006**, *110*, 4649–4656.
[28] A. D. Becke, *J. Chem. Phys.* **1993**, *98*, 5648–5652.
[29] C. T. Lee, W. T. Yang, R. G. Parr, *Phys. Rev. B* **1988**, *37*, 785–789.
[30] F. Furche, R. Ahlrichs, *J. Chem. Phys.* **2002**, *117*, 7433–7447.
[31] R. Ahlrichs, M. Bär, M. Haser, H. Horn, C. Kolmel, *Chem. Phys. Lett.* **1989**, *162*, 165–169.
[32] K. Andersson, P.-Å. Malmqvist, B. O. Roos, *J. Chem. Phys.* **1992**, *96*, 1218–1226.
[33] G. Karlström, R. Lindh, P.-Å. Malmqvist, B. O. Roos, U. Ryde, V. Veryazov, P.-O. Widmark, M. Cossi, B. Schimmelpfennig, P. Neogrády, L. Seijo, *Comp. Mat. Sci.* **2003**, *28*, 222–239.
[34] P. C. Hariharan, J. A. Pople, *Theor. Chim. Acta* **1973**, *28*, 213–222.
[35] M. M. Francl, W. J. Pietro, W. J. Hehre, J. S. Binkley, M. S. Gordon, D. J. Defrees, J. A. Pople, *J. Chem. Phys.* **1982**, *77*, 3654–3665.

Received: December 20, 2006
Revised: March 15, 2007
Published online on April 30, 2007

Paper V

J. M. Ortiz-Sánchez, R. Gelabert, M. Moreno and J. M. Lluch. Study of the photochemical properties and conical intersections of [2,2'-bipyridyl]-3-amine-3'-ol. *ChemPhysChem* 9(14): 2068 – 2076, 2008.

CHEMPHYSCHEM

DOI: 10.1002/cphc.200800322

Study of the Photochemical Properties and Conical Intersections of [2,2′-Bipyridyl]-3-amine-3′-ol

Juan Manuel Ortiz-Sánchez, Ricard Gelabert, Miquel Moreno,* and José M. Lluch[a]

The two isoelectronic bipyridyl derivatives [2,2′-bipyridyl]-3,3′-diamine and [2,2′-bipyridyl]-3,3′-diol are experimentally known to undergo very different excited-state double-proton-transfer processes, which result in fluorescence quantum yields that differ by four orders of magnitude. In a previous study, these differences were explained from a theoretical point of view, because of topographical features in the potential energy surface and the presence of conical intersections (CIs). Here, we analyze the photochemical properties of a new molecule, [2,2′-bipyridyl]-3-amine-3′-ol [BP(OH)(NH$_2$)], which is, in fact, a hybrid of the former two. Our density functional theory (DFT), time-dependent DFT (TDDFT), and complete active space self-consistent field (CASSCF) calculations indicate that the double-proton-transfer process in the ground and first singlet $\pi\rightarrow\pi^*$ excited state in BP(OH)(NH$_2$) presents features that are between those of their "parents". The presence of two CIs and the role they may play in the actual photochemistry of BP(OH)(NH$_2$) and other bipyridyl derivatives are also discussed.

1. Introduction

Organic molecules with acidic and basic functional groups connected by intramolecular hydrogen bonds are among the best-suited systems to undergo proton (or hydrogen) transfer upon photoexcitation. The advent of modern experimental techniques, such as time-resolved laser spectroscopy (with resolutions of a few femtoseconds) or coherent transient data, has provided a general picture of these excited-state intramolecular proton-transfer (ESIPT) processes as ultrafast and reversible, the whole cycle being completed in less than a few picoseconds.[1–4] These properties lead to very interesting potential applications and some well-known systems, such as derivatives of salicylic acid (SA) and the 2-(2′-hydroxyphenyl)benzazole (HBX) family, have for long been studied as photostabilizers, a very common technique used for the protection of organic polymers against photodegradation by UV sunlight.[5–10] In photostabilizers the ultrafast ESIPT process is followed by fluorescent or radiationless decay of the excited phototautomer leading to a very unstable (in the ground state) structure that quickly reverts to the original species, in this way closing the photocycle that is again ready to start the process. More recently, interest in these molecules has reemerged because of their potential use as optoelectronic devices, such as optical memories or optical switches.[11] Photoinduced switching of fluorescent properties is one of the most attractive concepts for the realization of a nondestructive readout system.[12–14] To have a good candidate for a photomemory it is necessary to obtain a stable photoproduct (most likely in the ground state) that will only revert to the original species through a new photoexcitation process, now at a quite different wavelength. The whole process that would be involved in an ideal optical photoswitch is depicted in Scheme 1.

The use of molecules that undergo a single ESIPT, such as the HBX and SA derivatives cited above, as optical memories has been considered in some detail[15] but usually the phototautomer relaxes to a structure in the ground state that is not stable, automatically reverting to the original species. Although there have been some systems specially designed to overcome this inconvenience (let us cite here a cleverly designed molecule, 7-hydroxy-(8-oxazine-2-one)-quinoline, recently proposed and theoretically studied by Sobolewski[16]), the more successful approaches to reversible single-molecule photoswitching

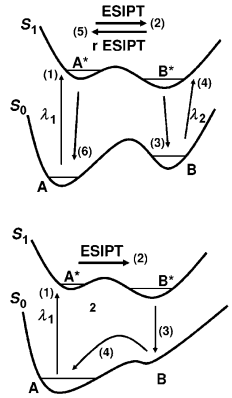

Scheme 1. Schematic representation of the processes involved in the photocycle of an ideal optical switch (top) and a photostabilizer (bottom). ESIPT and rESIPT refer to the direct and reverse excited-state intramolecular proton-transfer processes, respectively, while λ_1 and λ_2 refer to the wavelengths that trigger ESIPT and rESIPT, respectively. The numbering of events follows the sequential order of the photocycle steps.

[a] J. M. Ortiz-Sánchez, Dr. R. Gelabert, Dr. M. Moreno, Prof. J. M. Lluch
Departament de Química
Universitat Autònoma de Barcelona
08193 Bellaterra, Barcelona (Spain)
Fax: (+34) 93-581-2920
E-mail: mmf@qf.uab.es

have been obtained through mutations of large biochemical molecules, such as green fluorescent protein (GFP). In contrast to the single ESIPT process present in HBX, SA, and other related systems, GFP-like systems may undergo two or more ESIPT processes.[17,18] This opens the door to several reaction paths so that the possibility of obtaining a stable structure upon photoexcitation at a given wavelength largely increases. In fact, a GFP-like fluorescent protein called Dronpa has recently been proposed as a very promising candidate for a molecular photomemory.[19]

At a more modest size, there are also some organic molecules that may be subject to more than one ESIPT process. One of the simplest, and yet very interesting, among these systems is [2,2′-bipyridyl]-3,3′-diol ($BP(OH)_2$) which has been extensively studied from both the experimental[20–25] and theoretical[26] sides. From these studies it is now well established that the double ESIPT in $BP(OH)_2$ is a branched mechanism that consists of a concerted reaction channel where both protons simultaneously transfer, and a stepwise channel where one proton transfers first and the other follows upon completion of the first step. The characteristic times of both concerted and stepwise mechanisms are very different. The concerted channel and the first step of the stepwise mechanism are completed in about 100 fs, while the second proton-transfer step of the stepwise mechanism needs a much longer time of 10 ps to complete. Later on, a molecule quite similar to $BP(OH)_2$ with the two hydroxyl groups substituted by amino groups was studied by using femtosecond fluorescence upconversion techniques.[27] This new molecule, called [2,2′-bipyridyl]-3,3′-diamine ($BP(NH_2)_2$), has also been the subject of a recent careful quantum-electronic study.[28] Both experimental and theoretical works reveal quite striking differences between the two isoelectronic $BP(OH)_2$ and $BP(NH_2)_2$ species, as the quantum yield for $BP(NH_2)_2$ is four orders of magnitude lower and in this case there is no experimental evidence of the stepwise mechanism, though the whole process is still branched with different time constants that are now both on the order of femtoseconds. These differences are theoretically explained by the quite different energy profiles for the two proton-transfer processes in the ground (S_0) and first excited singlet (S_1) electronic states.[28] While for $BP(OH)_2$ the two proton-transfer processes are energetically feasible in S_1 and the two tautomeric species are also stable structures in S_0, for $BP(NH_2)_2$ there are no other stable structures in S_0 besides the original structure and the product of the double-proton transfer in S_1 is higher in energy than the point originally accessed upon photoexcitation. These topographical differences, along with the presence of a conical intersection (CI) between S_0 and S_1 in the region of the single-proton transfer, may explain the observed differences between both molecules.

Herein, we propose a new molecule, also isoelectronic with $BP(OH)_2$ and $BP(NH_2)_2$, which is, in fact, a hybrid of both and possesses one hydroxyl and one amino group. The molecular structure of this molecule, called [2,2′-bipyridyl]-3-amine-3′-ol [$BP(OH)(NH_2)$], along with those of their "parents" $BP(OH)_2$ and $BP(NH_2)_2$, are shown in Scheme 2. The interest of this molecule, synthesized some years ago,[29] lies in the fact that it could

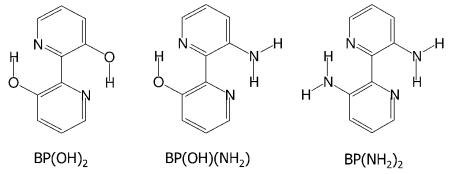

Scheme 2. Molecular structures of [2,2′-bipyridyl]-3,3′-diol (left), [2,2′-bipyridyl]-3-amine-3′-ol (center), and [2,2′-bipyridyl]-3,3′-diamine (right).

have properties that are intermediate between the quite disparate ones of $BP(OH)_2$ and $BP(NH_2)_2$. Besides, now there are two different asymmetric single-proton-transfer processes but just one double-proton-transfer product. Therefore there are, at least, three feasible ESIPT channels, a fact that increases the probability of obtaining an energy profile for the whole process compatible with the use of this molecule as a molecular photoswitch.

2. Results and Discussion

As explained in the Introduction, the asymmetric structure of the $BP(OH)(NH_2)$ molecule leads to two different single-proton-transfer processes, thus involving two single-proton-transferred intermediates, as depicted in Scheme 3. To distinguish between these different chemical species, we adopt here a nomenclature similar to that used in our previous publication on bipyridyl derivatives,[28] which is based on the nature of the functional groups presented in each molecule. In that sense, the reactant and product of the double-proton transfer are renamed as enol-amine (EA) and keto-imine (KI), respectively, whereas the intermediates corresponding to single-proton transfers are respectively renamed as enol-imine (EI) and keto-amine (KA). As a matter of fact, these two intermediates are a superposition of several canonical valence-bond structures,

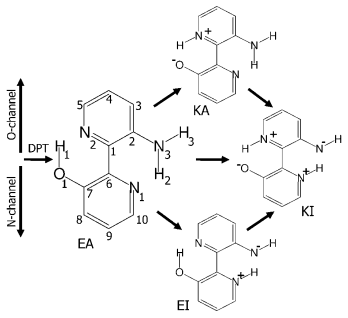

Scheme 3. Concerted and stepwise mechanisms for double-proton transfer in $BP(OH)(NH_2)$, including the nomenclature and atom numbering used in this work. The charges shown are formal charges in the context of a Lewis structure and do not necessarily correspond to the actual charge distribution. DPT denotes the double-proton-transfer channel.

with participation of an enol-imine and a keto-amine structure, respectively. Let us also use O-channel and N-channel to refer to the mechanisms that start with O-H···H transfer and N-H···H transfer, respectively. This nomenclature (along with the atom numbering used herein) is also used in Scheme 3. As is customary, we will use an asterisk to denote structures located in the first singlet excited electronic state S_1.

The topographical features of the proton-transfer process in both S_0 and S_1 states were obtained for the BP(OH)(NH_2) molecule and have also been compared to the results previously obtained for $BP(OH)_2$ and $BP(NH_2)_2$.[26,28] All the stationary points in S_0 were localized by full minimization and characterized at the DFT level of calculation, while only the zero-order stationary points in the S_1 state were directly located at the time-dependent DFT (TDDFT) level. At present, the characterization of stationary points within the TDDFT scheme requires computation of the numerical second derivatives (due to the unavailability of analytic second derivatives), which is a fairly expensive calculation. Thus, we have foregone these calculations. To approximately localize the transition-state structures for the proton-transfer processes in S_1, relaxed potential energy profiles for both concerted and stepwise proton transfer were computed using as a reaction coordinate the difference between distances for the proton and donor and acceptor atoms, thus encompassing the full range from a minimum of reactants to that of products.

The exploration of the electronic ground state at the DFT level led to the localization of two energy minima corresponding to the reactant (EA) and product (KI) tautomers. The whole double-proton-transfer process happens to be endoergic in S_0 with an energy difference between EA and KI of 18.19 kcal mol^{-1}. These optimized structures contain a molecular plane of symmetry (i.e. they belong to the C_S group of symmetry), but the frequency analysis reveals that the planar EA minimum presents an imaginary frequency (133 i cm^{-1}). Optimization of this structure brings forth the pyramidalization of the NH_2 group and leads to a structure only 0.04 kcal mol^{-1} below the former. In view of this, in the discussion below we restrict ourselves to the C_S (planar) symmetry group. For the reactant molecule (EA) our predicted value of the vertical excitation energy for the $S_0 \rightarrow S_1$ ($\pi \rightarrow \pi^*$) transition is 3.59 eV ($\lambda = 346$ nm). We remark that this result is, as could be somehow expected, intermediate between the values previously calculated using the same methodology for $BP(OH)_2$ (3.80 eV) and $BP(NH_2)_2$ (3.22 eV).[28]

All attempts to locate an energy minimum corresponding to the two intermediates of the stepwise mechanisms in S_0 (EI and KA) reverted to the original EA minimum. This situation is intermediate between the ones observed for $BP(OH)_2$ (where all the possible energy minima were located) and $BP(NH_2)_2$ (where only the reactant minimum was present). Thus, the transition-state structure linking the EA and KI structures corresponds to a concerted double-proton-transfer process. This structure (located 18.22 kcal mol^{-1} above the EA energy minimum) presents an imaginary frequency (777 i cm^{-1}) that corresponds to the N_3···H_2···N_1 proton-transfer process (see atom numeration in Scheme 3). The same structure presents a large real frequency of 2762 cm^{-1}, which corresponds to the H_1–N_2 stretching movement. An H_1–N_2 bond is already formed at the time the H_2 proton is being transferred from N_3 to N_1; thus the transition-state structure linking the EA and KI structures corresponds to a concerted but very asynchronous double-proton-transfer process.

Our first approach to the topology of the S_1 state led to the direct optimization of the EA* and KI* tautomers, both in C_S symmetry. In this electronic excited state, the double-proton transfer becomes a slightly exoergic process with an energy difference between KI* and EA* of 2.51 kcal mol^{-1}. In contrast to the results obtained for S_0, two energy minima were also located for the intermediates corresponding to both single-proton-transfer channels (EI* and KA* tautomers). The intermediate of the N-channel (EI*), also belonging to a C_S symmetry, is located 2.2 kcal mol^{-1} below EA* and 0.31 kcal mol^{-1} above KI*. However, the optimization of the intermediate of the O-channel (KA*) was not so straightforward. Our first attempt to locate an energy minimum in the KA* region by free optimization in S_1 led to a twisted conformation of the two pyridyl rings ($\angle C_7$-C_6-C_1-$N_2 = 86.5^\circ$) with a relative energy 23.19 kcal mol^{-1} below the energy minimum of the reactants. The situation is similar to that observed in our previous work on the $BP(NH_2)_2$ system, in which a strongly twisted intermediate also appeared by free optimization. However, in that case the intermediate was not located as the energy of the excited state matched that of the ground state. For $BP(NH_2)_2$ this ultimately led to the localization of a CI between the ground and first singlet excited electronic states.

According to several authors,[27,30,31] the existence of a twisted conformation on bipyridyl- or biphenyl-type systems indicates the presence of CIs which lead to efficient nonradiative deactivation paths of the fluorescent state. Later on we will also discuss this point for BP(OH)(NH_2). These results come from the fact that the localized HOMO→LUMO transition implies a charge-transfer state which might be overstabilized by the TDDFT method, as stated in several theoretical reports.[32–41] Recently, the charge-transfer problem when molecules are twisted has been discussed.[42] As observed in a previous work,[28] forcing absolute planarity (i.e., C_S symmetry) in the geometry optimization causes the molecular orbitals involved in the description of the charge-transfer state to become delocalized over the two pyridyl rings, thus leading to a C_S restricted planar stationary point which is no longer of the charge-transfer type. In the present case, forcing absolute planarity on the KA* intermediate leads to a stationary point 7.43 kcal mol^{-1} below the reactants.

To complete this electronic structure study on S_1, relaxed potential energy profiles were computed for the two stepwise proton-transfer mechanisms to estimate the locations of the transition-state structures for the different single-H transfers. Planarity of the molecule was imposed in these calculations. This is not a problem for the N-channel as the EI* intermediate is planar, but the planar KA* intermediate (C_S) is the end point for the O-channel and not the more stable C_1 symmetry, which is believed to be artificially stabilized by TDDFT as discussed above. This planar KA* is also used to build up the path for

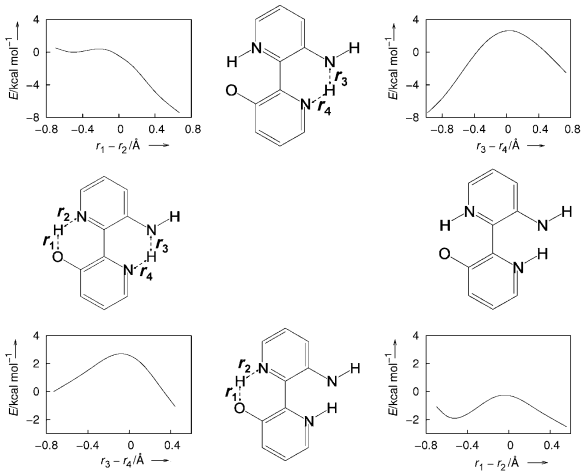

Figure 1. Relaxed potential energy profiles in S_1 for the two stepwise proton-transfer mechanisms in BP(OH)(NH_2). All energies (in kcal mol^{-1}) are relative to the EA* minimum. Distance differences are expressed in Å.

the second H-atom transfer that finally obtains the KI* minima. The maxima along these reaction paths can be considered a good estimation of the transition-state structures of the different single-proton-transfer processes in S_1, as represented in Figure 1 (where the four different reaction coordinates considered are also displayed). An estimation of the transition-state structure for the concerted double-transfer process was also performed as follows: a series of geometries were generated through a linear interpolation between the EA* and KI* minima structures, in mass-weighted Cartesian units. For each geometry, a TDDFT single point calculation was performed and the highest energetic point along the energy profile was optimized fixing the four distances. As the energy difference between the optimized geometry and the point along the reaction coordinate is less than 2 kcal mol^{-1}, it can be considered as a good candidate of the transition-state structure of the concerted mechanism. It lies 13.51 kcal mol^{-1} above the EA* minimum.

We summarize in Figure 2 the general landscape for the proton-transfer process in the BP(OH)(NH_2) molecule in both the S_0 and S_1 states. Energies (in kcal mol^{-1}) are given relative to the minimum-energy structure in S_0 (EA) and the Frank–Condon vertical excitation in S_1. Lines connecting the different stationary points correspond to the computed reaction paths that, in S_1, were also used to find the transition states (TS*) whose energy is also indicated (Figure 2). As planarity of the molecule is imposed, the C_1 KA* minimum does not appear. Later we will discuss the role of this and other nonplanar structures in the photochemistry of BP(OH)(NH_2). The dashed lines on the left of the S_1 profile show the results of the concerted mechanism (as discussed above). The larger energy barrier of the concerted path as compared with those of the single-H transfer processes precludes the involvement of such a mechanism in the excited state. In fact, the "transition state" of the double-proton path is most likely a second-order saddle point (the second imaginary frequency being one that breaks the concertedness). We highlight the complexity of the profile in the excited electronic state as compared with the much simpler one (just two minima linked by transition-state structures) of S_0.

A careful look at the two stepwise mechanisms reveals that from the initial EA* minimum the O-channel is energetically favored. However, the N-channel involves an energy barrier just 2.33 kcal mol^{-1} higher. If we now take into consideration the fact that the Franck–Condon (FC) or vertical excitation energy (i.e., the energy of EA* with the geometry optimized for the ground state) puts the system above the energy of both TS*(EA*→EI*) and TS*(EA*→KA*), we conclude that both channels are open from an energetic point of view. If the reaction takes place along the N-channel it may well end up at the KI* final product as this is the more stable

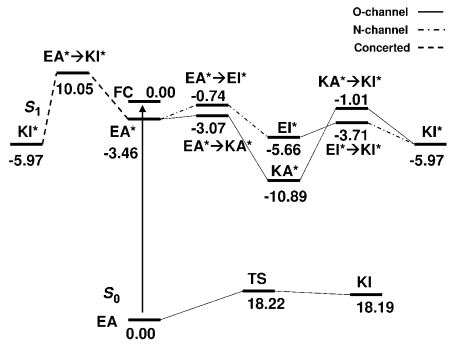

Figure 2. Relative energies (in kcal mol^{-1}) of the planar structures in S_0 (bottom) and S_1 (top) relevant to the double-proton transfer in BP(OH)(NH_2), referred to the EA minimum in S_0 and to the FC excitation energy in S_1.

structure along the path. Conversely, if the reaction starts along the O-channel the product of the first singlet proton transfer is now the most stable species although, again, the energy of the FC excitation is enough to surpass the second transition-state structure so that the KI* product is also accessible.

To obtain more information about the possible photochemistry of BP(OH)(NH_2) from our topographical study, let us com-

Table 1. Geometrical distances,[a] electronic densities,[b] and Laplacians[c] at the bond critical points of the selected bonds. See Scheme 3 for atomic numeration.

	O_1–H_1			N_2–H_1			N_1–H_2			N_3–H_2		
	r	ρ	$\nabla^2\rho$	r	ρ	$\nabla^2\rho$	r	ρ	$\nabla^2\rho$	r	ρ	$\nabla^2\rho$
EA*	1.03	0.29	−1.46	1.55	0.078	0.19	1.77	0.047	0.12	1.04	0.31	−1.65
EI*	1.02	0.31	−1.63	1.62	0.067	0.12	1.05	0.30	−1.61	1.74	0.051	0.11
KA*	1.71	0.050	0.13	1.04	0.31	−1.70	1.99	0.030	0.083	1.01	0.34	−1.82
KI*	1.61	0.062	0.16	1.05	0.30	−1.61	1.04	0.32	−1.67	1.78	0.046	0.11

[a] r in Å. [b] ρ in eÅ^{-3}. [c] $\nabla^2\rho$ in eÅ^{-5}.

pare the evolution of the intramolecular hydrogen bonds along the different stationary points located for both proton-transfer channels. Table 1 presents the distances between the two transferring hydrogen atoms and the corresponding acceptor/donor atoms for the reactants and products and the two planar single-proton intermediates. Along with the distances, Table 1 also presents the value of the charge density and its Laplacian at the bond critical points located for both the covalent X–H bond and the hydrogen bond X···H. As expected the Laplacian of the covalent bonds is always negative, which indicates concentration of charge in that region, whereas the hydrogen bonds have a positive value of the Laplacian that corresponds to a charge depletion.[43]

As expected, there is a direct relationship between the X···H distances and the electron density at the bond critical point so that we can discuss both values together. For all the stationary points analyzed the covalent X–H distances are almost equal (with differences no larger than 0.04 Å) and so are the electronic densities at the bond critical points. As for the hydrogen bonds, they present slightly more disperse values. Even so, the differences are quite small between the reactant EA*, product KI*, and intermediate EI* structures. The more dissimilar results appear in the planar KA* intermediate as it shows clearly weaker hydrogen bonds. In fact, the long distance (1.99 Å) between N_1 and H_2 casts doubts about the existence of a hydrogen bond there. However, the localization of a bond critical point and the charge analysis confirm that this bond still exists though quite weak. In any case, the weaker hydrogen bonds for the KA* intermediate fit well with the result, discussed above, that in this case the lowest-energy KA* structure is not planar (C_S) but one where both aromatic rings are twisted almost 90°. This structure does not possess any intramolecular hydrogen bonds, as the O_1···H_1 and N_1···H_2 distances are now quite large (3.16 and 2.86 Å, respectively) so that no bond critical points are found. Even if the low energy of this structure is somehow unphysical because of the problems of the TDDFT method in dealing with charge-transfer excited states, as discussed above, it is interesting to further analyze what electronic factors are coming into play to make the twisted structure more stable and why a similar effect is not at first obtained for the equivalent EI* intermediate.

Figure 3 depicts several energy profiles that were obtained for the two single-proton intermediates through internal rotation of the two pyridyl rings without reoptimization of the geometries. Figure 3a shows the energy profile when the KA* (C_1) minimum is rotated. Because of the loss of symmetry of the original structure, the energy profile is not symmetric on both sides of the 0° (planar) structure. Also, this planar structure is a maximum of energy in this profile, though this result is somewhat biased as the fixed geometry of the twisted intermediate is used along the whole energy profile. By taking as a starting structure the KA* (C_S) geometry we obtain the energy

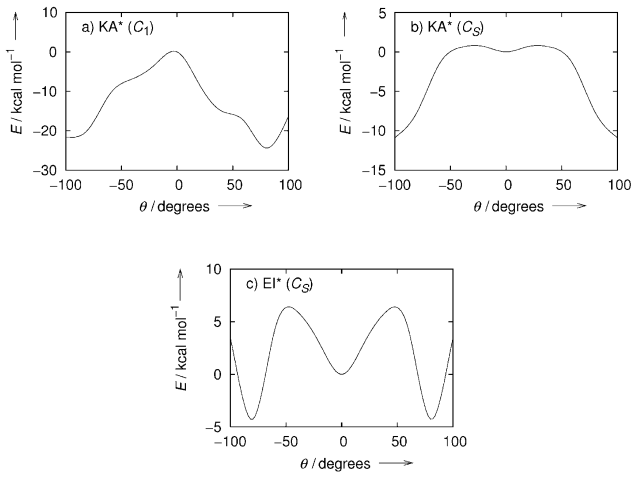

Figure 3. Energy profiles (in kcal mol^{-1}) for the internal rotation of the two pyridyl rings without reoptimization of the geometry. a) KA* intermediate starting from the C_1 symmetry minimum. b) KA* intermediate starting from the C_S symmetry minimum. c) EI* intermediate starting from the C_S symmetry minimum. θ refers to the $\angle C_7$-C_6-C_1-N_2 angle (see Scheme 3 for atom numbering).

profile depicted in Figure 3b. This also shows that twisting is a favored process, though now the planar structure is a relative minimum with a very shallow depth of about 0.5 kcal mol^{-1} that will likely disappear if the geometry were to be reoptimized. Things are different for the EI* intermediate (Figure 3c). The initial geometry in this case is the planar one (as this is the only stationary point located so far) and so the energy profile is symmetric around the 0° point. Now the energy sharply increases upon loss of planarity. However, after a maximum of energy about 6 kcal mol^{-1} above the initial structure, the energy drops sharply until a new minimum is found when the two pyridyl rings are almost orthogonal. Interestingly, this twisted structure is actually more stable (by ca. 4 kcal mol^{-1}) than the original planar one. This result clearly indicates the presence of an additional stationary point corresponding to the twisted structure of the EI* intermediate. As in the KA* case this C_1 structure is more stable than the planar (C_S) one although, probably because the intramolecular hydrogen bonds are stronger in the planar EI* geometry than in the planar KA* case, there is now a barrier to overcome for the twisting that is not present in the KA* region.

The loss of the C_S symmetry in the twisted intermediates induces pyramidalization around the nitrogen atoms. Starting from the twisted KA* structure and forcing planarity of all the nitrogen bonds leads to a structure that is destabilized by 15.48 kcal mol^{-1}. Conversely, a structure that retains the planarity of the two rings (twisting angle = 0°) but allows the nitrogen ligands to go out of the plane is located 12.37 kcal mol^{-1} above the totally planar one (C_S). As expected, pyramidalization clearly enlarges the two hydrogen bonds (the $O_1\cdots H_1$ and $N_1\cdots H_2$ distances are now 1.85 and 2.04 Å, respectively). However, the electronic density analysis still reveals the presence of bond critical points even though quite weakened. Globally these additional calculations show that pyramidalization of the nitrogen centers favors the twisting of the two rings but is not favorable enough to break up the intramolecular hydrogen bonds of the planar structure. Analogous results appeared when studying the EI* region, though in this case the stabilization of the twisted structure is not so remarkable. Then there are additional interactions that come into play in the 90° twisted minima. We can speculate that these are related to the interaction between the π electrons of one pyridyl ring and the lone pairs of the oxygen and nitrogen atoms of the other ring. It is conceivable that the single oxygen atom (with three lone pairs) present in the KA* structure interacts better with the π system than the nitrogen atom in the EI* structure that still has a hydrogen bonded and just one lone pair.

To discuss the expected photochemistry of BP(OH)(NH_2), a major point of interest is the likely presence of CIs along the whole energy profile. Although not properly localized, CIs are suspected for BP(NH_2)$_2$ and BP(OH)$_2$ in the region of the single-proton-transfer intermediate upon twisting of the two pyridyl rings.[28] As the system studied here is a hybrid between these two molecules, a similar behavior is to be expected. In fact, the lowering in energy of the single-proton-transfer intermediates upon twisting and the small energy difference between S_0 and S_1 calculated for these twisted minima (4.06 and 10.60 kcal mol^{-1} for the KA* and EI* C_1 structures, respectively) are clear indications of the presence of CIs. However, as explained in the Computational Methods section, the single-configuration TDDFT method is not suited to deal with such a multiconfigurational region of the potential hypersurface so at this point we resorted to the complete active space self-consistent field (CASSCF) method. Within this method we were able to fully localize CIs in both the KA* and EI* regions; their geometry is depicted in Figure 4. Note that, as expected, both CIs are quite

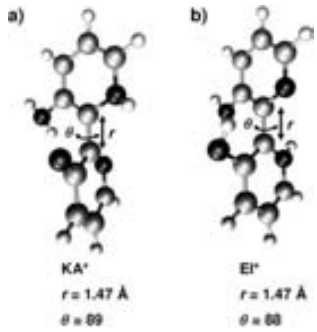

Figure 4. Geometry of the CIs located using the CASSCF method for the BP(OH)(NH_2) molecule in the regions corresponding to single-proton transfer. a) CI located in the KA* region. b) CI located in the EI* region. r and θ refer to the C_6–C_1 distance and the $\angle C_7$-C_6-C_1-N_2 angle, respectively (see Scheme 3 for atom numbering).

similar to the already analyzed twisted intermediates, but a direct comparison of geometries and energies is meaningless as different levels of calculation were used. Finally, we also succeeded in characterizing the two modes that break the degeneracy of the ground and first singlet excited states. The gradient difference (GD) mode is trivially identified as the twisting of the two pyridyl rings. Less evident is the characterization of the interstate or derivative-coupling (DC) mode. In both CIs the DC mode can be mainly ascribed to the stretching of the carbon–carbon (C_1–C_6) inter-ring distance (Figure 5).

Finally, we are able to discuss the likely photochemistry of BP(OH)(NH_2) and compare it with that of their isoelectronic analogues, BP(OH)$_2$ and BP(NH_2)$_2$. To do so we have devised a "full picture" of the energy variations along the different molecular motions that will likely play a role. Figure 6 shows such a picture in a very schematic way. The two different paths that arise from the fact that there are two protons to be transferred in a stepwise manner are considered by using opposite directions of the proton-transfer coordinate. This way, both directions of the proton-transfer coordinate end up at the same KI* structure.

Radiation of a suitable energy (3.59 eV according to our best calculations) puts the system in the first singlet excited electronic state S_1. Within the FC principle, the geometry is frozen along the electronic excitation so that the molecule is no longer in a minimum-energy structure but in a very unstable

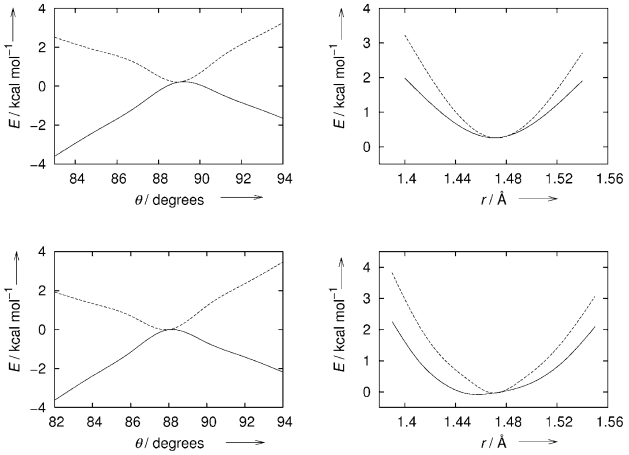

Figure 5. Energy profiles along the modes that break the degeneracy of the S_0 (——) and S_1 (·····) electronic states for the CIs located in the KA* region (left) and in the EI* region (right). Gradient difference (top) ascribed to the twisting angle of the two pyridyl rings. Derivative coupling (bottom) ascribed to the stretching of the carbon–carbon inter-ring distance. r and θ refer to the C_6–C_1 distance and the $\angle C_7$-C_6-C_1-N_2 angle, respectively (see Scheme 3 for atom numbering).

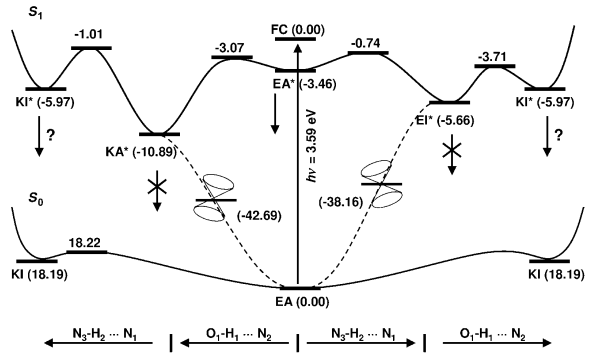

Figure 6. Model for the photochemistry of BP(OH)(NH_2) as inferred from the electronic results obtained in this work. Energies (in kcal mol^{-1}) in the ground state (S_0) are referred to the EA minimum, whereas energies in the first singlet excited electronic state S_1 are referred to the FC vertical excitation. All energies are DFT/TDDFT, except those for the CIs, which are given as the CASSCF energy difference between the geometry at the CI and the FC structure. Solid lines represent reaction paths that maintain the planar (C_S) symmetry whereas out-of-plane reaction paths are indicated by dashed lines. A double-cone symbol is posted on the regions of the CIs between S_0 and S_1. The arrows at the bottom indicate the proton that is transferred along the path.

conformation that may relax to the EA* minimum-energy structure from where it can fluoresce back to the S_0 state. However, as the transition-state structures for the first proton transfers are well below the energy of the FC structure, the system will most likely proceed to either (or both) of the single-proton-transfer structures KA* or EI*. From these two structures a radiative decay back to S_0 is less favorable as there is no minimum-energy structure corresponding to single-proton-transfer processes in S_0. However, a second proton transfer may take place to produce the KI* tautomer. Within our calculations KI* is a stable structure in S_0, but the very shallow depth of the S_0 minimum makes it unlikely that this structure may support many vibrational levels so that KI* fluorescence may be quite a slow process. Probably, the systems arriving at KI* will revert to EI* or KA*, finally relaxing to S_0 by means of CIs. Within this reasoning we predict that the quantum yield of the fluorescence in BP(OH)(NH_2) will be quite low, similar to that observed for BP-(NH_2)$_2$ ($\approx 10^{-5}$), but perhaps not as low since in the latter case there was no minimum at all in the region corresponding to the double-proton transfer in S_0.[28]

All the reasoning of the previous paragraph was restricted to the planar (C_S) structures without considering the out-of-plane motion of the molecule. All the C_S structures are linked by reaction paths depicted in Figure 6 as solid curves. Taking into account the out-of-plane motion (mainly represented by the twisting angle between the two pyridyl rings but including also, as discussed earlier, the pyramidalization of the NH_2 groups), there are lower-energy C_1 structures available in the regions corresponding to the single-proton transfers in S_1. These structures lead to the CIs (indicated in Figure 6 by a double-cone symbol). Because, as discussed above, TDDFT fails on such twisted geometries, the energies ascribed to the CIs in Figure 6 were obtained by assuming that the energy difference between the FC structure of the reactant and the corresponding CI at the TDDFT level is equal to the energy difference calculated at the CASSCF level between each CI and the FC structure. The CIs are connected to the C_S reaction path through arbitrary reaction paths (Figure 6, dashed lines). Once the CI is reached the system may deactivate to the ground electronic state and in doing so, it will probably end up at the most stable EA minimum. Again, dashed lines are used in Figure 6 to depict these hypothetical reaction paths. At this point the photochemical cycle has been closed and a new photoactivation is able to start the process again.

3. Conclusions

The information gathered herein on the energies of the more relevant points along the whole potential energy surfaces of the ground (S_0) and first singlet excited (S_1) electronic states is not enough to foresee the photochemical behavior of BP(OH)(NH_2). We can speculate that its behavior will be somehow intermediate between those observed for $BP(OH)_2$ and $BP(NH_2)_2$.[24,27] The fluorescence quantum yield will probably be low but not as low as in the $BP(NH_2)_2$ case. After vertical excitation, a single-proton-transfer event (leading either to EI* or KA* structures, our data neither discard nor favor any one of them) is the more likely process. Once there the system may deactivate to S_0 by losing the planar symmetry and accessing the corresponding CI or proceed to the KI* structure through a second proton-transfer event. The former path is lower in energy but again both channels are energetically open. The concerted double-proton-transfer path (detected experimentally for the $BP(OH)_2$ system[24]) is unlikely now as it implies a large energy barrier (see Figure 2). If the double-proton-transfer final product KI* is reached it may deactivate to S_0, but this process may be inefficient if the very shallow minimum of KI in the ground state does not support any vibrational state. In addition to this, the systems arriving at KI* might revert again to EI* or KA* and thus relax to S_0 through the CIs. This ESIPT scenario is rather similar to several simply hydrogen-bonded systems recently discussed.[44–47] To shed more light on the actual photochemistry of BP(OH)(NH_2), molecular dynamics studies should be carried out. These simulations could quantify the actual fraction of systems that react through the O- and N-channels and, more critically, the efficiency of the nonradiative processes through the CIs. However, these calculations are expected to be quite complex as so many channels are open and so many degrees of freedom are involved for this unsymmetrical system. Additionally, experimental work on this quite interesting molecule is needed. First of all, the absorption and fluorescence spectra ought to be acquired to obtain the fluorescence quantum yield (and reveal up to what point the system evolves after photoexcitation), but to really grasp the photochemical mechanisms of this molecule time-resolved experiments (surely at a femtosecond time resolution) are compulsory.

Computational Methods

Electronic DFT-based methods were used to explore the topology of the ground (S_0) and first $\pi\pi^*$ singlet excited (S_1) electronic states. DFT and TDDFT[48,49] optimizations were performed for the S_0 and S_1 states, respectively. TDDFT was successfully used to study other related ESIPT systems.[49–51] The three-parameter hybrid functional of Becke with the correlation functional of Lee, Yang, and Parr (B3LYP)[52,53] was chosen. The Turbomole program (version 5.4),[54,55] which implements analytical gradients at the TDDFT level,[55,56] was used to perform the TDDFT calculations.

An intrinsic reaction coordinate (IRC) calculation for connecting the transition-state structure with the reactant minimum in S_0 was performed at the DFT level with the Gaussian 03 package.[57] As we stated in a previous report,[58] the B3LYP functionals used in the Gaussian 03 and Turbomole packages differ very little in the relative stability of the calculated points, which implies a very minor effect on our results. This small difference comes from the use of a different form of the local correlation functional: the Gaussian 03 package uses the VWN(III) local correlation functional, whereas Turbomole uses VWN(V).[59]

Multireference CASSCF[60] calculations were carried out with the MOLCAS program (Version 6.4).[61] The electronic energy of the S_0 and S_1 states was obtained by using a state average with equal weights for both states, with an active space of ten electrons and ten molecular orbitals, which includes the last five occupied and the first five unoccupied orbitals. We note that this active space is probably not large enough to correctly describe the whole potential energy surface, but it was used just to analyze the presence of CIs between the S_0 and S_1 states. A larger active space would be necessary to compare the different regions of the potential energy surface. CIs were localized through minimization of the absolute value of the energy difference between the states that cross with the added condition that the energy of the state is the lowest possible that satisfies the first condition.

In all cases, to obtain a good description of the proton- and charge-transfer processes on excited states, the 6-31G(d,p)[62,63] basis was used for the hydrogen and carbon atoms, while additional diffuse functions (6-31G+(d,p) basis)[62,63] were added to the oxygen and nitrogen atoms.

Acknowledgements

The authors wish to thank Prof. J. M. Anglada and Prof. J. M. Bofill for helpful discussions on localizing conical intersections. We are grateful for financial support from the Ministerio de Educación y Ciencia and the Fondo Europeo de Desarrollo Regional through Project CTQ2005-07115/BQU, and from the Generalitat de Catalunya (2005SGR00400). Use of computational facilities at the Centre de Supercomputació de Catalunya is also acknowledged.

Keywords: conical intersections · excited states · femtochemistry · proton transfer · reaction mechanisms

[1] H. Bouas-Laurent, H. Durr, *Pure Appl. Chem.* **2001**, *73*, 639.
[2] P. F. Barbara, L. E. Brus, P. M. Rentzepis, *J. Am. Chem. Soc.* **1980**, *102*, 5631.
[3] P. T. Chou, Y. C. Chen, W. S. Yu, Y. H. Chou, C. Y. Wei, Y. M. Cheng, *J. Phys. Chem. A* **2001**, *105*, 1731.
[4] E. T. J. Nibbering, T. Elsaesser, *Chem. Rev.* **2004**, *104*, 1887.
[5] H. J. Heller, H. R. Blattmann, *Pure Appl. Chem.* **1974**, *36*, 141.
[6] N. S. Allen, *Polym. Photochem.* **1983**, *3*, 167.
[7] G. Woessner, G. Goeller, P. Kollat, J. J. Stezowski, E. Daltrozzo, M. Neureiter, H. E. A. Kramer, *J. Phys. Chem.* **1984**, *88*, 5544.
[8] G. Woessner, G. Goeller, J. Rieker, H. Hoier, J. J. Stezowski, E. Daltrozzo, M. Neureiter, H. E. A. Kramer, *J. Phys. Chem.* **1985**, *89*, 3629.
[9] G. Goeller, J. Rieker, J. A. Maier, J. J. Stezowski, E. Daltrozzo, M. Neureiter, H. Port, M. Wiechmann, H. E. A. Kramer, *J. Phys. Chem.* **1988**, *92*, 1452.
[10] S. J. Formosinho, L. G. Arnaut, *J. Photochem. Photobiol. A* **1993**, *75*, 21.
[11] M. Irie, *Chem. Rev.* **2000**, *100*, 1685.
[12] Y. C. Liang, A. S. Dvornikov, P. M. Rentzepis, *Proc. Natl. Acad. Sci. USA* **2003**, *100*, 8109.
[13] L. Giordano, T. M. Jovin, M. Irie, E. A. Jares-Erijman, *J. Am. Chem. Soc.* **2002**, *124*, 7481.
[14] A. Fernández-Acebes, J.-M. Lehn, *Chem. Eur. J.* **1999**, *5*, 3285.

[15] M. Sauer, *Proc. Natl. Acad. Sci. USA* **2005**, *102*, 9433.
[16] A. L. Sobolewski, *Phys. Chem. Chem. Phys.* **2008**, *10*, 1243.
[17] O. Vendrell, R. Gelabert, M. Moreno, J. M. Lluch, *J. Am. Chem. Soc.* **2006**, *128*, 3564.
[18] O. Vendrell, R. Gelabert, M. Moreno, J. M. Lluch, *J. Phys. Chem. B* **2008**, *112*, 5500.
[19] S. Habuchi, R. Ando, P. Dedecker, W. Verheijen, H. Mizuno, A. Miyawaki, J. Hofkens, *Proc. Natl. Acad. Sci. USA* **2005**, *102*, 9511.
[20] H. Zhang, P. van der Meulen, M. Glasbeek, *Chem. Phys. Lett.* **1996**, *253*, 97.
[21] D. Marks, H. Zhang, M. Glasbeek, P. Borowicz, A. Grabowska, *Chem. Phys. Lett.* **1997**, *275*, 370.
[22] P. Toele, H. Zhang, M. Glasbeek, *J. Phys. Chem. A* **2002**, *106*, 3651.
[23] D. Marks, P. Prosposito, H. Zhang, M. Glasbeek, *Chem. Phys. Lett.* **1998**, *289*, 535.
[24] P. Prosposito, D. Marks, H. Zhang, M. Glasbeek, *J. Phys. Chem. A* **1998**, *102*, 8894.
[25] O. K. Abou-Zied, *J. Phys. Chem. B* **2007**, *111*, 9879.
[26] R. Gelabert, M. Moreno, J. M. Lluch, *ChemPhysChem* **2004**, *5*, 1372.
[27] P. Toele, M. Glasbeek, *Chem. Phys. Lett.* **2005**, *407*, 487.
[28] J. M. Ortiz-Sánchez, R. Gelabert, M. Moreno, J. M. Lluch, *ChemPhysChem* **2007**, *8*, 1199.
[29] L. Kaczmarek, *Pol. J. Chem.* **1985**, *59*, 1141.
[30] K. Tokumura, O. Oyama, H. Mukaihata, M. Itoh, *J. Phys. Chem. A* **1997**, *101*, 1419.
[31] W. Rettig, V. Kharlanov, M. Maus, *Chem. Phys. Lett.* **2000**, *318*, 173.
[32] L. Serrano-Andrés, M. Merchán, *J. Mol. Struct. Theochem* **2005**, *729*, 99.
[33] R. Gelabert, M. Moreno, J. M. Lluch, *J. Phys. Chem. A* **2006**, *110*, 1145.
[34] M. J. G. Peach, P. Benfield, T. Helgaker, D. Tozer, *J. Chem. Phys.* **2008**, *128*, 044118.
[35] M.-S. Liao, Y. Lu, S. Scheiner, *J. Comput. Chem.* **2003**, *24*, 623.
[36] A. L. Sobolewski, W. Domcke, *Chem. Phys.* **2003**, *294*, 73.
[37] A. Dreuw, M. Head-Gordon, *J. Am. Chem. Soc.* **2004**, *126*, 4007.
[38] S. Anand, H. B. Schegel, *Mol. Phys.* **2006**, *104*, 933.
[39] E. Fabiano, F. Della Sala, G. Barbarella, S. Lattante, M. Anni, G. Sotgiu, C. Hättig, R. Cingolani, G. Gigli, *J. Phys. Chem. B* **2006**, *110*, 18651.
[40] E. Perpete, J. Preat, J.-M. Andre, D. Jacquemin, *J. Phys. Chem. A* **2006**, *110*, 5629.
[41] X. Xu, Z. Cao, Q. Zhang, *J. Phys. Chem. A* **2006**, *110*, 1740.
[42] J. Plötner, A. Dreuw, *Chem. Phys.* **2008**, *347*, 472.
[43] R. W. F. Bader, H. Essen, *J. Chem. Phys.* **1984**, *80*, 1943.
[44] A. L. Sobolewski, W. Domcke, *Phys. Chem. Chem. Phys.* **2006**, *8*, 3410.
[45] A. L. Sobolewski, W. Domcke, *J. Phys. Chem. A* **2007**, *111*, 11725.
[46] A. L. Sobolewski, W. Domcke, C. Hättig, *J. Phys. Chem. A* **2006**, *110*, 6301.
[47] J. D. Coe, T. J. Martinez, *Mol. Phys.* **2008**, *106*, 537.
[48] R. Bauernschmitt, R. Ahlrichs, *Chem. Phys. Lett.* **1996**, *256*, 454.
[49] A. Dreuw, M. Head-Gordon, *Chem. Rev.* **2005**, *105*, 4009.
[50] A. L. Sobolewski, W. Domcke, *Phys. Chem. Chem. Phys.* **1999**, *1*, 3065.
[51] A. J. A. Aquino, H. Lischka, C. Hattig, *J. Phys. Chem. A* **2005**, *109*, 3201.
[52] A. D. Becke, *J. Chem. Phys.* **1993**, *98*, 5648.
[53] C. T. Lee, W. T. Yang, R. G. Parr, *Phys. Rev. B* **1988**, *37*, 785.
[54] F. Furche, R. Ahlrichs, *J. Chem. Phys.* **2002**, *117*, 7433.
[55] R. Ahlrichs, M. Bär, M. Haser, H. Horn, C. Kolmel, *Chem. Phys. Lett.* **1989**, *162*, 165.
[56] C. Van Caillie, R. D. Amos, *Chem. Phys. Lett.* **2000**, *317*, 159.
[57] Gaussian 03 (Revision C.02), M. J. Frisch, G. W. Trucks, H. B. Schlegel, G. E. Scuseria, M. A. Robb, J. R. Cheeseman, J. A. Montgomery, Jr., T. Vreven, K. N. Kudin, J. C. Burant, J. M. Millam, S. S. Iyengar, J. Tomasi, V. Barone, B. Mennucci, M. Cossi, G. Scalmani, N. Rega, G. A. Petersson, H. Nakatsuji, M. Hada, M. Ehara, K. Toyota, R. Fukuda, J. Hasegawa, M. Ishida, T. Nakajima, Y. Honda, O. Kitao, H. Nakai, M. Klene, X. Li, J. E. Knox, H. P. Hratchian, J. B. Cross, V. Bakken, C. Adamo, J. Jaramillo, R. Gomperts, R. E. Stratmann, O. Yazyev, A. J. Austin, R. Cammi, C. Pomelli, J. W. Ochterski, P. Y. Ayala, K. Morokuma, G. A. Voth, P. Salvador, J. J. Dannenberg, V. G. Zakrzewski, S. Dapprich, A. D. Daniels, M. C. Strain, O. Farkas, D. K. Malick, A. D. Rabuck, K. Raghavachari, J. B. Foresman, J. V. Ortiz, Q. Cui, A. G. Baboul, S. Clifford, J. Cioslowski, B. B. Stefanov, G. Liu, A. Liashenko, P. Piskorz, I. Komaromi, R. L. Martin, D. J. Fox, T. Keith, M. A. Al-Laham, C. Y. Peng, A. Nanayakkara, M. Challacombe, P. M. W. Gill, B. Johnson, W. Chen, M. W. Wong, C. Gonzalez, J. A. Pople, Gaussian, Inc., Wallingford, CT, **2004**.
[58] J. M. Ortiz-Sánchez, R. Gelabert, M. Moreno, J. M. Lluch, *J. Phys. Chem. A* **2006**, *110*, 4649.
[59] S. H. Vosko, L. Wilk, M. Nusair, *Can. J. Phys.* **1980**, *58*, 1200.
[60] K. Andersson, P.-Å. Malmqvist, B. O. Roos, *J. Chem. Phys.* **1992**, *96*, 1218.
[61] MOLCAS (Version 6.2), K. Andersson, M. Barysz, A. Bernhardsson, M. R. A. Blomberg, Y. Carissan, D. L. Cooper, M. P. Fischer, L. Gagliardi, C. de Graaf, B. A. Hess et al., Lund University, Sweden, **2000**.
[62] P. C. Hariharan, J. A. Pople, *Theor. Chim. Acta* **1973**, *28*, 213.
[63] M. M. Francl, W. J. Pietro, W. J. Hehre, J. S. Binkley, M. S. Gordon, D. J. Defrees, J. A. Pople, *J. Chem. Phys.* **1982**, *77*, 3654.

Received: May 29, 2008
Published online on August 29, 2008

8

Appendixes

"To divide a cube into two other cubes, a fourth power or in general any power whatever into two powers of the same denomination above the second is impossible, and I have assuredly found an admirable proof of this, but the margin is too narrow to contain it."

Pierre de Fermat, on the margin of his copy of Diophantus' Arithmetica

A

Manuscript I

The Bipyridyl Derivatives as Photomemory Devices. A Comparative Electronic-Structure study.

Juan Manuel Ortiz-Sánchez[a], Ricard Gelabert[a], Miquel Moreno[a]*, José M. Lluch[a], José M. Anglada[b], José M. Bofill[c]

Abstract: The two isolectronic bipyridyl derivatives [2,2'-bipyridyl]-3,3'-diamine ($BP(NH_2)_2$) and [2,2'-bipyridyl]-3,3'-diol ($BP(OH)_2$) are experimentally known to undergo very different excited-state double-proton transfer processes, which result in fluorescence quantum yields that differ by four orders of magnitude. Such differences have been theoretically explained in terms of topographical features in the potential energy surface and the likely presence of conical intersections. The hypothetical hybrid compound [2,2'-bipyridyl]-3-amine-3'-ol ($BP(OH)(NH_2)$) presents intermediate photochemical features of its "ancestors". Here we analyze the photochemical properties of a whole family of "dark" (not fluorescent) states that can be accessed from each bipyridyl derivative upon irradiation of light of a given wavelength, and their potential application as photomemory devices. In light of our density functional theory (DFT), time-dependent DFT (TDDFT), and complete active space self-consistent field (CASSCF) calculations, $BP(NH_2)_2$ is the more likely candidate to become a photomemory device.

Introduction

Hydrogen bonds are of universal importance in chemistry and biochemistry. The properties of hydrogen bonds in the electronic ground state have been investigated since long ago. The use of powerful experimental methods[1] and the possibility of very accurate theoretical methods being applied to rather large molecular systems that easily reach the size of biological interesting systems has led to a very clear picture of the structure and chemical properties of these systems.[2,3]

Much less is known about the properties and reactivity of hydrogen bonds in excited electronic states and their crucial role in a plethora of photochemical processes of chemical and biochemical relevance. The most interesting phenomenon of these systems is that they may proceed through an excited state intramolecular proton transfer (ESIPT). The time scale of the ESIPT process and the presence or absence of a barrier for the proton transfer in the excited state was a matter of dispute for years[4-6] that was settled with the advent of ultrafast techniques globally known as femtochemistry and now it is well established that ESIPT are ultrafast processes usually lasting no more than a few hundreds of femtoseconds.

Probably the more thoroughly studied molecules exhibiting ESIPT are several families of aromatic systems with intramolecular hydrogen bonds. The interest in these systems was, at first, mostly technologically driven because of their potential use as photostabilizers and sunscreens for the protection of organic polymers and biological tissues (including our own skin).[7,8] The generic mechanism of photostabilizers involves an ultrafast proton (or hydrogen) transfer in the excited state followed by fluorescent or radiationless decay of the excited phototautomer leading to a very unstable structure in the ground state that quickly reverts to the original species. Figure 1(a) schematically depicts the process involved in the simplest mechanism: the molecule absorbs radiation at a short (dangerous) wavelength λ_1. Once in the excited singlet state (S_1) the ESIPT reaction takes place through a barrierless (or near barrierless) process. The phototautomer, the more stable species in S_1, fluoresces back to the ground state S_0 emitting a longer (harmless) wavelength λ_2. As said above the obtained tautomer in S_0 is very unstable so that it quickly reverts to the initial species that is able to start again the whole photocycle. This

[a] Llic. J. M. Ortiz-Sánchez, Dr. R. Gelabert, Prof. M. Moreno and Prof. J. M. Lluch.
Departament de Química
Universitat Autònoma de Barcelona
08913 Bellaterra, Barcelona (Spain)
Fax: (+34) 93 581 2920
E-mail: mmf@qf.uab.es

[b] Dr. J. M. Anglada
Departament de Química Biològica i Modelització Molecular
I.Q.A.C.-C.S.I.C.
08034 Barcelona, Barcelona (Spain)

[c] Prof. J. M. Bofill
Departament de Química Orgànica & Institut de Química Teòrica i Computacional
(IQTCUB), Universitat de Barcelona
08028 Barcelona, Barcelona (Spain)

correlative sequence of processes is indicated in Figure 1(a) by numbers within parenthesis that go from (1) to (4).

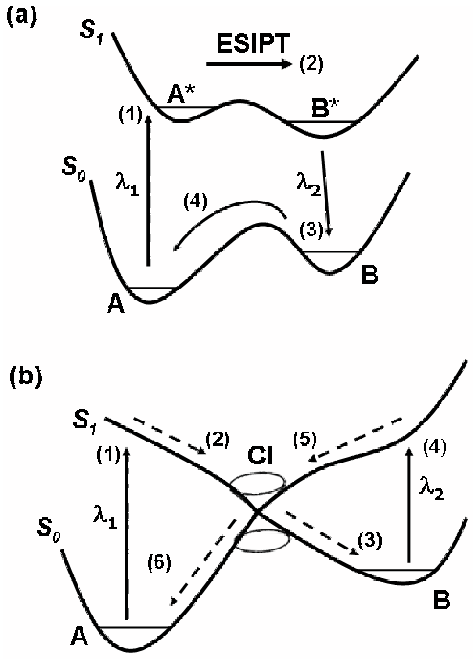

Figure 1. Schematic representation of the process involved in the photocycle of (a): a photostabilizer and (b): an ideal optical photoswitch. ESIPT in (a) refer to the excited-state intramolecular proton-transfer process while the double cone in (b) refers to a conical intersection (CI) region of low energy. λ_1 refers to the wavelengths that photoexcite A whereas λ_2 in (a) refers to the emission of B* while in (b) it indicates the wavelength that excite. The numbering of events follows the sequence of the photocycle steps.

This simple and easy-to-understand picture is not however the usual case as most of the photostabilizers do not actually emit any wavelength (that is, they do no fluoresce). In these cases the deactivation of the excited state has to take place through a radiationless path. A likely mechanism for the highly effective deactivation of fluorescent states, first proposed by Mataga,[9] involved the curve-crossing of the initially accessed (brilliant) state with a non-fluorescent dark state that would be the responsible of the deactivation process. At the time it was proposed, this model remained speculative as it could not be supported by accurate electronic-structure calculations. Since then, the number of theoretical studies of excited electronic states has grown spectacularly and now the presence of such true crossings between different electronic states (conical intersections) is known to be ubiquitous and essential in order to explain the actual photochemistry and photophysics of virtually any molecular system.[10]

In its plainest form, the mechanism of a photostabilizer that fully quenches fluorescence is indicated in Figure 1(b): After photoexcitation that absorbs λ_1 the ESIPT process leads to a tautomer that is not stable with respect to a deforming coordinate (usually torsion of the aromatic rings and/or a pyramidalization of the proton acceptor group). Following this coordinate a conical intersection (CI) with the ground state is reached. At this geometry, the $S_1 \rightarrow S_0$ nonadiabatic transition occurs within a fraction of the torsional process so that it is also ultrafast.[11] Once the system is again in the ground state the most likely process involves the return to the (more stable) initial species in the ground state thus closing the photocycle in the usual manner. Alternatively the CI may also connect with a different tautomer (obtained through rotation of the interring bond) in the ground state. If this isomeric species is stable enough, a so called photochromic species is obtained as the final product of the photoexcitation.

The formation of stable photochromic species is undesired for molecular photostabilizers so that a very small barrier for the reformation of the original species is expected. However, there are very well known examples of organic molecules with quite stable photochromic species such as the family of aromatic Schiff bases.[12,13] Recently, interest in photochromic systems has suddenly increased because the intriguing possibility to use them as molecular optical switches or photomemories. The use of organic molecules for the future realization of digital processors and storage media at the miniaturized level is at present a hot topic in the applied science world.[14-16] A molecule showing the simple scheme of Figure 1(b) could be a good candidate for a molecular photomemory if the photocromic species is stable enough. To accomplish that, additional stabilization of this isomer should be possible, for instance through the formation of a new hydrogen bond. Additionally, the photocromic form should absorb at a very different wavelength in comparison with the original absorption (λ_2 in Figure 1(b)) and this excitation would have to revert the system to the original form also through an ultrafast process. Again, a correlative number within parenthesis in Figure 1(b) indicates the whole sequence: (1) photoexcitation of the A species, (2) barrierless photochromic process in S_1, (3) transition via conical intersection reaching the B species in S_0, (4) photoexcitation of the B especies, (5) reverse photochromic process, and (6) closing of the photocycle by accessing again the conical intersection finally reverting to the A species in S_0. Finally, in order to be able to "read" the memory, there should exist a physical property, easy to measure, that could be used to clearly discriminate between the two isomers. This idea was recently explored by Sobolewski who theoretically designed a molecule that would fulfill all these conditions.[17]

In the past years we have studied a series of molecules isoelectronic to the [2,2'-bipyridyl]-3,3'-diol [hereafter referred as $BP(OH)_2$], one of the simplest molecules that is experimentally known to suffer a double proton transfer in the excited state.[18-22] In addition to the parent molecule study,[23] we have performed additional works that deal with the isoelectronic derivatives [2,2'-bipyridyl]-3,3'-diamine [$BP(NH_2)_2$][24] and [2,2'-bipyridyl]-3-amine-3'ol [$BP(OH)(NH_2)$][25]. In spite of the great similarity of the three molecular systems (the only change being the substitution of one or two hydroxyl groups by amino ones, see Scheme 1), they show quite different photochemical behaviors. One of the more striking differences, that arise from time resolved femtochemistry experiments, are the fluorescence quantum yields that differ by more than four orders of magnitude between $BP(OH)_2$ and $BP(NH_2)_2$.[26] Our previous theoretical works, mainly devoted to a systematic analysis of the stationary points in both the ground (S_0) and first singlet (S_1) excited electronic states, provided a nice theoretical ground that explained the differences between both systems and the hybrid $BP(OH)(NH_2)$ for which no experimental data is yet available.

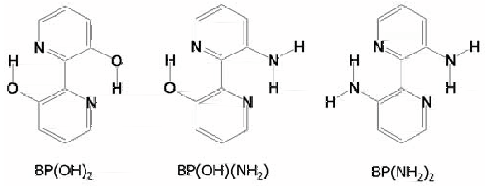

Scheme 1. Molecular structures of the three bipyridyl compounds studied here.

One of the key features that differentiate the three systems so largely is the likely presence of conical intersections (CIs) between S_1 and S_0. These CIs appear in the regions of the potential energy surface corresponding to a single proton transfer upon rotation of the two pyridyl rings and it appears that they are energetically accessible from the Franck-Condon initial excitation area for all the considered systems. In our previous works,[23-25] the different photochemical behaviors of the three systems were discussed in light of the different energies and geometries of the stationary points in S_0 and S_1 and the CIs. However, in these analyses the fate of the molecule beyond the CI was not considered. Up to this point we could conclude that these systems rank well to become good photostabilizers. In this paper we take a step beyond and look more carefully at the molecular motions that may follow in S_0 after passing the CI. In this way we disclose the presence of an, up to now, unknown set of photochromic structures that cannot be directly accessed by photoexcitation but that may eventually become the product of the full photochemical process. If these "dark" molecular species happened to be the main product after passage through the CI, the bipyridyl systems studied here could be one of the smallest and simplest photostable molecular memories known so far. Then our theoretical work may open the door to exciting new possibilities in the design of sub-nanostructures as building blocks for the next generation of digital processors and storage devices.

Results and Discussion

As said in the introduction section, we previously performed several studies of three isoelectronic bipyridyl derivatives.[23-25] We have reconsidered the three systems in this paper. We shall begin the study with $BP(NH_2)_2$, the molecule with the lowest quantum fluorescence yield as this points to a more likely access to the conical intersection and, consequently, to the dark states. Later on we will consider the $BP(OH)_2$ molecule, the best studied system from the experimental and theoretical points of view. Finally we will analyze the hybrid $BP(OH)(NH_2)$ that is almost experimentally unknown but also very interesting due to the asymmetry of the molecule that allows for a larger number of reaction paths. As there is no way to discuss our new results (the dark states) without also considering the "bright" states that were previously obtained (using the same level of calculation) and analyzed by us,[23-25] Figures 2 to 9 depict the structures in two different formats: black-filled letters, numbers and characters refer to the dark states (new results) whereas white-filled letters, numbers and characters are used for the bright (previously obtained) states of the different studied systems. This differentiation also allows for a more clear discussion in what follows.

$BP(NH_2)_2$

This molecule was theoretically analyzed by us in a previous work.[24] In that work the stationary states of the ground (S_0) and first singlet excited electronic state (S_1), which results from an allowed $\pi\pi^*$ excitation, were carefully located. Results are summarized in Figures 2 and 3. Figure 2 depicts the energies of the different stationary points (and the conical intersection structure) on both the S_0 and S_1 electronic states and the reaction paths (as discussed in the methodological section) that connect them. Figure 3 gives a schematic view of the more relevant structures found along the different photochemical paths as well as the numbering used from now on to refer to the atoms involved in a particular intramolecular

motion. It is hard to follow Figure 2 without taking a look at Figure 3 so that both Figures will be analyzed together. Even if Figure 2 shows the structures along a unique direction, all the reaction paths are obviously multidimensional. Solid lines connecting any pair of stationary points (minima or transition states) indicate a single Proton transfer. Arrows at the foot of the Figure indicate the transferring atom. Dashed lines are used in the Figure to indicate out-of-plane motions (mainly rotation around the C_1–C_2 bond)

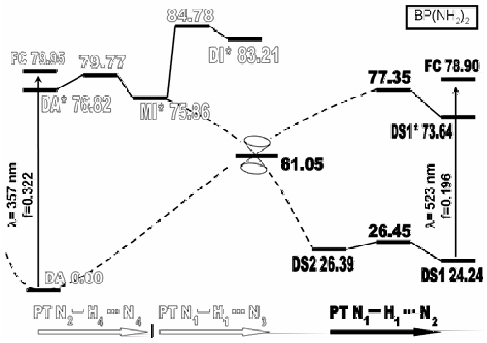

Figure 2. Relative energies (in kcal mol^{-1}) of the planar structures in S_0 (bottom) and S_1 (top) relevant to the double proton transfer and the rotation of the two pyridine rings in $BP(NH_2)_2$. Solid lines represent reaction paths that maintain the planar symmetry whereas out-of-plane reaction paths are indicated by dashed lines. A double-cone symbol is posted on the region of the conical intersection between S_0 and S_1. Arrows at the bottom indicate the proton that is transferred along any given path. The vertical arrows correspond to light absorptions relevant to the whole photochemical process (see text). White-filled letters, numbers and characters are used for processes in the bright zone that were already studied in a previous work,[24] whereas the dark region, first discussed here, is indicated by black-filled letters, numbers and characters.

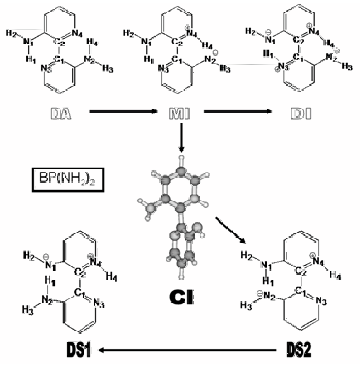

Figure 3. Schematic picture and numeration of atoms for the geometries of the stationary points and the conical intersection region of $BP(NH_2)_2$ in S_0 and S_1. The name of the structures and the meaning of the white-filled and black-filled letters is analogous to that of Figure 2.

In the bright side of S_0, the $BP(NH_2)_2$ possess only one minimum energy structure. As in our previous work, we name it diamine (DA) to indicate the positions of the transferring hydrogen atoms. This is the only existing chemical species prior to any photochemical reaction. Note that the fully optimized minimum is not perfectly planar as a small amount of pyramidalization takes place in the amino groups and the two pyridyl rings are also slightly rotated. However, all the energies considered in Figure 2 refer to fully planar geometries (with the obvious exception of the conical intersection as noted below). This does not produce large energy differences (for instance the difference in energy between the planar and optimized DA structures in S_0 is just 0.39 kcal mol^{-1}) Irradiation of light of 357 nm, quite similar to the maximum of absorption experimentally measured at 370 nm,[26] puts the system in the excited S_1 state. This electronic transition is clearly allowed as it has an oscillator strength of 0.322 (also indicated in Figure 2). Because of the Franck-Condon principle, the initial geometry accessed (leftmost FC in Figure 2) in S_1 is not the relaxed one corresponding to the DA* minimum that lies 3.13 kcal mol^{-1} below FC (note that, as it is customary, we are using an asterisk to refer to excited state structures). In fact, the energy of the FC structure allows the system to overcome the small energy barrier for the transfer of a hydrogen atom so that the so called monoimine structure (MI*) can be accessed. Conversely, the second hydrogen transfer that would lead to the diimine (DI*) product is not energetically accessible so that only a single hydrogen transfer may take place in this system upon irradiation.

As in S_0 there is no minimum on the monoimine region, MI* can hardly fluoresce. A possible channel of deactivation would go through a back proton transfer that reverted to DA* that is more able to fluoresce. However, as hinted in our previous work, there is a lower energy conical intersection (CI) region between the ground and first singlet excited electronic states that can be accessed from the MI* structure upon rotation around the C_1-C_2 bond (that is, rotation of the two pyridyl rings). Given the multiconfigurational character of these regions, we have used, in a first step, the CASSCF approach to properly locate the conical intersection. In a second step, we have taken this geometry and we have employed the TDDFT method to find a minimum energy structure in the CI region along the optimization geometries with very small S_0-S_1 excitation energy (typically less than 1.5 kcal mol^{-1}). The geometry so obtained does not differ much from the CASSCF one. We are aware that the TDDFT method used in this paper is not suited to properly locate and characterize conical intersections. However, it has been shown[27] that TDDFT may still provide a decent hint for the location of such structures and for the determination of their energy, provided that one is lucky or smart enough to know where the CI is to be found.

The more prominent geometrical parameter that defines the CI region is the rotation angle around the C_1–C_2 bond of around 90º so that the two pyridine rings are almost orthogonal in the CI.

This structure is also characterized by the pyramidalization of the NH_2 group of around 135º (dihedral angle H_2–N_1–C–C_2).

Even if the TDDFT energy of the CI is just qualitatively accurate, its value, well below the energies of all the rest of excited state geometries, clearly points to a very easy internal conversion deactivation through this structure. In fact this is the more likely explanation to the very low quantum yield of fluorescence (10^{-5}) measured for $BP(NH_2)_2$.[26] A question that has not been yet considered but it is of crucial importance is: what is the fate awaiting the system beyond the CI? In our previous work it was implicitly assumed that the system, once again in the ground S_0 state, would revert to the DA original structure thus closing the photochemical cycle that would be ready to start again. In this sense $BP(NH_2)_2$ would be qualified as a good photostabilizer as it would absorb UV radiation without emitting dangerous radiation (in fact without emitting any radiation). In order to determine the fate of the process beyond the CI we have followed the gradient difference vector direction, which is one of the two independent vectors of the branching space.[28] This fate can be easily ascribed, in the present case, to the interring C_1-C_2 rotational angle. That breaking of symmetry between S_0 and S_1 leads, on one side, to the DA initial structure and, in the other side, to a rotated DA isomer. If this structure is stable (as we have found in our calculations) a photochromic product can be obtained. In Figures 2 and 3 we have labeled this new species as DS2.

As seen in Figure 3 the DS2 structure has also two intramolecular N–H···N bonds. The fully optimized DS2 geometry is also non planar though, as said above, the energies shown in Figure 2 correspond to planar geometries. Now the energy difference between optimized (non planar) and planar geometries is a little bit larger (1.31 kcal mol^{-1}) probably because the new intramolecular H-bond N_2···H_1 implies a more crowded cycle of 7 atoms instead of the (more usual) 6 atoms involved in the DA structure. In any case, it did not come as a surprise to find that an intramolecular Proton transfer may take place in DS2 leading to the more stable DS1 tautomer. The barrier for the hydrogen transfer between both tautomers is almost non-existent, 0.06 kcal mol^{-1} above DS2. As for DS1 it is located at 2.15 kcal mol^{-1} below DS2. Given the excess of energy that is expected to possess the system coming from S_1, DS1 is the more likely final product, that is, the photochromic species, resulting from the initial photoexcitation of DA. As clearly seen in Figure 3 DS1 is, in fact, a tautomer of the DA original structure as an equivalent DS1 form could be obtained through direct transferring of H_2 between N_1 and N_4 (of course such a transfer cannot take place directly). DS1 lies quite high in energy, 24.24 kcal mol^{-1} above the lowest DA minimum, so that its presence would not be relevant were if not for the likelihood of the photochemical route just discussed

Now we can discuss the candidacy of $BP(NH_2)_2$ to become a photomemory device. If the dark states are the main product after passage of the CI region (within our pure electronic calculations we have no possibility to further evaluate this point) then DS1 is expected to be a fairly stable species as the energy barrier for going back to DA in the ground electronic state is quite large. The only possible way to revert DS1 into DA would be new irradiation, that we have calculated to occur with a wavelength of 523 nm. As also shown in Figure 2, the first allowed transition from DS1 has an oscillator strength of 0.196. The accessed excited state is the S_1 $\pi\pi^*$ excited state where DS1* exists as a minimum energy structure and where a transition state for the back-proton transfer from N_2 to N_1 has been estimated to lie 3.71 kcal mol^{-1} above DS1*. However, as seen in Figure 2, the Franck-Condon vertical excitation (rightmost FC in Figure 2) puts the system higher in energy than that so that ESIPT is, again, energetically feasible. We have not been able to locate a minimum corresponding to the DS2* structure as the optimization provokes an internal rotation around the C_1–C_2 inter-ring bond leading again to the conical intersection region. Once there, the system will proceed most likely to DA. If this is so we will have a good photomemory molecular device. Then, at a first sight, the whole scheme shown in Figure 2 corresponds to a system that could be used as a molecular photomemory. The whole scenario is somewhat more complicated than the one previously schematized in Figure 1(b) but it clearly fulfills all the expected conditions for a photomemory. Let us summarize: a) $BP(NH_2)_2$ is a bistable system. b) The two stable structures in S_0 absorb (with high oscillator strength) at different wavelengths. c) Irradiation of one species mostly lead to the other species in an ultrafast process (there is no energetic barrier to be surmounted in any direction). d) The two forms of $BP(NH_2)_2$ have to be differentiated by some physical property. Here an obvious choice is the absorption of microwave radiation as the symmetric DA structure has a null molecular dipole moment and, hence, it does not absorb in the zone of molecular rotational transitions, but DS1 is not at all symmetric and it has a quite prominent molecular dipole moment of 1.826 D. If the calculations presented here are further confirmed, $BP(NH_2)_2$ may become one of the simplest isolated molecule known so far that is able to act as an efficient photomemory device.

Finally, it may be of interest to compare the intramolecular hydrogen bonds between the original DA structure and the most stable dark state DS1. Table 1 presents the obtained geometrical data (distances) as well as the electronic characteristics analyzed using the Atoms In Molecules (AIM) formulation of Bader.[29] The

value of the electronic density at the bond critical points is a measure of the strength of the bond. As usual, it can be directly related to the corresponding bond distances. As for the Laplacian of the charge density, also shown in Table 1, a negative value is obtained for all the X–H covalent bonds (charge is concentrated in this region) whereas a positive value, indicating a charge depletion, is seen for the hydrogen bonds H···X. Comparison of the two H-bonds present in both DA and DS1 structures show that the covalent X–H bonds are stronger for the DA case whereas the intramolecular H···X bonds are stronger in the DS1 case. In fact it is quite surprising to see how the N–H bond of the amino group has enlarged in going from the DA to the DS1 structure (from 1.017 to 1.055 Å). As discussed above, this geometrical distortion probably comes as a consequence of the overcrowded 7-atom ring that is involved in the intramolecular hydrogen bond between H_1 and N_1 in DS1. The fact that the electronic densities at the bond critical points are not at all so different between both cases sustains this hypothesis.

Table 1. Geometrical distances,[a] electronic densities,[b] and Laplacians[c] at the bond critical points of the X–H···Y bonds. See Figure 3 for atomic numeration.

$BP(NH_2)_2$				
Structure	Bond	r	ρ	$\nabla^2\rho$
DA	N_1-H_1	1.017	0.332	-1.78
	H_1···N_3	1.868	0.0387	0.107
	N_2-H_4	1.017	0.332	-1.78
	H_4···N_4	1.868	0.0387	0.108
Structure	Bond	r	ρ	$\nabla^2\rho$
DS1	N_2-H_1	1.055	0.296	-1.51
	H_1···N_1	1.631	0.0640	0.127
	N_4-H_4	1.033	0.327	-1.77
	H_4···N_3	1.837	0.0424	0.121

[a] r in A. [b] ρ in e A^{-3}. [c] $\nabla^2\rho$ in e A^{-5}

$BP(OH)_2$

This molecule is the more thoroughly studied of the three isoelectronic systems considered here and was also the subject of the first electronic calculations performed by us some time ago.[23,24] In light of the search for molecular photomemories, it is not as interesting as the previous one because of the quite high measured fluorescence yield of 0.32 that, in principle, would hinder the presence of other photochemical paths such as the one eventually leading to the dark states. In any case we have carried out a search identical to the one for $BP(NH_2)_2$ and the obtained results are graphically displayed in Figures 4 and 5 (entirely equivalents to Figures 2 and 3 for $BP(NH_2)_2$). Globally the whole scenario is not very different from the one found for $BP(NH_2)_2$ though some subtle differences lead to quite a different photochemistry.

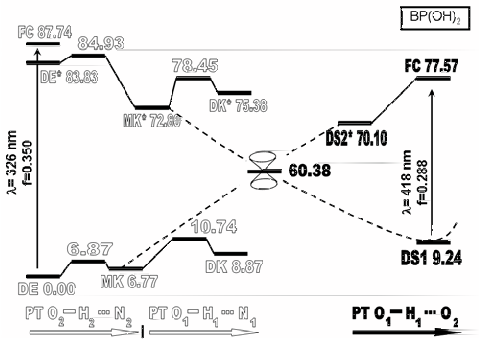

Figure 4. Relative energies (in kcal mol^{-1}) of the minimum-energy structures in S_0 (bottom) and S_1 (top) relevant to the double proton transfer and the rotation of the two pyridine rings in $BP(OH)_2$. Solid lines represent reaction paths that maintain the planar symmetry whereas out-of-plane reaction paths are indicated by dashed lines. A double-cone symbol is posted on the region of the conical intersection between S_0 and S_1. Arrows at the bottom indicate the proton that is transferred along any given path. The vertical arrows correspond to light absorptions relevant to the whole photochemical process (see text). White-filled letters, numbers and characters are used for processes in the bright zone that were already studied in previous works,[23,24] whereas the dark region, first discussed here, is indicated by black-filled letters, numbers and characters.

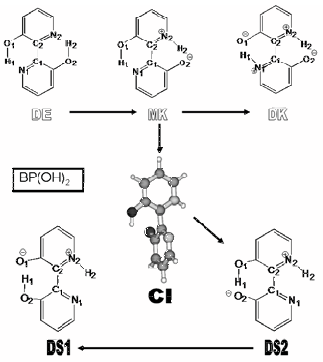

Figure 5. Schematic picture and numeration of atoms for the geometries of the stationary points and the conical intersection region of $BP(OH)_2$ in S_0 and S_1. The name of the structures and the meaning of the white-filled and black-filled letters is analogous to that of Figure 4.

The number of stationary points in the "bright" zone of the Figure is now larger: The ground electronic state S_0 displays three minima corresponding to the three possible protonation states. The most stable species is the dienol (DE) form. A single Proton transfer leads to the monoketo (MK) intermediate and an additional Proton transfer to the (final) diketo (DK) tautomer. The transition states linking the different minima have also been localized and are also depicted in Figure 4. Now all the stationary states directly located are fully planar. The first singlet excited electronic state S_1 comes from a $\pi\pi^*$ excitation. The S_0-S_1 transition is allowed (oscillator strength = 0.350) and the excitation wavelength has a maximum of absorption -Franck-Condon vertical transition- at 326 nm within our level of calculation (the experimental value is 340 nm). The relative stabilization of the tautomers dramatically changes in S_1 and the

more stable one is the MK* structure. However all the tautomeric forms are energetically available in S_1 as the FC structure lies higher in energy than any of them and also higher than the estimated energies of the transition states as seen in Figure 4.

A conical intersection has also been located in this case. The methodology used was the same outlined in the previous case and the characteristics of the located CI structure are also quite similar to the ones discussed for $BP(NH_2)_2$ with the two pyridine rings almost orthogonal to each other. The energy of this structure is also well below all the other ones in S_1 so that again the CI is energetically accessible from the S_1 potential energy surface. Again, this opens the door again to the dark states that can be obtained from relaxation of the CI in the ground state if the rotation between the two pyridyl rings does not bounce back (reverting to the original DE structure in S_0) but keeps going on leading to a 180º rotated planar structure. In this case the direct product of the rotation, DS2 using the same previous nomenclature, is not a stable structure as full optimization leads also to the spontaneous transfer of H_1 from O_1 to O_2 so that relaxation of the conical intersection directly leads to the DS1 tautomer.

The DS1 isomeric form of $BP(OH)_2$ is a photochromic species. It is a very stable structure and will only revert to the initial DE structure upon irradiation of a given wavelength, 418 nm according to our calculations. Within this wavelength the DS1 structure is excited up to the S_1 $\pi\pi^*$ state with a high oscillator strength (0.288). Contrary to the situation in S_0, there is no minimum energy structure DS1* in S_1 and the only located minimum corresponds to DS2*. This structure can be accessed directly from the Franck-Condon excitation and it has enough energy to lead again to the CI region where the system can evolve back to the bright states. Now the direct product of the full rotation is MK as it is a stable form of $BP(OH)_2$. However, MK will be reached with plenty of energy so that it will easily evolve to the more stable DE tautomer, in this way closing the whole photochemical cycle.

The Bader's AIM analysis of the DE and DS1 isomers of $BP(OH)_2$ is presented in Table 2. Results are quite similar to the ones previously discussed for $BP(NH_2)_2$. It is to be noted that here the N_2–H_2···N_1 intramolecular hydrogen bond in DS1 is quite weak. This result could be anticipated as it takes place through a 5-atom cycle. This fact prevents an additional path connecting DS2 to a structure mirroring DS1 involving the intramolecular transfer of the H_2 atom. Curiously enough, for $BP(NH_2)_2$ this intramolecular hydrogen bond was as strong as the other ones. As in the previous case the calculated dipolar moment of the DS1 photochromic species is large (5.890 D) and this physical property could be easily used to differentiate the DS1 state from the original DE symmetrical structure that has a null dipole moment. At the end, we have a very similar situation to the one discussed for $BP(NH_2)_2$ and, again, the conditions for a good photomemory device are fully accomplished. Without a molecular dynamics study of the competing processes considered here it is hard to tell whether the dark states will play a relevant role in the whole photochemistry of $BP(OH)_2$. As this (very complex) dynamical study is well beyond the scope of this paper we can only rely on the experimental data that indicates a high fluorescence yield, so that passing through the CI is probably not the preferred deactivation path of the photoexcited species, though there may still be a non negligible fraction of molecules going this way. Clearly, additional studies (both experimental and theoretical) are necessary to acquire a better knowledge of the fascinating possibilities of this deceivingly simple molecular system.

Table 2. Geometrical distances,[a] electronic densities,[b] and Laplacians[c] at the bond critical points of the X–H···Y bonds. See Figure 5 for atomic numeration.

$BP(OH)_2$				
Structure	Bond	r	ρ	$\nabla^2\rho$
DE	O_1-H_1	1.005	0.318	-1.75
	H_1···N_1	1.673	0.0581	0.123
	O_2-H_2	1.005	0.318	-1.75
	H_2···N_2	1.673	0.0581	0.123
Structure	Bond	r	ρ	$\nabla^2\rho$
DS1	O_2-H_1	1.052	0.271	-1.26
	H_1···O_1	1.410	0.0988	0.120
	N_2-H_2	1.029	0.330	-1.80
	H_2···N_1	1.941	0.0341	0.123

[a] r in A. [b] ρ in e A^{-3}. [c] $\nabla^2\rho$ in e A^{-5}

$BP(OH)(NH_2)$

For this asymmetric system there are two different paths for the intramolecular double hydrogen transfer depending on whether the first transfer involves the amino group (N-channel) or the hydroxyl group (O-channel). In order not to make the discussion too cumbersome, the two cases will be discussed together. Figures 6 and 7 depict the results for the N-channel whereas Figures 8 and 9 refer to the O-channel. For the bright states we are using the same nomenclature as in our previous theoretical work:[25] The initial form is the enol-amine (EA) whereas the product of the double hydrogen atom transfer is the keto-imine (KI) structure. A single H transfer leads from EA to the enol-imine (EI) or the keto-amine (KA) for the N- and O-channels respectively. As in $BP(NH_2)_2$, the stationary points are usually slightly out of plane, though in Figures 6 to 9 a planar geometry has been imposed with the obvious exception of the conical intersections that have the two pyridyl rings almost 90º twisted and an important degree of pyramidalization around the

nitrogen atoms. In fact, the geometries obtained here are quite similar to the ones properly located at the CASSCF level presented in our previous study of this molecule.[25]

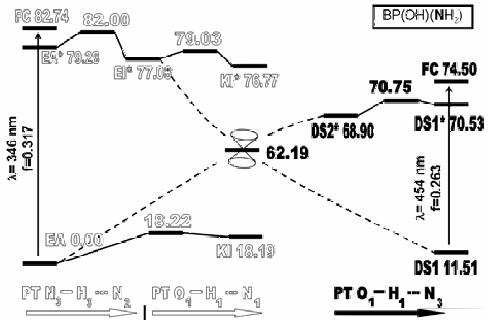

Figure 6. Relative energies (in kcal mol^{-1}) of the planar structures in S_0 (bottom) and S_1 (top) relevant to the double proton transfer and the rotation of the two pyridine rings in BP(OH)(NH_2) along the N-channel. Solid lines represent reaction paths that maintain the planar symmetry whereas out-of-plane reaction paths are indicated by dashed lines. A double-cone symbol is posted on the region of the conical intersection between S_0 and S_1. Arrows at the bottom indicate the proton that is transferred along any given path. The vertical arrows correspond to light absorptions relevant to the whole photochemical process (see text). White-filled letters, numbers and characters are used for processes in the bright zone that were already studied in a previous work,[25] whereas the dark region, first discussed here, is indicated by black-filled letters, numbers and characters.

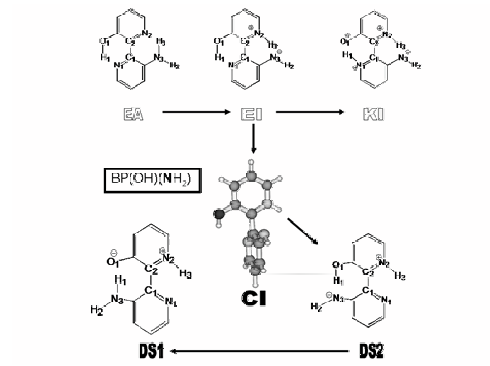

Figure 7. Schematic picture and numeration of atoms for the geometries of the stationary points and the conical intersection region of BP(OH)(NH_2) in S_0 and S_1 found along the N-channel. The name of the structures and the meaning of the white-filled and black-filled letters is analogous to that of Figure 6.

There are two minimum energy structures in the "bright" region of S_0, though the KI tautomer is barely stable as it lies only 0.03 kcal mol^{-1} below the transition state linking it to the original, and more stable, EA tautomer. The transition to the S_1 state from EA is allowed (oscillator strength: 0.317) and, as usual, it corresponds to a $\pi\pi^*$ electronic excitation. From the vertical accessed state (FC structure in Figures 6 and 8) several hydrogen-atom transfers are available. In the N-channel, Figure 6, the KI* product is the more stable one though the EI* structure is almost degenerate in energy. From this last structure, as in the previous cases, a conical intersection region can be accessed upon internal rotation of the two pyridyne rings. The CI is clearly the lowest energy structure in S_1 and, again, passage through it may lead to the dark states. Similarly to what was found for BP(OH)$_2$, only the DS1 structure (the one that has already transferred the hydrogen atom) is stable in S_0. From this photochromic species the reverse photochemical path can start through irradiation of light at 454 nm that puts the system in the $\pi\pi^*$ S_1 state with a quite high oscillator strength of 0.263. The initial accessed geometry (FC structure) has energy enough to proceed to the hydrogen-atom transfer leading to the now stable DS2* tautomer that, in turn, is able to access again the conical intersection region and so, revert back to the bright zone of the S_0 potential energy surface.

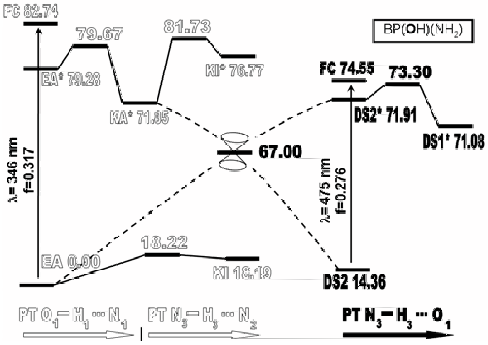

Figure 8. Relative energies (in kcal mol^{-1}) of the planar structures in S_0 (bottom) and S_1 (top) relevant to the double proton transfer and the rotation of the two pyridine rings in BP(OH)(NH_2) along the O-channel. Solid lines represent reaction paths that maintain the planar symmetry whereas out-of-plane reaction paths are indicated by dashed lines. A double-cone symbol is posted on the region of the conical intersection between S_0 and S_1. Arrows at the bottom indicate the proton that is transferred along any given path. The vertical arrows correspond to light absorptions relevant to the whole photochemical process (see text). White-filled letters, numbers and characters are used for processes in the bright zone that were already studied in a previous work,[25] whereas the dark region, first discussed here, is indicated by black-filled letters, numbers and characters.

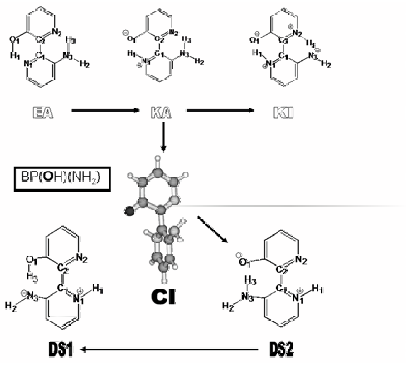

Figure 9. Schematic picture and numeration of atoms for the geometries of the stationary points and the conical intersection region of BP(OH)(NH_2) in S_0 and S_1 found along the O-channel. The name of the structures and the meaning of the white-filled and black-filled letters is analogous to that of Figure 8.

As for the O-channel path, it presents some peculiarities that are worth highlighting. In this case the KA* tautomer, obtained through a single Proton transfer, is the most stable structure in the bright zone of the S_1 potential energy surface. KA* is, in fact, the more stable minimum energy planar structure of $BP(OH)(NH_2)$ in S_1 so that the O-channel path is energetically favored over the N-channel path as discussed earlier.[25] As it is the norm in all the systems analyzed so far, a conical intersection region can be accessed from KA* leading to the dark region of the ground electronic state. Now the Proton transfer does not spontaneously occur and DS2 is the only stable form and the final photochromic species. From this point we can start the back Proton transfer with irradiation of 475 nm light that puts the system in the $\pi\pi^*$ S_1 state with a high oscillator strength (0.276). Once in the excited state, ESIPT might take place as DS1* is a stable species, even lower in energy than the optimized DS2* form. In any case, tautomerization in S_1 does not lead to any new photochemical path. Alternatively, internal rotation of the two pyridine rings in DS2* leads, energetically downhill, to the CI region where, as usual, the whole photochemical cycle can be closed through a full 180º rotation that leads again to the initial EA structure.

As in the previous cases, the AIM analysis was performed for the initial EA structure and the stable photochromic species in the N-channel (DS1) and the O-channel (DS2). Results are shown in Table 3. A global comparison of the values presented in Table 3 does not reveal any striking difference. In all the cases the two intramolecular hydrogen bonds are well constituted and so, intramolecular hydrogen transfer is available and internal rotation of the two pyridine rings is energetically costly. These two characteristics are essential in order to have a bistable system, a required condition for a photomemory molecular device. Here, the choice of the physical property that could be used to differentiate (read) the two stable forms of $BP(OH)(NH_2)$ is not so obvious as the original EA structure is no longer symmetric (i.e. it does not possess an inversion center) and so it has a permanent dipole moment of 3.001 D, smaller than the calculated value of the two dark states: 3.607 D (N-channel) and 5.411 D (O-channel) but not negligible so that EA will probably absorb microwave radiation. In that case a more careful look at the molecular properties of EA as compared to the ones of the dark states would be necessary to find a property to discriminate the two photochromic forms. For instance, an infrared (vibrational) absorption band found at clearly different wavelengths in the two forms would be enough for that purpose.

Table 3. Geometrical distances,[a] electronic densities,[b] and Laplacians[c] at the bond critical points of the X–H···Y bonds. See Figures 7 and 9 for atomic numeration.

$BP(OH)(NH_2)$				
Structure	Bond	r	ρ	$\nabla^2\rho$
EA	O_T-H_1	1.009	0.314	-1.69
	H_1···N_1	1.629	0.0651	0.128
	N_3-H_3	1.018	0.332	-1.78
	H_3···N_2	1.903	0.0357	0.0988
Structure	Bond	r	ρ	$\nabla^2\rho$
N-channel DS1	N_3-H_1	1.041	0.309	-1.62
	H_1···O_1	1.610	0.0592	0.164
	N_2-H_3	1.031	0.329	-1.78
	H_3···N_1	1.878	0.0389	0.114
Structure	Bond	r	ρ	$\nabla^2\rho$
O-channel DS2	N_3-H_3	1.041	0.309	-1.62
	H_3···O_1	1.610	0.0592	0.164
	N_1-H_1	1.031	0.329	-1.78
	H_1···N_2	1.878	0.0389	0.114

[a] r in A. [b] ρ in e A^{-3}. [c] $\nabla^2\rho$ in e A^{-5}

Globally, the photochemistry of $BP(OH)(NH_2)$ is more complex than the ones of the precedent systems because here the asymmetry of the molecule increases the number of reaction paths but no great differences arise in the global plot. In the absence of dynamical simulations and, in this case, any experimental data, it is hard to say whether the photochemistry of this molecule will differ from that of the two precedent isolectronic systems. At first sight, the fluorescence quantum yield of $BP(OH)(NH_2)$ should not be high as the more stable EI* and KA* species, resulting from single Proton transfers, have no corresponding minimum energy structure in S_0 and KI, the product of the full double Proton transfer, is barely stable. Low fluorescence is a prior condition to access the conical intersection region, a fact that opens the door to the formation of the photochromic species. Attainment of these, up to now, unknown isomeric species may depend on a subtle balance within the geometries and energies of the numerous stationary points and conical intersection regions located in both the ground and first singlet excited electronic states so that it cannot be easily anticipated whether a given molecular system will be better suited to become an ideal photomemory device.

Conclusion

In the previous section the potential energy surfaces of the ground (S_0) and first singlet excited (S_1) electronic states of three bipyridyl isoelectronic species have been carefully analyzed. In all the systems the energies of the tautomers corresponding to the single and double hydrogen-atom transfer and the transition states linking them have been calculated. Also, the presence of conical intersections between S_0 and S_1 that are reached upon internal rotation of the two pyridyl rings has been confirmed in the region of

the single hydrogen-atom transfer and, most interesting, the existence of a whole family of "dark" states has been disclosed. These dark states can only be accessed upon irradiation of light of a given wavelength and they are predicted to be stable in normal conditions so that they may act as photochromic species. Radiation with a light of a quite different wavelength would easily revert the process transforming the photochromic species into the "original" one that would be able to start again the process. As a whole, the photochemistry of the three bipyridyl compounds would conform to the properties of an ideal photomemory as detailed in the introduction section. Comparison of the photocycle for an "ideal" photomemory (Figure 1b) and the actual behavior of the three studied compounds (Figures 2, 4, 6 and 8) is another clear proof in favor of this argument.

In light of the results presented in this paper, the more likely candidate to become a photomemory device is the $BP(NH_2)_2$ system as in this case, following the initial excitation, the path to the conical intersection seems the most likely one given that fluorescence is known to proceed with a quite low quantum yield (~10^{-5}), and this result can be envisaged from our theoretical results as explained in the previous section. For $BP(OH)_2$, the more thoroughly studied system from the experimental point of view, the quantum yield of fluorescence is much higher (0.32) so that the internal conversion path through the conical intersection is a less likely process, again in accord with our theoretical calculations. In any case, the other conditions required for a photomemory device are fully accomplished by the two systems: The photochromic species is stable enough; there is a physical property (absorption of microwave radiation) able to easily discriminate the two forms and light of a different wavelength can reverse the whole process. As for the "hybrid" $BP(OH)(NH_2)$, there is no previous experimental work on it and we only know from the previous literature that it has been synthesized.[30] The whole photochemistry is expected more complex as now the asymmetry of the molecule allows for two hydrogen transfer channels depending on whether the first transferred hydrogen departs from a hydroxyl or an amino group. A full comparison of our results allow us to predict a quantum yield for $BP(OH)(NH_2)$ intermediate between the one of $BP(OH)_2$ and $BP(NH_2)_2$. In any case, there is no way to further assess the possibility to reach the different photochromic species without performing an ambitious (and expensive) dynamical study that consider all the subtleties of the potential energy surfaces of S_0 and S_1 and their crossing regions. Work devoted to this aim is presently in progress in our laboratory.

The very rich photochemistry of the bipyridyl compounds allows for discussion on additional applications in the technological field. Even if, from now on, the discussion goes on a more speculative track, it is worth mentioning the possibility to use the bipyridyl systems as molecular motors and/or rotors.[31,32] Given that the initial and photochromic forms in S_0 are interchanged through internal rotation, a continuous irradiation using the two wavelengths that activate the interconversion would result in a continuous internal rotation of the molecule. That is, we have a molecule that is able to absorb radiation and transform the energy into mechanical (rotational) energy. To really have a molecular motor it would be necessary to additionally restrict the internal rotation to proceed always in the same direction.[33] This could be accomplished, for instance, through addition of some bulk substituent with enantiomeric character to the bipyridyl compound.

Another, up to now, unexplored field is the possibility to control the internal rotation of the bipyridyl systems by the surrounding media. As the initial species and its photochromic partner can only be interconnected through internal rotation, the full cycle is to be controlled by the rigidity of the external medium where the full reaction takes place. That is, the ability to internally rotate the two (bulk) pyridyl rings may be severely restricted depending on the viscosity of the medium specially when sizeable substituents are introduced in the rings. It could be expected that the more hindered the internal rotation, the lower the difference between the $BP(OH)_2$ and $BP(NH_2)_2$ quantum yields. By changing the electronic properties of the substituents (apolar, polar or even ionic) it could be possible to tune the system to be more sensitive to a specific property of the solvent. This fact opens the door to the use of these systems as molecular or nano viscometers an idea that was foreseen several years ago.[34] The usefulness of bipyridyl derivatives as molecular rotors and/or viscometers relies on the predominance of the photochromic species as the final product after irradiation of the original compound. For this reason, the few experimental data known up to now and our electronic results point to the $BP(NH_2)_2$ system as the more suited species to act not only as an ideal photomemory device but also as a molecular rotor and/or viscometer. In any case, we hope that the results and discussion presented in this paper may appeal the scientific curiosity of the chemistry world so that the bipyridyl systems, mainly the diamino and the hybrid systems, barely studied up to now, could be the subject of more ambitious works at the molecular level that may confirm (or deny) our tentatively proposed new applications.

Computational Details Section

Electronic density functional based methods have been used to explore the topology of the ground (S_0) and first $\pi\pi^*$ singlet excited (S_1) electronic states. Density Functional Theory (DFT) and Time Dependent-DFT (TDDFT)[35,36] optimizations have been performed for the S_0 and S_1 states respectively. TDDFT has been successfully used to study other related ESIPT systems.[36-38] The three parameter hybrid functional of Becke with the correlation functional of Lee, Yang and Parr (B3LYP)[39,40] has been chosen. The Turbomole program (version 5.4)[41,42], which implements analytical gradients at the TDDFT level, has been used to perform the TDDFT calculations.

Also Atoms In Molecules (AIM) analysis have been performed at the DFT level with the Gaussian03 package.[43] As we stated in a previous work,[44] the B3LYP functionals used in the Gaussian03 and Turbomole packages differ very little in the relative stability of the calculated points, which implies a very little effect on our results. This small difference comes from the use of a different form of the local correlation functional: The Gaussian03 package uses the VWN(III) local correlation functional, whereas Turbomole uses VWN(V).[45]

Multireference Complete Active Space Self-Consistent Field method (CASSCF)[46] calculations have been carried out with the MOLCAS program (Version 6.4).[47] The electronic energy of S_0 and S_1 states has been obtained, using a state-average with equal weights for both states, with an active space of 10 electrons and 10 molecular orbitals which includes the 5 highest occupied and the 5 lowest unoccupied molecular orbitals. Note that this active space is probably not large enough to correctly describe the whole potential energy surface but it has been used just to analyze the presence of conical intersections between the S_0 and S_1 states. A larger active space would be necessary to compare the different regions of the potential energy surface.

In all cases, to obtain a good description of the proton and charge transfer processes on excited states, the 6-31G(d,p)[48,49] basis has been used for the hydrogen and carbon atoms, while additional diffuse functions (6-31G+(d,p) basis)[48,49] have been added to the oxygen and nitrogen atoms.

Acknowledgements

We are grateful for financial support from the Ministerio de Ciencia e innovación through project CTQ2008-02403/BQU, CTQ2008-06536/BQU, CTQ2008-02856/BQU and from the Generalitat de Catalunya (2005SGR00400 and 2005SGR00117). Use of computational facilities at the Centre de Supercomputació de Catalunya is also acknowledged.

1. G. C. Pimentel, A. L. McClellan, *The Hydrogen Bond*; Freeman, San Francisco, 1960.
2. S. Scheiner, *Acc. Chem. Res.* 1985, *18*, 174.
3. M. V. Basilevsky, M. V. Vener, *Russian Chem. Rev.* 2003, *72*, 1.
4. S. J. Formosinho, L. G. Arnaut, *J. Photochem. Photobiol. A* 1993, *75*, 21.
5. (a) S. M. Ormson, R. G. Brown, *Prog. React. Kinet.* 1994, *19*, 45; (b) D. Le Gourrierec, S. M. Ormson, R. G. Brown, *Prog. React. Kinet.* 1994, *19*, 211.
6. A. Douhal, F. Lahmani, A. H. Zewail, *Chem. Phys.* 1996, *207*, 477.
7. H. J. Heller, H. R. Blattmann, *Pure Appl. Chem.* 1972, *30*, 145; 1974, *36*, 141.
8. J. –E. A. Otterstedt, *J. Chem. Phys.* 1973, *58*, 5716.
9. N. Mataga, *Pure Appl. Chem.* 1984, *56*, 1255.
10. W. Domcke, D. R. Yarkony, H. Köppel (Eds.), *Conical Intersections. Electronic Structure , Dynamics and Spectroscopy*; World Scientific Publishing, 2004.
11. E. Gindensperger, I. Burghardt, L. S. Cederbaum, *J. Chem. Phys.* 2006, *124*, 144103.
12. J. M. Ortiz-Sánchez, R. Gelabert, M. Moreno, J. M. Lluch, *J. Chem. Phys.* 2008, *129*, 214308.
13. E. Hadjoudis, I. M. Mavridis, *Chem. Soc. Rev.* 2004, *33*, 579.
14. H. Mori, E. Miyoshi, *Bull. Chem. Soc. Jpn.* 2007, *80*, 1335.
15. M. Sauer, *Proc. Natl. Acad. Sci. U. S. A.* 2005, *102*, 9433.
16. F. M. Raymo, *Adv. Mater.* 2002, *14*, 401.
17. A. L. Sobolewski, *Phys. Chem. Chem. Phys.* 2008, *10*, 1243.
18. H. Zhang, P. Van der Meulen, M. Glasbeek, *Chem. Phys. Lett.* 1996, *253*, 97.
19. D. Marks, H. Zhang, M. Glasbeek, P. Borowicz, A. Grabowska, *Chem. Phys. Lett.* 1997, *275*, 370.
20. P. Toele, H. Zhang, M. Glasbeek, *J. Phys. Chem. A* 2002, *106*, 3651.
21. D. Marks, P. Prosposito, H. Zhang, M. Glasbeek, *Chem. Phys. Lett.* 1998, *289*, 535.
22. P. Prosposito, D. Marks, H. Zhang, M. Glasbeek, *J. Phys. Chem. A* 1998, *102*, 8894.
23. R. Gelabert, M. Moreno, J. M. Lluch, *ChemPhysChem* 2004, *5*, 1372.
24. J. M. Ortiz-Sánchez, R. Gelabert, M. Moreno, J. M. Lluch, *ChemPhysChem* 2007, *8*, 1199.
25. J. M. Ortiz-Sánchez, R. Gelabert, M. Moreno, J. M. Lluch, *ChemPhysChem* 2008, *9*, 2068.
26. P. Toele, M. Glasbeek, *Chem. Phys. Lett.* 2005, 407, 487.
27. B. G. Levine, C. Ko, J. Quenneville, T. J. Martinez, *Mol. Phys.* 2006, 104, 1039.
28. J. M. Anglada, J. M. Bofill, *J. Comput. Chem.* 1997, 18, 992.
29. R. W. F. Bader, H. Essen, *J. Chem. Phys.* 1984, 80, 1943.
30. L. Kaczmarek, *Pol. J. Chem.* 1985, 59, 1141.
31. G. S. Kottas, L. I. Clarke, D. Horinek, J. Michl, *Chem. Rev.* 2005, 105, 1281.
32. Z. Dominguez, T.-A. Khunog, H. Dang, C. N. Sanrame, J. E. Nuñez, M. A. Garcia-Garibay, *J. Am. Chem. Soc.* 2003, 125, 8827
33. J. Vicario, M. Walko, A. Meetsma, B. L. Feringa, *J. Am. Chem. Soc.* 2006, 128, 5127

34. P. Turkewitsch, B. Wandelt, R. R. Ganju, G. D. Darling, W. S. Powell, *Chem. Phys. Lett.* 1996, *260*, 142.
35. R. Bauernschmitt, R. Ahlrichs, *Chem. Phys. Lett.* 1996, 256, 454.
36. A. Dreuw, M. Head-Gordon, *Chem. Rev.* 2005, 105, 4009.
37. A. L. Sobolewski, W. Domcke, *Phys. Chem. Chem. Phys.* 1999, 1, 33065.
38. A. J. A. Aquino, H. Lischka, C. Hattig, *J. Phys. Chem. A* 2005, 109, 3201.
39. A. D. Becke, *J. Chem. Phys.* 1993, 98, 5648.
40. C. T. Lee, W. T. Yang, R. G. Parr, *Phys. Rev. B* 1988, 37, 785.
41. F. Furche, R. Ahlrichs, *J. Chem. Phys.* 2002, 117, 7433.
42. R. Ahlrichs, M. Bär, M. Haser, H. Horn, C. Kolmel, *Chem. Phys. Lett.* 1989, 162, 165.
43. Gaussian 03, Revision C.02, M. J. Frisch, G. W. Trucks, H. B. Schlegel, G. E. Scuseria, M. A. Robb, J. R. Cheeseman, J. A. Montgomery, Jr., T. Vreven, K. N. Kudin, J. C. Burant, J. M. Millam, S. S. Iyengar, J. Tomasi, V. Barone, B. Mennucci, M. Cossi, G. Scalmani, N. Rega, G. A. Petersson, H. Nakatsuji, M. Hada, M. Ehara, K. Toyota, R. Fukuda, J. Hasegawa, M. Ishida, T. Nakajima, Y. Honda, O. Kitao, H. Nakai, M. Klene, X. Li, J. E. Knox, H. P. Hratchian, J. B. Cross, V. Bakken, C. Adamo, J. Jaramillo, R. Gomperts, R. E. Stratmann, O. Yazyev, A. J. Austin, R. Cammi, C. Pomelli, J. W. Ochterski, P. Y. Ayala, K. Morokuma, G. A. Voth, P. Salvador, J. J. Dannenberg, V. G. Zakrzewski, S. Dapprich, A. D. Daniels, M. C. Strain, O. Farkas, D. K. Malick, A. D. Rabuck, K. Raghavachari, J. B. Foresman, J. V. Ortiz, Q. Cui, A. G. Baboul, S. Clifford, J. Cioslowski, B. B. Stefanov, G. Liu, A. Liashenko, P. Piskorz, I. Komaromi, R. L. Martin, D. J. Fox, T. Keith, M. A. Al-Laham, C. Y. Peng, A. Nanayakkara, M. Challacombe, P. M. W. Gill, B. Johnson, W. Chen, M. W. Wong, C. Gonzalez, and J. A. Pople, Gaussian, Inc., Wallingford CT, 2004.
44. J. M. Ortiz-Sánchez, R. Gelabert, M. Moreno, J. M. Lluch, *J Phys. Chem. A* 2006, 110, 4649.
45. S. H. Vosko, L. Wilk, M. Nusair, *Can. J. Phys.* 1980, 58, 1200.
46. K. Andersson, P-A. Malmqvist, B. O. Ross, *J. Chem. Phys.* 1992, 96, 1218.
47. MOLCAS (version 6.2), K. Andersson, M. Barysz, A. Bernhardsson, M. R. A. Blomberg, Y. Carissan, D. L. Cooper, M. P. Fischer, L. Gagliardi, C. de Graaf, B. A. Hess *et al.*, Lund University, Sweden, 2000.
48. P. C. Hariharan, J. A. Pople, *Theor. Chim. Acta* 1973, 28, 213.
49. M. M. Franci, W. J. Pietro, W. J. Hehre, J. S. Binkley, M. S. Gordon, D. J. Defrees, J. A. Pople, *J. Chem. Phys.* 1982, 77, 365

B

Electronic methods

B.1 *Ab initio* methods

It might be daring to state that the comprehension of the chemical phenomena lies entirely on the understanding of the chemical bond. Nevertheless, *The Nature of the Chemical Bond*, by Linus Pauling (1939), is one of the very first published text books on theoretical chemistry, a book that still keeps its validity today. Heitler and London introduced in 1927 the first theoretical wave function of the ground state of H_2, which included only covalent contributions to the bond:

$$\Psi_{HL}(\vec{x_1}, \vec{x_2}) = \frac{1}{\sqrt{2}} \left[\psi_A(\vec{r_1})\psi_B(\vec{r_2}) + \psi_A(\vec{r_2})\psi_B(\vec{r_1})\right] \times \Theta(S_1, S_2) \qquad \text{(B.1)}$$

where $\psi_X(\vec{r})$ is the atomic orbital centered on the atom X, $\vec{x} = (\vec{r}, S)$ is the collective spatial-spin coordinate, and $\Theta(S_1, S_2)$ is the normalized singlet spin wave function. That idea would be later refined by Pauling, Slater and van Vleck in 1931, who elaborated the Valence Bond (VB) theory, which allowed the inclusion of ionic contributions to the bond. At the same time, Hund and Mulliken developed a different approach to the chemical bond, which would be known as Molecular Orbital (MO) theory. In contrast to the VB theory, the N-electron wave function in MO theory is built up as an antisymmetrized Slater determinant (or antisymmetrized linear combination):

$$\Psi_{MO}(N) = \frac{1}{\sqrt{N!}} \begin{vmatrix} \chi_1(1) & \chi_2(1) & \dots & \chi_n(1) \\ \chi_1(2) & \chi_2(2) & \dots & \chi_n(2) \\ \vdots & \vdots & \ddots & \vdots \\ \chi_1(N) & \chi_2(N) & \dots & \chi_n(N) \end{vmatrix} \tag{B.2}$$

where each function χ constitutes a molecular spin-orbital, expressed as a normalized linear combination of the atomic orbitals, according to the linear combination of atomic orbitals (LCAO-MO) approach. Note that the wave function can be either constructed with one molecular orbital Ψ_{MO}, or a linear combination of several other Ψ_{MO}.

When $\Psi_{MO}(N)$ (Eq. B.2) is expanded, the resulting expression for the wave function contains both the covalent and non-bonding ionic contributions to the chemical bond. Hence, for some time, it was believed that both VB and MO approaches could give the same description of the electronic structure, and the choice of one description or another was left to convenience. However, when Roothaan introduced the concept of basis functions (as a way to represent the atomic orbitals from which $\chi_n(N)$ is built), it was found that Ψ_{MO} was easier to handle if it was written in terms of antisymmetrized products of orthonormal molecular orbitals.[1] For that reason, most of the theoretical methods developed in order to solve the electronic Schrödinger equation are based on the MO theory rather than on the VB theory.

The resolution of the electronic Schrödinger equation based on the MO theory procedure is as follows: given a finite basis set, the coefficients of the molecular orbital expansion are determined in order to obtain the minimum electronic energy from Ψ_{MO}. Besides, according to the variational theorem, the energy thus obtained is as close as possible, but aboveto respect the exact solution. Depending on the basis set size and the number of spin-spatial configurations included in the molecular orbital expansion, a plethora of hyerarchic quantum chemical methods have been developed since the early 1930s, known as *ab initio* methods or molecular orbital approach methods.

B.1.1 The Hartree-Fock approach

The Hartree-Fock (HF) approximation constitutes the simplest of the possible models that we can construct within the MO theory. Within a finite basis set, the N-electron HF wave function is built up with one single configuration Ψ_{MO}(Eq. B.2). After the BO approximation is summoned, the nuclear kinetic energy operator and nucleus-nucleus potential energy operator are ommitted from the molecular Hamiltonian, and the resulting Hamiltonian can be factorized into one term contaning only the one-electron operators and a second term which consists on the bielectronic electron-electron repulsion:

$$\hat{H} = \sum_{i=1}^{N} \hat{h}(i) + \sum_{i<j}^{N} \frac{1}{r_{ij}} \tag{B.3}$$

where $\hat{h}(i)$ contains the kinetic energy of the electron i and the attractive potential energy created by the nuclei of the molecule:

$$\hat{h}(i) = \sum_{i=1}^{N} \left[\frac{-\nabla_i^2}{2} + \sum_{\alpha=1}^{M} \frac{-Z_\alpha}{\mid \vec{r_i} - \vec{R_\alpha} \mid} \right] \tag{B.4}$$

At this point, we would like to calculate the electronic energy associated to the trial wave function Ψ_{HF}. Since the wave function Ψ_{HF} (Eq. B.2) is normalized, we can evaluate the expected value for the corresponding energy as:

$$E_{HF} = \langle \Psi_{HF} \mid \hat{H} \mid \Psi_{HF} \rangle \tag{B.5}$$

This equation implies a dependence between the energy and the trial wave function Ψ. Since Ψ is not a function of parameters but of spin-orbitals, according to Eq. B.2, E is a functional of Ψ, and may be represented as $E[\Psi]$. Replacing Eq. B.2 into Eq. B.5, and given that the $\hat{h}_i$ operator only operates over the electron i, and the second term in Eq. B.3 cannot be separated into monoelectronic integrals, we arrive at the HF energy associated to the determinant Ψ_{HF}:

$$E = \sum_{i=1}^{N} h_{ii} + \frac{1}{2} \sum_{i=1}^{N} \sum_{j=1}^{N} (J_{ij} - K_{ij}) \tag{B.6}$$

where:

$$h_{ii} = \langle \chi_i(1) \mid \hat{h}(1) \mid \chi_i(1) \rangle \tag{B.7}$$

$$J_{ij} = \langle \chi_i(1)\chi_j(2) \mid \frac{1}{r_{12}} \mid \chi_i(1)\chi_j(2) \rangle \tag{B.8}$$

$$K_{ij} = \langle \chi_i(1)\chi_j(2) \mid \frac{1}{r_{12}} \mid \chi_j(1)\chi_i(2) \rangle \tag{B.9}$$

h_{ii}, J_{ij} and K_{ij} correspond to the mono-electronic, Coulomb and exchange integrals, respectively. The exchange integral, which does not have any classical correspondence, arises because of the antisymmetric nature of the determinant wave function.

Eq. B.6 provides the electronic energy derived from a wave function Ψ_{HF}, built up from a starting set of spin-orbitals $\chi_N(N)$. The question which may arise now is: is this set of spin-orbitals $\{\chi_i\}_{i=1}^{N}$ the one which minimizes the energy? Most probably not. To this purpose, the HF method employes the variational principle in order to find the optimal molecular orbitals with which the energy of such a polielectronic function will be stationary. In other words, with the HF method we find the best function within a restricted set

of functions (only one determinant), using the word "best" in a variational context. Thus, the Slater determinant (Eq. B.2) that minimizes the energy in Eq. B.5 is the one for which a small change in the wave function implies a null change in the energy:

$$\begin{aligned} E[\Psi + \delta\Psi] &= \langle \Psi \mid \hat{H} \mid \Psi \rangle + \langle \delta\Psi \mid \hat{H} \mid \Psi \rangle \\ &+ \langle \Psi \mid \hat{H} \mid \delta\Psi \rangle + \langle \delta\Psi \mid \hat{H} \mid \delta\Psi \rangle \end{aligned} \tag{B.10}$$

the second and third terms represent the first-order variation of the energy δE, which must be zero:

$$\delta E = \langle \Psi \mid \hat{H} \mid \delta\Psi \rangle + \langle \delta\Psi \mid \hat{H} \mid \delta\Psi \rangle = 0 \tag{B.11}$$

Given that the spin-orbitals $\{\chi_i\}_{i=1}^{N}$ must be orthonormal functions:

$$\langle \chi_i \mid \chi_j \rangle = \delta_{ij} \tag{B.12}$$

the optimal Slater determinant must satisfy Eqs. B.11 and B.12. The problem of finding the best spin-orbitals is a problem of minimizing a function submitted to restrictions, and the Lagrange multipliers procedure must be adopted:

$$L = E - \sum_{i=1}^{N} \sum_{j=1}^{N} \varepsilon_{ij} g_{ij} \tag{B.13}$$

where L is the Lagrangian function to be minimized, g_{ij} are the terms corresponding to the restrictions, and ε_{ij} are the Lagrange multipliers to be determined. Replacing Eq. B.6 into Eq. B.13, the set of spin-orbitals which minimize the energy are:

$$\hat{f}(1)\chi_i(1) = \sum_{j=1}^{N} \varepsilon_{ij}\chi_j(1) \quad i = 1, 2, \ldots, N \tag{B.14}$$

These set of equations are known as the HF equations, where $\hat{f}(1)$ is the Fock operator:

$$\hat{f}(1) = \hat{h}(1) + \sum_{j=1}^{N} (\hat{J}_j(1) - \hat{K}_j(1)) \tag{B.15}$$

This operator contains the monoelectronic operator $\hat{h}(1)$ and the bielectronic operators $\hat{J}$ and $\hat{K}$:

$$\hat{J}_j(1)\chi_i(1) = \left(\int \chi_j^*(2) \frac{1}{r_{12}} \chi_j(2) d\tau_2 \right) \chi_i(1) \tag{B.16}$$

$$\hat{K}_j(1)\chi_i(1) = \left(\int \chi_j^*(2) \frac{1}{r_{12}} \chi_i(2) d\tau_2 \right) \chi_i(1) \tag{B.17}$$

$\hat{J}$ and $\hat{K}$ are known as the Coulomb and exchange operators, respectively. According to Eq. B.14, the HF equations are written as a linear eigenvalue equation, however, they might best be described as a pseudo-eigenvalue equations since the Fock operator has a functional dependence on the solutions $\{\chi_i\}$, through the Coulomb and exchange operators. Thus the HF equations are really nonlinear equations and have to be solved by iterative procedures. That is the reason why the Hartree-Fock method is also known as Self Consistent Field method (SCF).

The Fock equations in the form of Eq. B.14 imply an integro-diferential mathematical problem which is far from being feasible for the majority of molecular systems, and new approximations need to be introduced. In 1951, Roothaan and Hall proposed to express the molecular orbitals as a linear combination of a set of basis functions. Such functions are centered in the atoms within the molecule, and are usually named as atomic orbitals (AO). So now, given a molecular orbital Ψ_i expressed as a lineal combination of the set of basis functions φ_v:

$$\Psi_i = \sum_{v=1}^{K} c_{vi} \varphi_v \tag{B.18}$$

replacing (B.18) in (B.14) we arrive at:

$$\sum_{v=1}^{K} c_{vi}\langle\varphi_\mu(1) \mid \hat{f}(1) \mid \varphi_v(1)\rangle = \sum_{\mu=1}^{K} c_{vi}\epsilon_i\langle\varphi_\mu(1) \mid \varphi_v(1)\rangle \quad \mu = 1, 2, 3, \ldots, K \tag{B.19}$$

where the integrals on the first member correspond to the matrix elements of the Fock operator in the basis φ_v ($F_{\mu v}$), whereas the integrals in the second term are the overlap integrals of the basis functions φ_v ($S_{\mu v}$). Then, Eq. B.19 can be rewritten as:

$$\sum_{v=1}^{K}[F_{\mu v} - \epsilon_i S_{\mu v}]c_{vi} = 0 \quad \mu = 1, 2, 3, \ldots, K \tag{B.20}$$

which are known as the Roothann-Hall equations. Note that the integro-diferential problem presented in Eqs. B.15 has been replaced by a set of algebraic equations, in which the only procedure is to evaluate the best expansion coeficients c_{vi} given an accepted and unquestionable set of atomic orbitals. Given that the ground state of a large number of molecules, both in their equilibrium geometry region and vicinities, are well described with only one electronic configuration, the HF approximation gained a lot of success over the years; even though the energy obtained is just qualitatively correct.

The HF method can be applied both to closed and open shell systems. For open-shell systems, the use of an unrestricted open-shell set of spin orbitals leads to unrestricted open-shell wave functions via the Pople-Nesbet equations. As no open-shell systems have been treated in this thesis, the derivation of the Pople-Nesbet equations have been skipped, but the interested reader can find the information elsewhere.[2,3]

The mathematical importance of the HF approximation is undeniable, as it represents the starting point for more accurate methods. Only a few computational methods of quantum chemistry bypass the HF approximation.

However, if such algorithms cannot be automatically implemented in a kind of routine or blackbox procedure, we would be still calculating by hand the most simple molecules such as water or methane. For that reason, not only the developers but also the people who worked to implement such algorithms deserve our attention. The excellent work of Obara and Saiko[4] represent a good example of several efficient algorithms (which can be easily coded) that can be used to compute mono- and bi-electronic integrals for electronic methods such as HF.

B.1.2 Post Hartree-Fock methods

As has been presented in the previous section, the HF *ansatz* of the electronic wave function corresponds to an antisymetrized product of spin-orbital functions. The physical consequence of this method is that each electron feels the mean potential field generated by all the other electrons. This is clearly an unphysical situation, as the motion of a single electron depends on the instantaneous position of every electron and thus, their movement is said to be correlated. This is the so called electronic correlation. The HF *ansatz* is the reason why the SCF methodology is inadequate to quantitatively describe the majority of the polielectronic systems. In order to correct this inacuracy, it is necessary to add the electronic correlation to the wave function. To do so, three major methodologies, known as post Hartree-Fock methods, have been developed: Configuration Interaction (CI), Many Body Perturbation Theory (MBPT) and Coupled Cluster (CC) methods. In what follows in the present section, only the Configuration Interaction method will be presented, as this method has been employed in some of the calculations of this thesis. For further information about Many Body Perturbation Theory and Coupled Cluster approach, the reader is directed to some excellent text books on quantum chemistry.[3,5,6]

The CI method is the simplest of the aforementioned post HF methods, conceptually speaking. Basically, the wave function is built as a linear combination of determinants formed with the spin-orbitals obtained from the HF

method:

$$\Psi_{CI} = c_0\Psi_0 + \sum_S c_S\Psi_S + \sum_D c_D\Psi_D + \sum_T c_T\Psi_T + \dots \tag{B.21}$$

where Ψ_0 is the HF determinant, and Ψ_S, Ψ_D, Ψ_T,... are determinants which represent single, double, triple,... excitations of the fundamental determinant Ψ_0 *i.e.* to replace one, two, three,... occupied spin orbitals with virtual spin orbitals. The exact electronic energy can be obtained, if the atomic orbitals basis set is complete, and every possible excited determinant is considered. However, such a calculation is far from being feasible for the majority of the molecular systems due to the huge number of excited states. Instead of that, the monoelectronic basis set of atomic orbitals must be truncated. Now, if we consider all the possible determinants within a finite monoelectronic basis set, it is possible to obtain the exact eigenvectors and eigenfunctions for that space. The resulting solutions are known as full configuration interaction (FCI) solutions, in other words, the exact solutions within a given basis space. Nevertheless, even the FCI solutions are only accessible for small molecular systems, which forces to truncate both the monoelectronic and polielectronic basis sets. These two limitations are the main error sources in every quantum chemical calculation.

B.1.3 Configuration Interaction with Single Excitations

If we limit the expansion of the wave function to only singly excited determinants formed by replacing, with respect to the reference wave function, one occupied spin orbital with a virtual spin orbital, the CI method is reduced to the Configuration Interaction Singles (CIS) approach:

$$\Psi_{CIS} = \sum_{ia} c_i^a\Psi_i^a(r) \tag{B.22}$$

where $\Psi_i^a(r)$ denotes the singly excited Slater determinant formed replacing the occupied orbital i with the virtual orbital a, and c_i^a are the expansion

coefficients. Since the singly excited determinants constitute electronic excited configurations of the molecule, it is possible to derive expression for the computation of excitation energies and total energies within electronic excited states. Replacing Eq. B.22 into the electronic Schrödinger equation, and projecting onto $\langle \Psi_j^b \mid$, yields:

$$\sum_{ia} \langle \Psi_j^b \mid \hat{H} \mid \Psi_i^a \rangle c_i^a = E_{CIS} \sum_{ia} c_i^a \delta_{ij} \delta_{ab} \tag{B.23}$$

where:

$$\langle \Psi_j^b \mid \hat{H} \mid \Psi_i^a \rangle = (E_0 + \varepsilon_a - \varepsilon_i)\delta_{ij}\delta ab + (ia \mid\mid jb) \tag{B.24}$$

with Eqs. B.23 and B.24, it is easy to obtain an expression for the CIS excitation energies, defined as $\omega_{CIS} = E_{CIS} - E_0$:

$$\begin{aligned} &\sum_{ia} \{(\varepsilon_a - \varepsilon_i)\delta ij\delta_{ab} + (ia \mid\mid jb)\} c_i^a = \\ &\omega_{CIS} \sum_{ia} c_i^a \delta_{ij}\delta_{ab} \langle \Psi_j^b \mid \hat{H} \mid \Psi_i^a \rangle = \\ &(E_0 + \varepsilon_a - \varepsilon_i)\delta_{ij}\delta ab + (ia \mid\mid jb) \end{aligned} \tag{B.25}$$

where ϵ_a and ϵ_i are the orbital energies of the single-electron orbitals φ_a and φ_i, respectively, and $(ia \mid\mid jb)$ corresponds to the antisymmetrized two-electron integrals. Eq. B.25 can be rewritten as a secular equation:

$$(\mathbf{H} - \omega)\mathbf{X} = 0 \tag{B.26}$$

where $\mathbf{H}$ is the matrix representation of the Hamiltonian in the space of the singly excited determinants, $\mathbf{X}$ is the matrix of the CIS expansion coefficients, and ω is the diagonal matrix of the excitation energies. Thus, solving Eq. B.26 to obtain the excitation enrgies ω, is only a matter of diagonalizing the matrix $\mathbf{H}$.

Besides, we can obtain an analytic expression for the total energy of electronic excited state from Eq. B.25 by adding E_0 and multiplying from the left with the corresponding CIS vectors:

$$E_{CIS} = E_{HF} + \sum_{ia} (c_i^a)^2 (\epsilon_a - \epsilon_i) + \sum_{ia,jb} c_i^a (ia \mid\mid jb) \tag{B.27}$$

Note that according to Eq. B.27, E_{CIS} is analytically differentiable with respect to external parameters, for example, nuclear displacements and external fields. This allows for the application of analytic gradient techniques for the calculation of excited-state properties, such as equilibrium geometries and vibrational frequencies. That is the reason of why the CIS approach was widely employed for many years in the treatment of excited electronic states.[7]

Despite these advantages, the CIS method presents some important flaws. First, electron correlation is neglected, as according to Brillouni's theorem, the solutions of these equations are orthogonal to the ground state.[2] Thus, excitation energies are largely overestimated by $\sim$1 eV. Second, CIS does not obey the Thomas-Reiche-Kuhn dipole sum, which states that the sum of transition dipole moments must be equal to the number of electrons. Thus, transition moments cannot be expected to be more than qualitatively accurate.[8] And third, the computational cost for CIS calculations scales with n^4, being n the number of occupied molecular orbitals. Thus, large basis set calculations become easily very expensive. In order to overcome these limitations, it is necessary to go beyond the CI approach.

B.1.4 Complete Active Space Self-Consistent Field methods

As we have previously said, the CIS method is not able to include the electronic correlation of a given system, by virtue of Brillouni's theorem. Nevertheless, this situation can be overcome if not only mono-excited but multi-excited determinants are included in the wave function's expansion. Alternatively, the molecular orbitals coefficients of each determinant can also

be optimized, so that they are not the same as in the ground state, and hence not longer orthogonal to the solutions of the CI equations. Among the methodologies adressed to the optimization of both the coefficients of the determinants and the molecular orbitals coefficients of each determinant, the multiconfigurational self-consistent field (MCSCF) approach should be mentioned. There exist many molecular systems in which several excited electronic configurations are in close degeneracy with the ground state. For these systems, the appropiate wave function should contemplate the multiconfigurational nature of the electronic structure, and the MCSCF approach is very suitable.

The main restriction of the MCSCF methods is the size of the reference wave function. Within a few configurations, the computational cost grows exponentially. A possible solution for that limitation is the choice of a reduced configurational space which has chemical relevance for the system under study. Such a choice must be done based on chemical criteria and (why not?) chemical intuition, according to the information available on the system. This is the main idea of the most popular MCSCF method among the theoretical chemical community, the complete active space SCF (CASSCF) method,[9–11] developed by B. O. Ross and collaborators at the University of Lund.

Within this method, the configurational space is specified by a number of active orbitals and electrons, with which all the possible configurations (consistent with a given spatial and spin symmetry) will be formed. Thus, the CASSCF wave function is a FCI in the configurational space defined by the active space. For example, one might define an active space (11,8), meaning that 11 valence electrons are distributed between all configurations that can be constructed from 8 molecular orbitals. However, the number of configurations quickly increases with the number of active orbitals, along with the computational cost.

In order to perform a consistent CASSCF study of a chemical reaction, the active space describing reactants, products, transition states, interme-

diates... should be the same. Thus, the choice of the active space must be flexible enough to consistently describe all the chemical processes under study. Along a chemical reaction, the energetic order of the orbitals which are relevant to describe the change in the electronic structure are likely to change (and they probably will do) from reactants to products. An active space large enough to foresee and include such changes easily becomes unfeasible. Mainly for that reason, CASSCF methods are very well suited for spectroscopy studies, but more limited for reactivity. It is precisely the choice of the active space the main argument which both detractors and supporters use to justify the rejection and the greatness, respectively, of this kind of methodologies. It is true that the selection of the active space is not a black-box procedure. It might not be straightforward, but it is far from being impossible for most cases. It helps a lot to know something about the electronic structure of the system under study. As a general rule, the active space should contain those molecular orbitals whose occupation numbers will significantly vary from 2 and 0 along the chemical process.

The CASSCF method includes the static correlation, also called long range interaction, which describes the effect of quasidegeneracies between configurations. The dynamic correlation, which reflects the short range electron-electron interaction, can be properly described by variational methods, like the multireference-CI (MRCI) method,[12] or by perturbation theory, like the CAS perturbation theory to second order (CASPT2) method.[13,14]

The *ansatz* of the wave function according the MRCI method is:

$$\Psi_{MRCI} = \Psi_{ref} + \Psi_{SD} \tag{B.28}$$

where Ψ_{ref} is a reference function, for example a CASSCF function or part of it, and Ψ_{SD} represents single and double replacement configurations. However, as previously commented, the CI methods grow quickly out of hand, and are only feasible for small molecules. A second procedure to include the dynamic correlation is by using the perturbation theory, up to second order. In second order perturbation theory, we solve a set of linear equations:

$$(\hat{H}_0 - E_0)\Psi_1 = -(\hat{H}_1 - E_0)\Psi_0 \tag{B.29}$$

where Ψ_1 is the first order wave function and $\hat{H}_1$ is the perturbation, defined as $\hat{H} - \hat{H}_0$. Then, the second order energy is given as:

$$E_2 = \langle \Psi_0 \mid \hat{H}_1 \mid \Psi_1 \rangle \tag{B.30}$$

Thus, only terms in Ψ_1 that interact with the reference function Ψ_0 will contribute to the second order energy. Ψ_0 is the CASSCF reference function and $\mid \Psi_1\rangle$ can be defined as:

$$\mid \Psi_1\rangle = \sum_{pq,rs} C_{pq,rs}\hat{E}_{pq}\hat{E}_{rs} \mid \Psi_0\rangle \tag{B.31}$$

where the indices q, s refer to inactive or active orbitals, and p, r refer to active or secondary orbital.

Because the CASSCF method is a multiconfigurational approach, it is very suitable to compute regions of the PES where energy crossing points occur, like conical intersections. A minimum energy crossing point (MECP) can be obtained by finding the lowest energy of the excited state at which two states are degenerate. Hence, in an optimization calculation, the energy difference berween the two states can be used as a constraint:

$$r = E_1 - E_0 \tag{B.32}$$

However, this constraint condition will only lead to a single MECP. If we are interested in exploring the seam of a conical intersection, for example, we should also explore the spatial extension of the intersection subspace by combining the constraint of the intersection in Eq. B.32 with those employed for a minimum energy path search.

B.2 Electronic density-based methods

The theoretical methods presented so far, are enclosed within the MO theory, in which the energy of the system is a functional of the well known wave function ($E[\Psi]$). That functional relationship could be read as "by placing an appropiate wave function Ψ inside the [ ], we can obtain the energy E". The functional $E[\Psi]$ is perfectly known, as seen in Eq .B.5. However, the Ψ is a function which depends on the $3N$ spatial coordinates of the N particles describing the system. The dependence of so many variables makes Ψ a very complex mathematical function to deal with in order to obtain the energy.

The density functional theory (DFT) provides a very similar framework (conceptually speaking) to the one of the *ab initio* methods, in the way we can express the energy of the system as a functional of a different magnitude: the electronic density $\rho(\vec{r})$. Density provides information about how something is distributed in space, and for a chemical system, electron density tells us where the electrons are likely to be. Because of the electronic density is a function which depends only on 3 spatial coordinates, it becomes an attractive function to work with, in contrast to the $3N$-dimensional wave function Ψ. Hence, in the DFT scheme, the number of variables is considerably reduced. However, with regard to the *ab initio* methods, the main disadvantage of DFT is that the functional $E[\rho(\vec{r})]$ is not known, and only approximations to it can be made.

B.2.1 Density Functional Theory

The electronic density of a system of N-electrons can be defined as:

$$\rho(\vec{r}) = N \int \mid \Psi(\vec{r}_1, \vec{r}_2, \ldots, \vec{r}_N,) \mid^2 d\vec{r}_2, \ldots, d\vec{r}_N \tag{B.33}$$

and its corresponding quantum operator is:

$$\hat{\rho}(\vec{r}) = \langle \Psi \mid \sum_{i=1}^{N} \delta(\vec{r} - \vec{r_i}) \mid \Psi \rangle \tag{B.34}$$

The main difference between the wave function Ψ and the electronic density $\rho(\vec{r})$ is that the latter is an observable magnitude, whereas the former not. Through X-ray crystallography experiments, the electronic density, defined in the real space $\vec{r}$, can be determined using the expression:

$$\rho(\vec{r}) = \int \frac{d\vec{q}}{(2\pi)^3} F(\vec{q}) e^{i\vec{q}\cdot\vec{r}} \tag{B.35}$$

where $F(\vec{q})$ is the Fourier transform of the electronic density defined in the reciprocal space $\vec{q}$. Since its development by Sir William Henry Bragg and Sir William Lawrence Bragg,[15] X-ray crystallography has become one of the most piercing experimental techniques to unveil the structure of molecules, from inorganic compounds to large biomolecules.[16–18] But it also provides the starting point for the development of the DFT methods.

A single molecule can be fully characterized if the atomic number of the nuclei, their positions, and the total number of electrons are known *i.e.* $\{Z_\alpha, \vec{R}_\alpha, N\}$. The question that now arises is: if we knew the electronic density of a molecule, by X-ray crystalography for example, could we obtain from it the information $\{Z_\alpha, \vec{R}_\alpha, N\}$? The answer is yes.

The total number of electrons can be straightforward obtained integrating the electronic density over all the electronic space:

$$\int \rho(\vec{r}) d\vec{r} = N \tag{B.36}$$

The position of the nuclei can be obtained by taking into account that the electronic density is a maximum over the nuclei. Thus, the maxima of the $\rho(\vec{r})$ function directly give $\{\vec{R}_\alpha\}$. Finally, according to Kato's nucleus-electron cusp condition,[19,20] the derivative of the logarithm of the electronic density gives the atomic numbers of the nuclei:

$$-\frac{1}{2}\left(\frac{\partial \log \rho(\vec{r})}{\partial \vec{r}}\right)_{\vec{r}\to\vec{R}_\alpha} = Z_\alpha, \quad \forall \quad \alpha \tag{B.37}$$

However, it has to be noted that Kato's theorem is only valid in the electronic ground state.[1] To sum up, with the electronic density it is possible to have

a complete knowledge of a molecule ($\{Z_A, \vec{R}_A, N\}$), which in turn allows us to derive its corresponding Hamiltonian operator (plus the electron-electron repulsion operator). From its solution, we can obtain its associated wave function, and therefore all the observable properties of the system:

$$\rho(\vec{r}) \Rightarrow \{Z_\alpha, \vec{R}_\alpha, N\} \Rightarrow \hat{H} \Rightarrow \Psi \Rightarrow \text{Observable molecular properties}$$

From this explanation, it cannot be inferred that the relationship between $\rho(\vec{r})$ and the corresponding wave function of the system is unique. Otherwise, all the formulation of the DFT theory would fall into a problem of ambiguity. This can be clarified by means of the Hohenberg-Kohn theorem (HK). Hohenberg and Kohn proved, by *reductio ad absurdum*, that two different external potential could not generate the same electron density. The justification of the HK theorem is widely known in theoretical chemistry, and can be found in many reference works.[1,21]

Accepting the univocal correspondence between external potentials, wave functions and electronic densities, any molecular property A can be then determined by the density $\rho(\vec{r})$ of the ground state:

$$\Psi_0 = \Psi_0[\rho(\vec{r})] \Rightarrow \langle A_0 \rangle = A[\rho(\vec{r})] = \langle \Psi_0[\rho(\vec{r})] \mid \hat{A} \mid \Psi_0[\rho(\vec{r})] \rangle \tag{B.38}$$

Concretely for the electronic energy of a molecule:

$$E[\rho] = T_e[\rho] + E_{en}[\rho] + E_{ee}[\rho] \tag{B.39}$$

where $T_e[\rho]$ is the electronic kinetic energy, $E_{en}[\rho]$ is the electron-nucleus energy interaction and $E_{ee}[\rho]$ is the electron-electron energy interaction. Even though the HK theorem is mathematically exact and states the univocal correspondence $\rho(\vec{r}) \leftrightarrow \hat{H}$, it cannot unveil the explicit analytic form of such functionals, except for local one-particle operators, like the external (nuclear) potential. Therefore, approximate solutions have to be adopted in order to

generate accurate expressions of the unknown functional. Some important contributions are the statistical mechanical approach by Thomas and Fermi,[1] or the constrained search procedure of M. Levy.[22] Here only the Kohn-Sham (KS) implementation of DFT will be presented, as it has gained ground within the quantum chemical community, mainly due to its similarity with the SCF method.

According to the KS model, for each real system of interacting electrons with ground state density $\rho(\vec{r})$, there exists a suitable chosen model system of non-interacting electrons which exhibits the same ground state density $\rho_S(\vec{r})$:

$$\rho_S(\vec{r}) = \sum_{i=1}^{N/2} 2 \mid \varphi_i(r) \mid^2 = \rho(\vec{r}) \tag{B.40}$$

In that way, Equation B.39 can be rewritten as:

$$E[\rho] = T_S[\rho] + E_{en}[\rho] + J[\rho] + E_{xc}[\rho] \tag{B.41}$$

where $J[\rho]$ is the classical electron-electron Coulomb interaction energy, $T_S[\rho]$ is the kinetic energy of a non-interacting N-electron system (which is an approximation to the the real $T_e[\rho]$) and $E_{xc}[\rho]$ is the so-called exchange-correlation energy term:

$$T_S[\rho] = \sum_{i=1}^{N} \langle \Psi_i \mid -\frac{1}{2}\nabla^2_{(1)} \mid \Psi_i \rangle \tag{B.42}$$

$$E_{xc}[\rho] = T_e[\rho] - T_S[\rho] + E_{ee}[\rho] - J[\rho] \tag{B.43}$$

where $\nabla^2_{(1)}$ is the one-particle kinetic term. The KS procedure for minimizing the energy in Eq. B.40 reminds us of the HF procedure. One has to find a set of orthogonal molecular orbitals Ψ_i which minimize the energy. With these restrictions, the KS equations become:

$$\hat{h}_{KS}(1)\Psi_i = \big[-\frac{1}{2}\nabla^2_{(1)} + \hat{v}_{ef}(1)\big]\Psi_i = \epsilon_i\Psi_i \tag{B.44}$$

where $\hat{v}_{ef}(1)$:

$$\hat{v}_{ef}(1) = \hat{V}_{en}(1) + 2\sum_{i=1}^{N}\hat{J}_i(1) + \hat{V}_{xc}(1) \tag{B.45}$$

is an effective potential which includes the electron-nucleus attractive potential V_{en}, the classical electron-electron repulsive potential $\sum_{i=1}^{N} J_i(1)$, and the exchange-correlation potential $\hat{V}_{xc} = \frac{\partial E_{xc}}{\partial\rho(\vec{r})}$. Given that the effective potential depends on the total electronic density via Eq. B.45, the KS equations represent a self-consistent field (SCF) problem that has to be solved in iterative fashion. However, the KS equations are formally simpler than the Fock equations because the effective potential is local, in contrast to the non-local nature of the exchange of the Fock operator (see Eq. B.17). Besides, the KS procedure takes electron correlation into account, while HF does not. Even though the mathematical development of Kohn and Sham is exact, there is a very important weak point of the whole theory: The analytic form of the exchange-correlation functional $E_{xc}[\rho]$ is not known.

The reliability of a DFT calculation then lies in the capacity of generating approximate $E_{xc}[\rho]$ functionals. In that direction, three major approaches have been developed. Slater proposed in the early 1950s the local-density approximation (LDA), where the functional is considered to depend only on the electronic density at the coordinate where the functional is evaluated. Under such approximation, an analytic expression for the $E_{xc}[\rho]$ functional can only be obtained for a homogeneous electron gas. For that system, Dirac developed the expression for the exchange energy:

$$E_x^{LDA}(\rho) = -\frac{3}{2}\left(\frac{3}{4\pi}\right)^{1/3}\int \rho^{4/3}(\vec{r})d\vec{r} \tag{B.46}$$

The expression for the correlation energy was obtained from Monte Carlo calculations by Vosko, Wilk and Nusair in 1980,[23] called the VWN func-

tional. Even though the homogeneous electron gas approximation worked surprisingly well for small molecules, it soon became clear that such an approximation was too simple in order to treat larger molecular systems.

One way to correct the limitations of the LDA functionals is to consider that the functional also depends on the gradient of the density at the same coordinate where it is evaluated, which is the basis of the generalized gradient approximations (GGA). Usually, GGA functionals start off from known LDA functionals, adding correcting terms to the gradient. Some of the most well-knonw GGA functionals are the Becke's functional of 1988 (B88), the Perdew and Wang functions of 1991 (PW91), or the Lee, Yang and Parr functional (LYP). These functionals can be combined among them to give the new functionals like BPW91 or BLYP. In spite of the improvements that the GGA functionals supposed, difficulties in expressing the exchange part of the energy still arise. They could be relieved by including a component of the exact exchange energy calculated from HF theory. Functionals of this type are known as hybrid functionals, like the B3-LYP, probably the most widely used functional among the quantum chemical community.

In many cases, with GGA and hybrid functionals it is possible to achieve results with a similar precision compared to post-HF methods (like MP2), but with a substantially lower computational cost. For that reason, DFT methods have become an important alternative in the study of many-electron systems.

B.2.2 Time-Dependent DFT

The traditional KS formulation of the DFT is limited to time-independent systems, that is, ground states (lowest energy states of a given symmetry and multiplicity). However, many molecular properties in quantum mechanical electronic structure theory can be considered to be the result of the response of a time-dependent perturbation, like excitation energies or oscillator strengths. If one wants to apply the DFT formalism to these situations one could, for instance, first establish an analogous time-dependent

version of the HK theorem, and then reformulate the KS procedure in a time-dependent scheme. These steps lead to the theoretical foundation of the Time-Dependent Density Functional Theory (TDDFT), which is mainly concerned with the change in molecular properties induced by an external and perturbing time-dependent field (often an electric field).

An aspect on TDDFT that might confuse people, is that the time dependence referred to in TDDFT is usually not time dependence of the nuclei (that is dynamics!). Instead, it is the time dependence of the electrons when the fixed nuclear framework is subject to a periodic radiation field.

The TDDFT method is based on the Runge-Gross (RG) theorem,[24] which is the time-dependent analogue of the HK theorem in the ground state DFT. The basic principle is very similar to the HK theorem: an univocal correspondence between an external time-dependent potential, the initial state on which the potential acts, and the resulting time-dependent electronic density is proved. The interested reader can find an elegant proof of that theorem in Ref. 7.

The time-dependent KS equations can be derived in a similar fashion that the KS DFT equations. The existence of a model time-dependent system of non-interacting electrons with the same one-electron density as the true time-depedent system of interacting electrons, can be assured by virtue of the generalization of the RG theorem by van Leeuwen.[8] The resulting time-dependent Kohn-Sham equations are:

$$i\frac{\partial}{\partial}\varphi(\vec{r},t) = \left(-\frac{1}{2}\nabla^2 + v_{KS}(\vec{r},t)\right)\varphi(\vec{r},t) \tag{B.47}$$

where the time-dependent effective potential $v_{KS}(\vec{r},t)$ is:

$$v_{KS}(\vec{r},t) = v_e(r,t) + \int \frac{\rho(r',t)}{\mid r - r' \mid} d^3r' + \frac{\delta A_{xc}[\rho]}{\delta\rho(r,t)} \tag{B.48}$$

Here, δ denotes functional differentation (not function differentiation ∂). $v_e(r,t)$ is the time-dependent external potential, and the integral term approximates the electron-electron repulsion.

In order to approximate the effective potential (the last term in Eq. B.48) Runge and Gross adopted a Dirac's action formulation:[24]

$$A[\Psi] = \int \langle \Psi(t) \mid \hat{H} - i\frac{\partial}{\partial t} \mid \Psi(t) \rangle \tag{B.49}$$

Given the unique mapping between densities and wave functions, Runge and Gross treated the Dirac's action as a density functional and, derived a formal expression for the exchange-correlation component of the action, which determines the exchange-correlation potential by functional differentiation. However, approximate expression for the action functional are even less known than for the functional $E_{xc}[\rho]$ in DFT.[1] A practical solution for this problem is to assume the external potential to be time-independent, which constitutes the so-called adiabatic local density approximation (ALDA):

$$\frac{\delta A_{xc}[\rho]}{\delta \rho(r,t)} = \frac{\delta E_{xc}[\rho_t]}{\delta \rho_t(r)} \tag{B.50}$$

Since this replacement is *only* exact when the external potential is time-independent, one can argue that it should be a reasonable approximation when the external potential is only weakly time-dependent, and then the ground state exchange-correlation functional E_{xc} can be used.

In order to obtain excitation energies and oscillator strengths from the time-dependent KS equations, the KS wave function can be propagated in time, which is referred as known as real-time TDDFT.[8] However, the most widely used approach, and also the only one implemented in standard quantum chemistry packages, is the linear-response TDDFT. Basically, if a external perturbation is small enough so that it does not completely destruct the ground state structure of the system, one can analyze the linear response of the system. The variation of the system will depend (to first order) only on the ground state wave function, so that we can simply use all the properties of DFT. Within this context, excitation energies can be obtained in several ways. The most direct is through the introduction of a basis set in the KS orbitals and rewrite the time-dependent KS equations as secular equations,[8]

a procedure that recalls the one seen for the CIS level. In fact, CIS can be obtained as a limit of TDDFT when using a hybrid functional with 100% of HF exchange.

As electronic correlation is introduced in DFT via the electronic density $\rho(\vec{r})$ (and so it is in TDDFT), the values of vertical excitation energies are more accurate when compared with CIS. Moreover, TDDFT satisfies the Thomas-Reiche-Kuhn dipole sum. However, there exist some notorious disadvantages. It is well-known that TDDFT has severe problems with the correct description of Rydberg states, valence states of molecules exhibiting extended π systems, and doubly excited states; but most important, TDDFT systematically overstabilizes charge-transfer states.[25,26] To our knowledge, some semiquantitative procedures have been proposed to correct this shortcoming of TDDFT,[27–30] but the correct TDDFT description of such states is still an unsolved problem.

Bibliography

[1] J. M. Mercero, J. M. Matxain, X. Lopez, D. M. York, A. Largo, L. A. Eriksson and J. M. Ugalde. Theoretical methods that help understanding the structure and reactivity of gas pahse ions. *Int. J. Mass Spectrom.*, 240(1):37 – 99, 2005.

[2] A. Szabo and N. S. Ostlund. *Modern quantum chemistry: Introduction*. Dover, New York, 1983.

[3] I. N. Levine. *Quantum chemistry*. Prentice Hall, 5th Edition, 2000.

[4] S. Obara and A. Saika. Efficient recursive computation of molecular integrals over Cartesian Gaussian functions. *J. Chem. Phys.*, 84(7):3963 – 3974, 1986.

[5] F. Jensen. *Introduction to computational chemistry*. John Wiley & Sons, Engalnd, 1999.

[6] C. J. Cramer. *Essentials of computational chemistry: Theories and models*. John Wiley & Sons, England, 2002.

[7] J. B. Foresman, M. Head-Gordon, J. A. Pople and M. J. Frisch. Toward a systematic molecular orbital theory for excited states. *J. Phys. Chem.*, 96(1):135 – 149, 1992.

[8] A. Dreuw and M. Head-Gordon. Single-refence ab initio methods for the calculation of excited states of large molecules. *Chem. Rev.*, 105(11):4009 – 4037, 2005.

[9] H. Werner. *Matrix-formulated direct multiconfiguration self-consistent field and multiconfiguration reference configuration-interaction methods*, pages 1 – 63. Advances in Chemical Physics 69. John Wiley & Sons, New York, Ab inition methods in Quantum Chemistry Part II edition, 1987.

[10] R. Shepard. *The multiconfiguration self-consistent field method*, pages 63 – 200. Advances in Chemical Physics 69. John Wiley & Sons, New York, Ab inition methods in Quantum Chemistry Part II edition, 1987.

[11] B. O. Ross. *The complete active space self-consistent field method and its applications in electronic structure calculations*, pages 399 – 455. Advances in Chemical Physics 69. John Wiley & Sons, New York, Ab initio methods in Quantum Chemistry Part II, 1987.

[12] B. O. Ross. A new method for large-scale CI calculations. *Chem. Phys. Lett.*, 15(2):153 – 159, 1972.

[13] K. Andersson, P.-Å. Malmqvist, B. O. Ross, A. J. Sadlej and K. Wolinski. Second-order perturbation theory with a CASSCF reference function. *J. Phys. Chem.*, 94(14):5483 – 5488, 1990.

[14] K. Andersson, P.-Å. Malmqvist and B. O. Ross. Second-order perturbation theory with a complete active space self-consistent field reference function. *J. Chem. Phys.*, 96(2):1218 – 1226, 1992.

[15] W. L. Bragg. *The diffraction of X-rays by crystals*, pages 370 – 382. Nobel Lectures, Physics 1901 – 1921. Elsevier Publishing Company, 1967.

[16] D. Crowfoot. X-ray single crystal photographs of insulin. *Nature*, 135:591 – 592, 1935.

[17] J. D. Dunitz, L. E. Orgel and A. Rich. The Crystal structure of ferrocene. *Acta Cryst.*, 9:373 – 375, 1956.

[18] J. Deisenhofer, O. Epp, K. Miki, R. Huber and H. Michel. Structure of the protein subunits in the photosynthetic reaction centre of (en italica Rhodopseudomonas viridis) at 3 Å resolution. *Nature*, 318(6047):618 – 624, 1985.

[19] T. Kato. On the eigenfunctions of many-particle systems in quantum mechanics. *Commun. Pure Appl. Math*, 10(2):151 – 177, 1957.

[20] E. Steiner. Charge densities in atoms. *J. Chem. Phys.*, 39(9):2365 – 2366, 1963.

[21] R. G. Parr and W. Yang. *Density-functional theory of atoms and molecules*. Oxford University Press, New York, 1989.

[22] M. Levy. Universal variational functionals of electron densities, first-order density matrices, and natural spin-orbitals and solution of the v-representability problem. *Proc. Natl. Acad. Sci.*, 76(12):6062 – 6065, 1979.

[23] S. H. Vosko, L. Wilk and M. Nusair. Accurate spin-dependent electron liquid correlation energies for local spin density calculations: A critical analysis. *Can. J. Phys.*, 58(8):1200 – 1211, 1980.

[24] E. Runge and E. K. U. Gross. Density-functional theory for time-dependent systems. *Phys. Rev. Lett.*, 52(12):997 – 1000, 1984.

[25] L. Serrano-Andrés and M. Merchán. Quantum chemistry of the excited state: 2005 review. *J. Mol. Struct.*, 729(1 – 2):99 – 108, 2005.

[26] R. Gelabert, M. Moreno and J. M. Lluch. The charge-transfer $\pi\pi^*$ excited state in the 7-Azaindole dimer. A hybrid configuration interactions singles/time-dependent density functional theory description. *J. Phys. Chem. A*, 110(3):1145 – 1151, 2006.

[27] A. Dreuw, G. R. Fleming and M. Head-Gordon. Charge-transfer state as a possible signature of a zeaxanthin-chlorophyll dimer in the non-photochemical quenching process in green plants. *J. Phys. Chem. B*, 107(27):6500 – 6503, 2003.

[28] Y. Tawada, T. Tsuneda, S. Yanagisawa, T. Yanai and K. Hirao. A long-range-corrected time-dependent density functional theory. *J. Chem. Phys.*, 120(18):8425 – 8433, 2004.

[29] M. Chiba, T. Tsuneda and K. Hirao. Excited state geometry optimizations by analytical energy gradient of long-range corrected time-dependent density functional theory. *J. Chem. Phys.*, 124(14):144106–1 – 144106–11, 2006.

[30] J. Neugebauer, O. Gritsenko and E. J. Baerends. Assessment of a simple correction for the long-range charge-transfer problem in time-dependent density-functional theory. *J. Chem. Phys.*, 124(21):214102–1 – 214102–11, 2006.

C

Mathematical derivation of the SMA's kinetic energy operator

According to our discussion on the dynamics of SMA in Section 5.1, our reduced SMA's dynamical model contains three significant fragments as for the ESIPT is concerned: the proton, the oxygen atom (attached to the aromatic ring) and the nitrogen-methyl segment. These fragments are related through the set of dynamical coordinates (R, r, ρ), as depicted in Figure 5.4 (c).

Assuming that the motion of the proton is restricted to a plane, a pair of Cartesian coordinates (x, y) can be assigned to each dynamical fragment. Hence, the kinetic energy operator can be initially written as:

$$\begin{aligned}\hat{T} &= -\frac{1}{2m_O}\left(\frac{\partial^2}{\partial x_O^2}+\frac{\partial^2}{\partial y_O^2}\right)-\frac{1}{2m_{NCH_3}}\left(\frac{\partial^2}{\partial x_{NCH_3}^2}+\frac{\partial^2}{\partial y_{NCH_3}^2}\right)\\ &\quad -\frac{1}{2m_H}\left(\frac{\partial^2}{\partial x_H^2}+\frac{\partial^2}{\partial y_H^2}\right)\end{aligned} \tag{C.1}$$

In order to derive a mathematical expression of $\hat{T}$ in terms of the dynamical set $\{R,\ r,\ \rho\}$, it is necessary to stablish the formal relationships between the six Cartesian coordinates in Eq. C.1 and the set (R, r, ρ). Given that both sets of coordinates must define the same space, we included three additional dynamical coordinates: the Cartesian coordinates of the center of mass $(x_{CM},\ y_{CM})$ and the in-plane global rotation angle (θ). From the representation of both sets of coordinates into a Cartesian coordinate system, as depicted in Figure 5.4 (d), it is possible to obtain the transformation relationships between the dynamical and Cartesian sets of coordinates:

$$R=\sqrt{\left(x_N-x_O\right)^2+\left(y_N-y_O\right)^2} \tag{C.2}$$

$$\begin{aligned}r &= \frac{\frac{1}{2}\left(x_{NCH_3}^2-x_O^2\right)+x_H\left(x_O^2-x_{NCH_3}^2\right)}{\sqrt{\left(x_O-x_{NCH_3}\right)^2+\left(y_O-y_{NCH_3}\right)^2}}\\ &+ \frac{\frac{1}{2}\left(y_{NCH_3}^2-y_O^2\right)+y_H\left(y_O^2-y_{NCH_3}^2\right)}{\sqrt{\left(x_O-x_{NCH_3}\right)^2+\left(y_O-y_{NCH_3}\right)^2}}\end{aligned} \tag{C.3}$$

$$\begin{aligned}\rho &= \left|\frac{x_H\left(y_O-y_{NCH_3}\right)+y_H\left(x_{NCH_3}-x_O\right)}{\sqrt{\left(x_O-x_{NCH_3}\right)^2+\left(y_O-y_{NCH_3}\right)^2}}\right|\\ &+ \left|\frac{x_O y_{NCH_3}-x_{NCH_3}y_O}{\sqrt{\left(x_O-x_{NCH_3}\right)^2+\left(y_O-y_{NCH_3}\right)^2}}\right|\end{aligned} \tag{C.4}$$

$$x_{CM} = \frac{m_O x_O + m_{NCH_3} x_{NCH_3} + m_H x_H}{m_O + m_{NCH_3} + m_H} \tag{C.5}$$

$$y_{CM} = \frac{m_O y_O + m_{NCH_3} y_{NCH_3} + m_H y_H}{m_O + m_{NCH_3} + m_H} \tag{C.6}$$

$$\theta = \arctan\left(\frac{y_{NCH_3} - y_O}{x_{NCH_3} - x_O}\right) \tag{C.7}$$

From Eqs. C.2-C.7, it is possible to express Eq. C.1 in terms of the dynamical set of coordinates, applying the chain rule. On the resulting expression of the kinetic energy operator, every second derivative term with respect to the center of mass can be separated, given the traslational motion of the center of mass has to be uncoupled from the internal motion. Taking 0 (for convenience) as the initial value for the angle θ, and assuming that the global in-plane rotation of the fragments are not significantly coupled to the proton transfer process (thus cancelling the derivative terms with respect to θ), we arrive to the final expression of $\hat{T}((R, r, \rho))$ introduced in Section 5.1:

$$\begin{aligned}
\widehat{T}_N = \; & - \frac{1}{2}\left(\frac{1}{m_{N-CH_3}} + \frac{1}{m_{O-ring}}\right)\frac{\partial^2}{\partial R^2} \\
& - \frac{1}{2}\left[\left(\frac{1}{m_{N-CH_3}} + \frac{1}{m_{O-ring}}\right)\left(\frac{1}{4} + \frac{\rho^2}{R^2}\right) + \frac{1}{m_H}\right]\frac{\partial^2}{\partial r^2} \\
& - \frac{1}{2}\left[\left(\frac{1}{m_{N-CH_3}} + \frac{1}{m_{O-ring}}\right)\left(\frac{1}{4} + \frac{r^2}{R^2}\right) + \frac{r}{R}\left(\frac{1}{m_{N-CH_3}} - \frac{1}{m_{O-ring}}\right) + \frac{1}{m_H}\right]\frac{\partial^2}{\partial \rho^2} \\
& + \frac{1}{2}\left(\frac{1}{m_{N-CH_3}} - \frac{1}{m_{O-ring}}\right)\frac{\partial}{\partial R}\frac{\partial}{\partial r} \\
& + \left[\frac{r\rho}{R^2}\left(\frac{1}{m_{N-CH_3}} + \frac{1}{m_{O-ring}}\right) + \frac{\rho}{2R}\left(\frac{1}{m_{N-CH_3}} - \frac{1}{m_{O-ring}}\right)\right]\frac{\partial}{\partial r}\frac{\partial}{\partial \rho} \\
& - \frac{1}{2R}\left(\frac{1}{m_{N-CH_3}} + \frac{1}{m_{O-ring}}\right)\frac{\partial}{\partial R}
\end{aligned}$$

(Continues on next page.)

$$+ \quad \frac{1}{2}\left[\frac{1}{R}\left(\frac{1}{m_{N-CH_3}}-\frac{1}{m_{O-ring}}\right)+\frac{r}{R^2}\left(\frac{1}{m_{N-CH_3}}+\frac{1}{m_{O-ring}}\right)\right]\frac{\partial}{\partial r}$$
$$+ \quad \frac{\rho}{2R^2}\left(\frac{1}{m_{N-CH_3}}+\frac{1}{m_{O-ring}}\right)\frac{\partial}{\partial \rho} \tag{C.8}$$

D

SMA's *Fortran77* routine

The construction of the PES corresponding to the dynamical simulations on SMA (see Paper II), was performed through the generation of 720 molecular geometries as a function of the set of dynamical coordinates (R, r, ρ). Here we present the *Fortran77* rutine coded to that end.

```
program SMAgeometry
implicit none
integer i,j
integer label1(12)
double precision x1(12,3)
integer label2(4)
double precision x2(4,3)
integer labelO,labelN,labelH
double precision xO(3),xN(3),xH(3)
double precision Rbig,Rsmall
double precision Nghost(3),Oghost(3)
```

```
      double precision Ulength,U(3),W(3)
      double precision deltaR,deltaRox,deltaRnit
      double precision UM,M(3),Vlength,V(3)
      double precision Mlength,Wlength,Hpos,dotprod
      double precision N(3),rho
C
C
      open (file='fragment_1.xyz',status='old',unit=10)
      do i=1,12
           read(10,*) label1(i),x1(i,1),x1(i,2),x1(i,3)
      end do
      close (unit=10)
      open (file='fragment_3.xyz',status='old',unit=10)
      do i=1,4
           read(10,*) label2(i),x2(i,1),x2(i,2),x2(i,3)
      end do
      open (file='fragment_oxigen.xyz',status='old',unit=10)
      read(10,*) labelO,xO(1),xO(2),xO(3)
      open (file='fragment_nitrogen.xyz',status='old',unit=10)
      read(10,*) labelN,xN(1),xN(2),xN(3)
      open (file='fragment_proto.xyz',status='old',unit=10)
      read(10,*) labelH,xH(1),xH(2),xH(3)
      read(5,*) Rbig,Rsmall,Rho
C
C
      do i=1,12
           write(6,*) label1(i),x1(i,1),x1(i,2),x1(i,3)
      end do
C
C
      do i=1,3
           Nghost(i)=xN(i)
           Oghost(i)=xO(i)
      end do
C
C
      Ulength=0.0d0
      do i=1,3
           U(i)=xO(i)-xN(i)
           M(i)=xH(i)-0.5d0*(xO(i)+xN(i))
           Ulength=Ulength+U(i)**2
```

```
            Mlength=Mlength+M(i)**2
         end do
         Ulength=sqrt(Ulength)
         Mlength=sqrt(Mlength)
         do i=1,3
            U(i)=U(i)/Ulength
            M(i)=M(i)/Mlength
         end do
C
C
         deltaR=Rbig-Ulength
C
C
         deltaRox=deltaR/(1.0d0+sqrt(16.0d0/29.0d0))
         deltaRnit=deltaR/(1.0d0+sqrt(29.0d0/16.0d0))
C
C
         do i=1,3
            xO(i)=Oghost(i)+U(i)*deltaRox
            xN(i)=Nghost(i)-U(i)*deltaRnit
         end do
         write(6,*) labelO,(xO(i),i=1,3)
         write(6,*) labelN,(xN(i),i=1,3)
C
C
         do i=1,4
            do j=1,3
               x2(i,j)=x2(i,j)-U(j)*deltaRnit
            end do
         end do
         do i=1,4
            write(6,*) label2(i),(x2(i,j),j=1,3)
         end do
C
C
         UM=0.0d0
         do i=1,3
            UM=UM+U(i)*M(i)
         end do
         UM=UM*Ulength*Mlength
         Wlength=0.0d0
```

```
        do i=1,3
             W(i)=(U(i)*Ulength)-(Ulength**2/UM)*M(i)*Mlength
             Wlength=Wlength+W(i)**2
        end do
        Wlength=sqrt(Wlength)
        do i=1,3
             W(i)=W(i)/Wlength
        end do
        Hpos=0.0d0
        do i=1,3
             Hpos=Hpos+M(i)*W(i)*Wlength*Mlength
        end do
        Vlength=0.0d0
        do i=1,3
             V(i)=xO(i)-xN(i)
             Vlength=Vlength+V(i)**2
        end do
        Vlength=sqrt(Vlength)
        do i=1,3
             V(i)=V(i)/Vlength
        end do
        do i=1,3
             N(i)=xH(i)-0.5d0*(xO(i)+xN(i))-Rsmall*V(i)
        end do
        dotprod=0.0d0
        do i=1,3
             dotprod=dotprod+N(i)*W(i)
        end do
C
C
        do i=1,3
            xH(i)=0.5d0*(xO(i)+xN(i))-Rsmall*V(i)+W(i)*(dotprod-rho)
        end do
        write(6,*) labelH,(xH(i),i=1,3)
C
C
        end
```

For the correct running of this routine, the SMA molecule is divided in five portions, and each portion is provided to the code via five external files: *fragment_1.xyz*, *fragment_2.xyz*, *fragment_nitrogen.xyz*, *fragment_oxigen.xyz* and *fragment_proto.xyz*.

Each file contains the atomic number and the Cartesian coordinates (in Å) of each atom. Concretely, files *fragment_1.xyz* and *fragment_2.xyz* display the aromatic ring and the C–H portion, and the the methyl group, respectively; whereas files *fragment_nitrogen.xyz*, *fragment_oxigen.xyz* and *fragment_proto.xyz* contain the position of the nitrogen, oxygen and the proton, respectively.

In what follows, we include an example of a starting SMA geometry divided on each file:

`fragment_1.xyz`

```
 6   -2.125116    1.667348    0.000000
 6   -0.738163    1.675638    0.000000
 6    0.000000    0.477899    0.000000
 6   -0.695501   -0.762654    0.000000
 6   -2.099322   -0.763131    0.000000
 6   -2.798877    0.436791    0.000000
 1   -2.681418    2.598766    0.000000
 1   -0.196868    2.619098    0.000000
 1   -2.611444   -1.719450    0.000000
 1   -3.885147    0.417720    0.000000
 6    1.454251    0.516427    0.000000
 1    1.919660    1.513936    0.000000
```

`fragment_2.xyz`

```
 6    3.616611   -0.431977    0.000000
 1    4.026540   -0.938431    0.881195
 1    4.026540   -0.938431   -0.881195
 1    3.964593    0.611673    0.000000
```

```
fragment_nitrogen.xyz

 7    2.172386   -0.548950    0.000000

fragment_oxigen.xyz

 8   -0.047815   -1.936263    0.000000

fragment_proto.xyz

 1    0.930067   -1.730178    0.000000
```